



The countryside charity  
Cambridgeshire  
and Peterborough

The Town Hall, Market Hill  
St Ives, Cambridgeshire  
PE27 5AL  
www.cprecams.org.uk  
Tel: 01480 396698  
Email: office@cprecams.org.uk

The Planning Inspectorate  
Temple Quay House  
Temple Quay  
Bristol  
BS1 6PN

Branch President  
Christopher Vane Percy  
Branch Chair  
Alan James  
Branch Vice-Chair  
Jane Williams

15 May 2023

Submitted by upload to:

<https://infrastructure.planninginspectorate.gov.uk/projects/eastern/medworth-energy-from-waste-combined-heat-and-power-facility/?ipcsection=submission>

Dear Sir

**Ref: EN010110: Medworth Energy from Waste Combined Heat and Power Facility at Algores Way, Wisbech, Cambridgeshire.**

The Cambridgeshire and Peterborough Branch of the Campaign to Protect Rural England (CPRE) is an apolitical, independent charity which works to maintain the thriving and beautiful countryside of Cambridgeshire and Peterborough, to encourage strong rural communities and to prevent urban sprawl into and other damage to the countryside.

In our submission of 14<sup>th</sup> November 2022, we set out our strong objections to the above application.

We now have significant additional information about a major issue arising from climate change which we believe is highly relevant to this application and to the practicability, viability and safety of the proposed installation.

CPRE continues to object strongly to this proposal and our purpose in writing today is to update, amplify, clarify and provide additional information relating to one of the issues previously raised. Please see our additional comments below.

#### **Increasing Flood Risk due to Climate Change**

In our submission of 14<sup>th</sup> November 2022, we set out in general terms our concerns about the effects of this proposal on climate change and our concerns about the risks to the plant from rising flood risk.

We exemplified this with the effects of heavier and prolonged rainfall during the winter of 2020/21. We consider that this was likely due to the combined effects of higher rainfall intensity, changes to global weather patterns prolonging the period of rainfall, and steadily rising sea levels.

Since we made our original submission, we have become aware of several scientific papers which are the result of studies into rising global sea levels due to the effects of global ice melt, particularly in Greenland and in Antarctica.

Newly published research into the increasing likelihood of rapid sea-level rise due to uncontrolled melting of South Polar ice and Greenland ice leads to the conclusion that current official estimates of projected sea level rise, and hence flood risk, are too low and that serious flooding of the Fens is almost inevitable sooner rather than later.

The current official estimates of sea level rise used in flood protection estimation and planning are based on either IPCC 2014, 1 metre by 2100, or IPCC 2019, 1.1 metre by 2100. For example, using IPCC 2014, the South Bank of the River Great Ouse is currently being raised to protect against 1 in 80-year events, a very low level of protection. The North Bank, now classed as a dam, is being raised to 1 in 10,000 year protection.

Due to timing, neither IPCC 2014 or IPCC 2019 takes into account the accelerated melt rate of the Greenland ice sheet leading to an estimated additional 10 inches of sea level rise, as recently announced by researchers in the article titled *"What's going on with the Greenland ice sheet? It's losing ice"*

The Cambridgeshire and Peterborough branch of the Campaign to Protect Rural England  
Registered address: Town Hall, Market Hill, St Ives, Cambridgeshire PE27 5AL  
Registered charity number: 242809

Cont'd...

*faster than forecast and now irreversibly committed to at least 10 inches of sea level rise*” by Alun Hubbard, Professor of Glaciology, Arctic Five Chair, University of Tromsø. Copy enclosed.

Similarly, the increasing risk of the collapse of the Thwaites glacier in the Antarctic, leading to an estimate of up to 10 feet of sea level rise will not have been taken into account. This risk is highlighted in the following publications.

*“Study: Antarctic 'doomsday' glacier could retreat faster than expected”*, an article by Lylla Younes, published in September 2022. Copy enclosed.

*“Rapid retreat of Thwaites Glacier in the pre-satellite era”*, an article in Nature Geoscience by Alistair G C Graham et al, published in September 2022. Copy enclosed.

*“Seafloor images explain Thwaites Glacier retreat”*, a post on the British Antarctic Survey website on 5<sup>th</sup> September 2022. Copy enclosed.

There is a further estimated potential 0.5 metre sea level rise from the Pine Island ice shelf according to this paper:

*“Scientists expose vulnerabilities of critical Antarctic ice shelf”*, a post on British Antarctic Survey website on 21<sup>st</sup> September 2022. Copy enclosed.

These reports indicate clearly that rapid change is occurring to major ice deposits in both the north and the south of the globe. Similar changes are occurring to ice deposits in major mountain ranges such as the Alps and the Himalayas. All of which will further contribute to global sea level rise and increased risk of flooding in low-lying areas such as the Fens.

On 14<sup>th</sup> February 2023, the United Nations Secretary General warned of these effects in an address to the Security Council. Copy enclosed.

Satellite telemetry indicates clearly that the rate of sea level rise around the globe is increasing inexorably and data from the Aviso web site shows that rate of increase graphically. On March 25<sup>th</sup> 2023, the rate of sea level rise measured at 3.57 mm per year. See website extract and image enclosed.

A further issue in the South East of England is land sinkage which is currently around 1 mm per year. See enclosed paper:

*“Crustal motions in Great Britain: evidence from continuous GPS, absolute gravity and Holocene sea level data”*, Teferle et al. Copy enclosed.

Adding the rate of sea level rise measured by satellite to the rate of ground level shrinkage due to crustal motion, would indicate a current effective rate of sea level rise of 4.57 mm per annum affecting the Fens.

These projections indicate a significant increase of flood risk to the Fens, including Wisbech, during the life of the proposed incinerator. Some sudden additional increase, such as that arising from a rapid disruption of the Thwaites Glacier, could bring forward the timing of significant flooding.

These considerations are without taking into account the effects of high-tide and increased tidal surges due to more extreme weather events.

Neither do they take into account the increased run-off being caused by unwise developments in the upstream flood plain which can no longer be vetoed by the Environment Agency.

### **Conclusion**

Our conclusion is that the flood risk to the proposed plant is increasing steadily and at a higher rate than predicted by IPCC 2014 or IPCC 2019 which are currently used to define flood risk when designing flood protection measures.

We do not blame anyone for this, particularly the Environment Agency. It is just a matter of fact that climate change is now causing changes much faster than previously projected.



Cont'd...

Consequently, we advise that the highest levels of caution be taken.

**CPRE Cambridgeshire and Peterborough urge the Planning Inspectorate not to approve this application.**

Please note that our submission is in respect of the proposed development. While we have taken every effort to present accurate information for your consideration, as we are not a decision maker or statutory consultee we cannot accept any responsibility for unintentional errors or omissions and you should satisfy yourselves on any facts before making decisions arising from our submission.

Yours faithfully,

**Alan James BScTech., PhD, MBCS, CITP, MIMMM, CEnv**  
Chairman - CPRE Cambridgeshire and Peterborough

**Enc.**

Article	What's going on with the Greenland ice sheet? It's losing ice faster than forecast and now irreversibly committed to at least 10 inches of sea level rise.	August 2022	Prof. Alun Hubbard.
Article	Study: Antarctic 'doomsday' glacier could retreat faster than expected.	Sept 2022	Lylla Younes
Publication	Rapid retreat of Thwaites Glacier in the pre-satellite era.	Sept 2022	Alistair G C Graham et al
Website post	Seafloor images explain Thwaites Glacier retreat.	Sept 2022	British Antarctic Survey
Website post	Scientists expose vulnerabilities of critical Antarctic ice shelf.	Sept 2022	British Antarctic Survey
Script	Sea Level Rise: Implications for International Peace and Security.	Feb 2023	UN Secretary General
Website Print	Aviso Satellite Altimetry Website Extract.	May 2023	Aviso
Image	Aviso Satellite Altimetry – Graph of Rate of Sea Level Rise.	May 2023	Aviso
Publication	Crustal motions in Great Britain: evidence from continuous GPS, absolute gravity and Holocene sea level data.	March 2009	Teferle et al

What's going on with the Greenland ice sheet? It's losing ice faster than forecast and now irreversibly committed to at least 10 inches of sea level rise.

Prof. Alun Hubbard.



A turbulent melt-river pours a million tons of water a day into a moulin, where it flows down through the ice to ultimately reach the ocean. Ted Giffords

## What's going on with the Greenland ice sheet? It's losing ice faster than forecast and now irreversibly committed to at least 10 inches of sea level rise

Published: August 29, 2022 7.04pm BST

**Alun Hubbard**

Professor of Glaciology, Arctic Five Chair, University of Tromsø

I'm standing at the edge of the Greenland ice sheet, mesmerized by a mind-blowing scene of natural destruction. A milewide section of glacier front has fractured and is collapsing into the ocean, calving an immense iceberg.

Seracs, giant columns of ice the height of three-story houses, are being tossed around like dice. And the previously submerged portion of this immense block of glacier ice just breached the ocean – a frothing maelstrom flinging ice cubes of several tons high into the air. The resulting tsunami inundates all in its path as it radiates from the glacier's calving front.

Fortunately, I'm watching from a clifftop a couple of miles away. But even here, I can feel the seismic shocks through the ground.



A fast-flowing outlet glacier calves a 'megaberg' into Greenland's Uummannaq Fjord. Alun Hubbard

Despite the spectacle, I'm keenly aware that this spells yet more unwelcome news for the world's low-lying coastlines.

As a field glaciologist, I've worked on ice sheets for more than 30 years. In that time, I have witnessed some gobsmacking changes. The past few years in particular have been unnerving for the sheer rate and magnitude of change underway. My revered textbooks taught me that ice sheets respond over millennial time scales, but that's not what we're seeing today.

A study published Aug. 29, 2022, demonstrates – for the first time – that Greenland's ice sheet is now so out of balance with prevailing Arctic climate that it no longer can sustain its current size. It is irreversibly committed to retreat by at least 59,000 square kilometers (22,780 square miles), an area considerably larger than Denmark, Greenland's protectorate state.

Even if all the greenhouse gas emissions driving global warming ceased today, we find that Greenland's ice loss under current temperatures will raise global sea level by at least 10.8 inches (27.4 centimeters). That's more than current models forecast, and it's a highly conservative estimate. If every year were like 2012, when Greenland experienced a heat wave, that irreversible commitment to sea level rise would triple. That's an ominous portent given that these are climate conditions we have already seen, not a hypothetical future scenario.

Our study takes a completely new approach – it is based on observations and glaciological theory rather than sophisticated numerical models. The current generation of coupled climate and ice sheet models used to forecast future sea level rise fail to capture the emerging processes that we see amplifying Greenland's ice loss.

## **How Greenland got to this point**

The Greenland ice sheet is a massive, frozen reservoir that resembles an inverted pudding bowl. The ice is in constant flux, flowing from the interior – where it is over 1.9 miles (3 kilometers) thick, cold and snowy – to its edges, where the ice melts or calves bergs.

In all, the ice sheet locks up enough fresh water to raise global sea level by 24 feet (7.4 meters).

David Attenborough takes us on a virtuoso tour of the Greenland ice sheet.

Greenland's terrestrial ice has existed for about 2.6 million years and has expanded and contracted with two dozen or so "ice age" cycles lasting 70,000 or 100,000 years, punctuated by around 10,000-year warm interglacials. Each glacial is driven by shifts in Earth's orbit that modulate how much solar radiation reaches the Earth's surface. These variations are then reinforced by snow reflectivity, or albedo; atmospheric greenhouse gases; and ocean circulation that redistributes that heat around the planet.

We are currently enjoying an interglacial period – the Holocene. For the past 6,000 years Greenland, like the rest of the planet, has benefited from a mild and stable climate with an ice sheet in equilibrium – until recently. Since 1990, as the atmosphere and ocean have warmed under rapidly increasing greenhouse gas emissions, Greenland's mass balance has gone into the red. Ice losses due to enhanced melt, rain, ice flow and calving now far exceed the net gain from snow accumulation.

Greenland's ice mass loss measured by NASA's Grace satellites.

### **What does the future hold?**

The critical questions are, how fast is Greenland losing its ice, and what does it mean for future sea level rise?

Greenland's ice loss has been contributing about 0.04 inches (1 millimeter) per year to global sea level rise over the past decade.

This net loss is split between surface melt and dynamic processes that accelerate outlet glacier flow and are greatly exacerbated by atmospheric and oceanic warming, respectively. Though complex in its manifestation, the concept is simple: Ice sheets don't like warm weather or baths, and the heat is on.



Meltwater lakes feed rivers that snake across the ice sheet - until they encounter a moulin. Alun Hubbard

What the future will bring is trickier to answer.

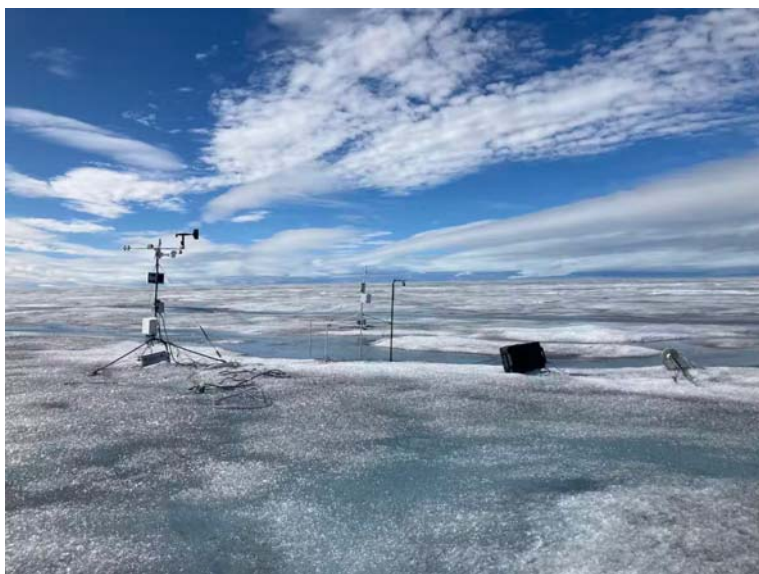
The models used by the Intergovernmental Panel on Climate Change predict a sea level rise contribution from Greenland of around 4 inches (10 centimeters) by 2100, with a worst-case scenario of 6 inches (15 centimeters).

But that prediction is at odds with what field scientists are witnessing from the ice sheet itself.

According to our findings, Greenland will lose at least 3.3% of its ice, over 100 trillion metric tons. This loss is already committed – ice that must melt and calve icebergs to reestablish Greenland's balance with prevailing climate.

We're observing many emerging processes that the models don't account for that increase the ice sheet's vulnerability. For example:

- Increased rain is accelerating surface melt and ice flow.
- Large tracts of the ice surface are undergoing bio-albedo darkening, which accelerates surface melt, as well as the impact of snow melting and refreezing at the surface. These darker surfaces absorb more solar radiation, driving yet more melt.



In August 2021, rain fell at the Greenland ice sheet summit for the first time on record. Weather stations across Greenland captured rapid ice melt. European Space Agency

- Warm, subtropical-originating ocean currents are intruding into Greenland's fjords and rapidly eroding outlet glaciers, undercutting and destabilizing their calving fronts.
- Supraglacial lakes and river networks are draining into fractures and moulins, bringing with them vast quantities of latent heat. This "cryo-hydraulic warming" within and at the base of the ice sheet softens and thaws the bed, thereby accelerating interior ice flow down to the margins.

## **The issue with models**

Part of the problem is that the models used for forecasting are mathematical abstractions that include only processes that are fully understood, quantifiable and deemed important.



Models reduce reality to a set of equations that are solved repeatedly on banks of very fast computers. Anyone into cutting-edge engineering – including me – knows the intrinsic value of models for experimentation and testing of ideas. But they are no substitute for reality and observation. It is apparent that current model forecasts of global sea level rise underestimate its actual threat over the 21st century. Developers are making constant improvements, but it's tricky, and there's a dawning realization that the complex models used for long-term sea level forecasting are not fit for purpose.



Author Alun Hubbard's science camp in the melt zone of the Greenland ice sheet. Alun Hubbard

There are also “unknown unknowns” – those processes and feedbacks that we don't yet realize and that models can never anticipate. They can be understood only by direct observations and literally drilling into the ice.

That's why, rather than using models, we base our study on proven glaciological theory constrained by two decades of actual measurements from weather stations, satellites and ice geophysics.

### **It's not too late**

It's an understatement that the societal stakes are high, and the risk is tragically real going forward. The consequences of catastrophic coastal flooding as sea level rises are still unimaginable to the majority of the billion or so people who live in low-lying coastal zones of the planet.



A large tabular iceberg that calved off Store Glacier within Uummannaq Fjord. Alun Hubbard



Personally, I remain hopeful that we can get on track. I don't believe we've passed any doom-laden tipping point that irreversibly floods the planet's coastlines. Of what I understand of the ice sheet and the insight our new study brings, it's not too late to act.

But fossil fuels and emissions must be curtailed now, because time is short and the water rises – faster than forecast.

Study: Antarctic 'doomsday' glacier could retreat faster than expected.  
Lylla Younes

# Study: Antarctica's 'doomsday glacier' could retreat faster than expected

“Thwaites is really holding on today by its fingernails, and we should expect to see big changes over small timescales.”



*NATA / OIB / Jeremy Harbeck*

Lylla Younes

---

Published

Sep 07, 2022

---

Topic

Climate + Science

---

Over the past decade, scientists studying sea level rise have turned their attention to western Antarctica, where one of the world's largest glaciers has dumped over a trillion tons of ice into the ocean since the early 2000s. The Thwaites glacier has been referred to as the "doomsday glacier" because its complete collapse could raise global sea levels by as much as 10 feet.

Whether and when this collapse happens depends in large part on how fast Thwaites' so-called grounding line — the bottom part of a glacier where ice, rock, and ocean meet — is eroded. This process is called glacier retreat, and scientists have long viewed it as typically being a slow process that can extend over millennia. However, a new study published Monday in the journal Nature Geoscience has upended those beliefs.

A team of researchers led by marine geophysicist Alastair Graham at the University of South Florida's College of Marine Science found that during the past two centuries, the glacier's grounding line has retreated much more rapidly than previously thought. During one 5.5-month period, for example, the body of ice eroded at a rate of 2.1 kilometers per year — twice the rate observed by satellites between 2011 and 2019.



**Reader support helps sustain our work. Donate today to keep our climate news free.**

ONE TIME	MONTHLY		
\$10	\$15	OTHER	<b>Donate</b>

These findings suggest that, in the future, the glacier’s retreat may be more rapid and unpredictable than scientists have hitherto expected. This only adds to worries that warming seas will push Thwaites to a tipping point of irreversible collapse and destabilize the surrounding West Antarctic ice sheet, with dire consequences for global sea level rise.

To support our nonprofit environmental journalism, please consider disabling your ad-blocker to allow ads on Grist. Here's How →

“Thwaites is really holding on today by its fingernails, and we should expect to see big changes over small timescales in the future — even from one year to the next — once the glacier retreats beyond a shallow ridge in its bed,” marine geophysicist and study co-author Robert Larter from the British Antarctic Survey said in a press release.

Glaciers are complex geological systems influenced by the interaction of land and sea. Those like Thwaites that terminate at the ocean are held back by giant ice shelves, floating platforms that form when ice flows down the land-based glaciers and pools over the ocean. Rising ocean temperatures have led to the weakening and fragmenting of these vital support structures: Last year, scientists reported that the ice shelf surrounding Thwaites could collapse within the next five years. The loss of the ice shelf means that the glacier must rely more heavily on the seafloor for stabilization.

That's why the team of scientists led by Graham decided to focus their efforts on the grounding line where the glacier breaks off from the ocean floor. Their goal was to gather data on how fast that line has moved in the past, in order to make projections about its future.

Understanding events in the pre-satellite era requires measuring geological remnants of prior events. In the case of Thwaites, that means tracking the rib-like ridges that formed along the ocean floor from the glacier's past retreat. To do this, the researchers dispatched a robot to capture high-resolution images of the seafloor in front of the glacier. Using those images, the researchers identified 160 parallel ridges that were created "like a footprint" by the glacier front as it retreated, moving with the daily tides. What surprised the scientists most was the speed at which these ridges were created, with rapid periods of retreat happening as recently as 50 years ago.

To support our nonprofit environmental journalism, please consider disabling your ad-blocker to allow ads on Grist. Here's How →

While these results throw Thwaites' future into greater question, Graham underscored that it is not too late to address the primary factor influencing the glacier's retreat: rising ocean temperatures.

"It's got the potential to become the doomsday glacier, but we're not quite there yet," he told Grist, adding that cutting global greenhouse gas emissions has the potential to reduce the rate at which the ocean is warming. "We still have, to some extent, some control over what Thwaites does."

---

**Support solutions-based climate news**

Your support keeps our unbiased, nonprofit news free.

**Donate Now**

## More

---

[Fix](#)

[Events](#)

[Visionaries Bureau](#)

[Become a Member](#)

[Advertising](#)

[Republish](#)

[Accessibility](#)

## Sustainability

---

As part of our commitment to sustainability, in 2021 Grist moved its office headquarters to the Bullitt Center in Seattle's vibrant Capitol Hill neighborhood. Known as one of the greenest commercial buildings in the world, since it opened its doors on Earth Day in 2013 the Bullitt Center has been setting a new standard for sustainable design.



© 1999-2023 Grist Magazine, Inc. All rights reserved.

Grist is powered by [WordPress VIP](#).

Design and build by [Upstatement](#).

[Terms of Use](#) | [Privacy Policy](#).





Rapid retreat of Thwaites Glacier in the pre-satellite era.

Alistair G C Graham et al



OPEN

# Rapid retreat of Thwaites Glacier in the pre-satellite era

Alastair G. C. Graham<sup>1</sup>✉, Anna Wåhlin<sup>2</sup>, Kelly A. Hogan<sup>3</sup>, Frank O. Nitsche<sup>4</sup>,  
Karen J. Heywood<sup>5</sup>, Rebecca L. Totten<sup>6</sup>, James A. Smith<sup>3</sup>, Claus-Dieter Hillenbrand<sup>3</sup>,  
Lauren M. Simkins<sup>7</sup>, John B. Anderson<sup>8</sup>, Julia S. Wellner<sup>9</sup> and Robert D. Larter<sup>3</sup>

**Understanding the recent history of Thwaites Glacier, and the processes controlling its ongoing retreat, is key to projecting Antarctic contributions to future sea-level rise. Of particular concern is how the glacier grounding zone might evolve over coming decades where it is stabilized by sea-floor bathymetric highs. Here we use geophysical data from an autonomous underwater vehicle deployed at the Thwaites Glacier ice front, to document the ocean-floor imprint of past retreat from a sea-bed promontory. We show patterns of back-stepping sedimentary ridges formed daily by a mechanism of tidal lifting and settling at the grounding line at a time when Thwaites Glacier was more advanced than it is today. Over a duration of 5.5 months, Thwaites grounding zone retreated at a rate of >2.1 km per year—twice the rate observed by satellite at the fastest retreating part of the grounding zone between 2011 and 2019. Our results suggest that sustained pulses of rapid retreat have occurred at Thwaites Glacier in the past two centuries. Similar rapid retreat pulses are likely to occur in the near future when the grounding zone migrates back off stabilizing high points on the sea floor.**

Ice loss from West Antarctica's second largest marine ice stream, Thwaites Glacier, is currently a major uncertainty for future sea-level projections<sup>1–3</sup>. Its bed deepens upstream to >2 km below sea level<sup>4</sup>, and warm, dense, deep water delivers heat to the present-day ice-shelf cavity, melting its ice shelves from below<sup>5</sup>. Together, these conditions make Thwaites Glacier susceptible to runaway retreat<sup>6</sup>. Satellite radar observations of change in the ice stream show that its fast-flowing trunk has sped up, thinned and widened since 2011, while there has been spatially variable grounding-line retreat<sup>7,8</sup>. Such changes have occurred as a consequence of reduced buttressing from weakened contact with a shallow ridge at the Eastern Ice Shelf terminus<sup>8–10</sup>, and fragmentation and subsequent detachment of the Thwaites Glacier Tongue (TGT) from a sea-bed pinning point<sup>11</sup> (Fig. 1a). As the stabilizing effects of these ice-shelf pinning points lessen<sup>12</sup>, future retreat of Thwaites becomes increasingly predicated on processes that occur in the grounding zone—the region in which the glacier comes afloat in the ocean. Sea-floor topography can help stabilize ice sheets against grounding-line retreat<sup>13</sup>, and grounding-line migration affects ice-sheet stability on timescales spanning months to millennia<sup>14</sup>. Currently, Thwaites is grounded on prominent sea floor ridges in a number of places<sup>15</sup>, and the evolution of grounding-zone processes here is critical to future ice retreat<sup>16,17</sup>. However, the processes operating at marine ice-stream margins are poorly resolved, presenting a challenge to understanding how quickly and through what mechanisms glaciers such as Thwaites can retreat from sites of sea-floor stabilization.

One place where information on patterns and processes of retreat might be studied is in former ice-sheet grounding zones. Offshore

of Thwaites Glacier, recent sonar mapping documented numerous sea-bed promontories where the ice was previously grounded<sup>18</sup>. Spectral analyses of this former bed topography indicate that these regions are geologically analogous to the modern grounding zone<sup>18</sup>, making them ideal sites to target the processes and behaviour of Thwaites in the recent past.

As present-day retreat partly represents adjustments to past imbalance<sup>19</sup>, it is important to constrain how glaciers such as Thwaites changed before observations were possible. Direct observations of grounding-line change and forcing extend back only 30–40 years for most of West Antarctica, and although ice-sheet retreat following the Last Glacial Maximum is mostly well constrained, data relating to the past 10,000 years of Thwaites Glacier history are scarce<sup>20</sup>. Substantial gaps therefore remain in our understanding of grounding-line behaviour in the pre-satellite era.

A recent detailed study of grounding-zone wedges offshore of the Antarctic Peninsula, formed during the last deglaciation, revealed delicate grounding-line landforms that record exceptionally fast rates of past retreat<sup>21</sup> demonstrating potential to resolve subannual rates of change from submarine landforms. However, Antarctic deglaciation at the time of this retreat was driven in part by sea-level rise from the melting of the Northern Hemisphere ice sheets<sup>22</sup>, meaning neither the time period nor forcing provide appropriate analogues for the near-future state of the West Antarctic Ice Sheet. In addition, although satellite monitoring since the 1990s has substantially improved the temporal resolution at which small-scale grounding zone changes can now be sensed<sup>2,23</sup>, so far, there has been no way of reconstructing rates of past grounding-line retreat over annual or even

<sup>1</sup>College of Marine Science, University of South Florida, St Petersburg, FL, USA. <sup>2</sup>Department of Marine Sciences, University of Gothenburg, Gothenburg, Sweden. <sup>3</sup>British Antarctic Survey, Natural Environment Research Council, Cambridge, UK. <sup>4</sup>Lamont-Doherty Earth Observatory, Columbia University, Palisades, NY, USA. <sup>5</sup>School of Environmental Sciences, University of East Anglia, Norwich, UK. <sup>6</sup>Department of Geological Sciences, University of Alabama, Tuscaloosa, AL, USA. <sup>7</sup>Department of Environmental Sciences, University of Virginia, Charlottesville, VA, USA. <sup>8</sup>Department of Earth, Environmental and Planetary Sciences, Rice University, Houston, TX, USA. <sup>9</sup>Department of Earth and Atmospheric Sciences, University of Houston, Houston, TX, USA. ✉e-mail: [alastairg@usf.edu](mailto:alastairg@usf.edu)

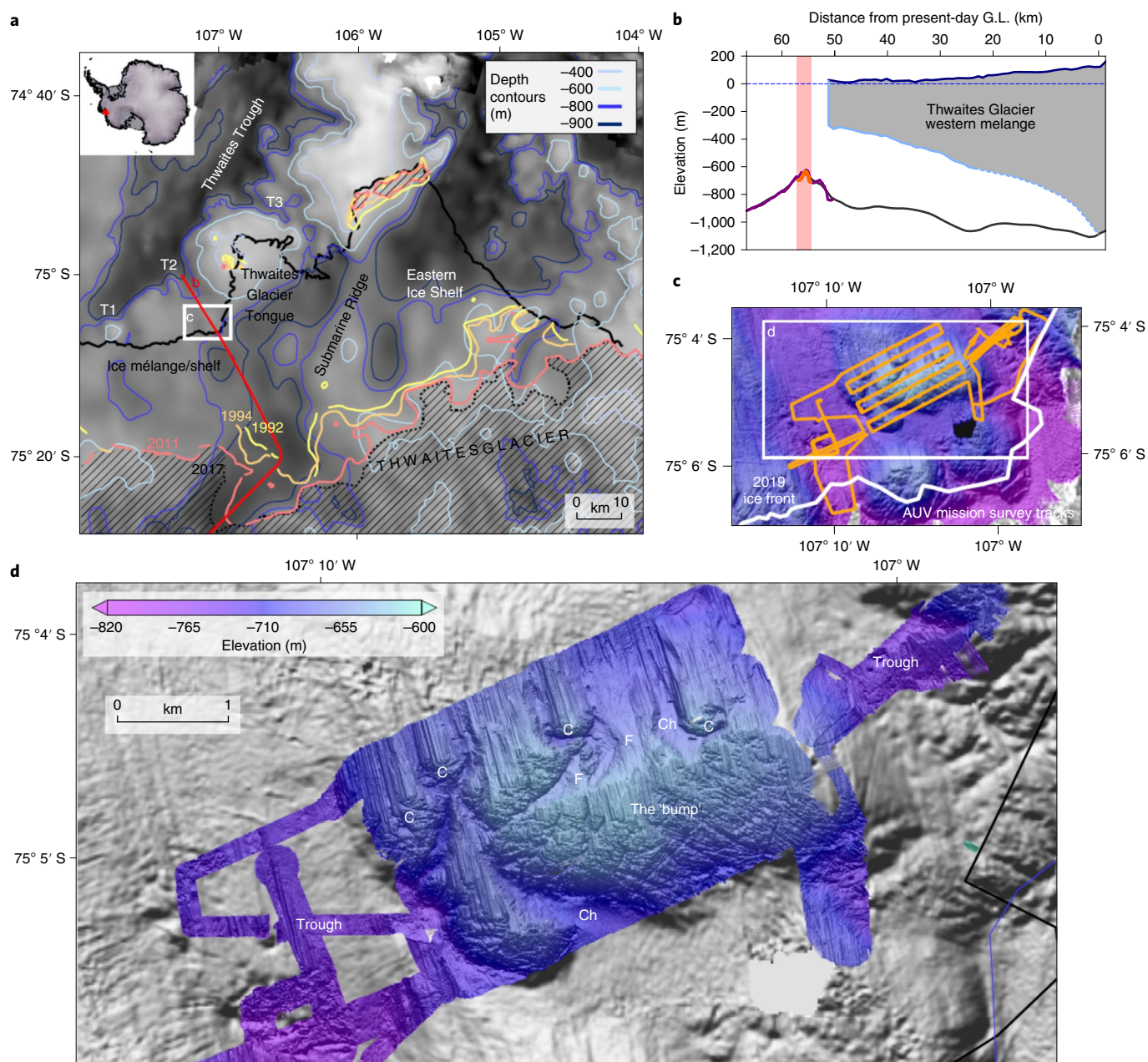


**Fig. 1 | Location map and context of the Thwaites Glacier study site.** **a**, Map of the southern Amundsen Sea embayment in the vicinity of Thwaites Glacier. Bathymetry/topography covering marine, sub-ice shelf and grounded glacier from ref. <sup>37</sup>. Previous grounding-line positions, as well as pinning points at the termini of the TGT and Eastern Ice Shelf, are shown in colour. Modern region of grounding hatched. T1-T3: tributary troughs. **b**, Long profile showing study site context. Pink bar and orange-shaded bathymetry show area of new survey. G.L., grounding line. **c**, AUV survey tracks at the apex of the Thwaites western ice mélangé and TGT. **d**, AUV multibeam swath bathymetry of 1.5 m resolution superimposed on a hillshade-rendered image of shipborne EM122 swath bathymetry collected on the same research cruise. F, fan; C, crag; Ch, channel.

subannual, let alone daily, time frames, for historical time periods (for example, pre-1990s) that might further improve simulations of future West Antarctic Ice Sheet evolution.

In this Article, to address vital questions about rates and processes of recent grounding-line retreat, we studied an isolated sea-floor promontory (the ‘bump’) at the southwest corner of the remnant TGT, downstream of what is now Thwaites Glacier’s fastest-flowing grounded section<sup>7</sup> (Fig. 1a). The bump, at ~630–670 m water depth, is deeper than the keel depths of modern icebergs or ice shelf drafts<sup>24</sup> so post-retreat processes are unlikely to have disturbed landforms produced during grounding-zone retreat

(Fig. 1b). The site lies within a broader tributary trough (T2 in Fig. 1) that is today a flow path for modified Circumpolar Deep Water (CDW) that circulates into and out of the ice-shelf cavity<sup>25</sup>. The bump is flanked to the east and west by two narrow subtroughs at approximately 800 m depth (Fig. 1d). We deployed an autonomous underwater vehicle (AUV) mounted with geophysical sensors to acquire high-resolution (sub-metre) multibeam bathymetry and acoustic imagery from sidescan sonar, flying at an altitude of 50–90 m from the sea floor. Approximately 13 km<sup>2</sup> of new geophysical data were obtained over a 19 h mission across the bump (Fig. 1c).



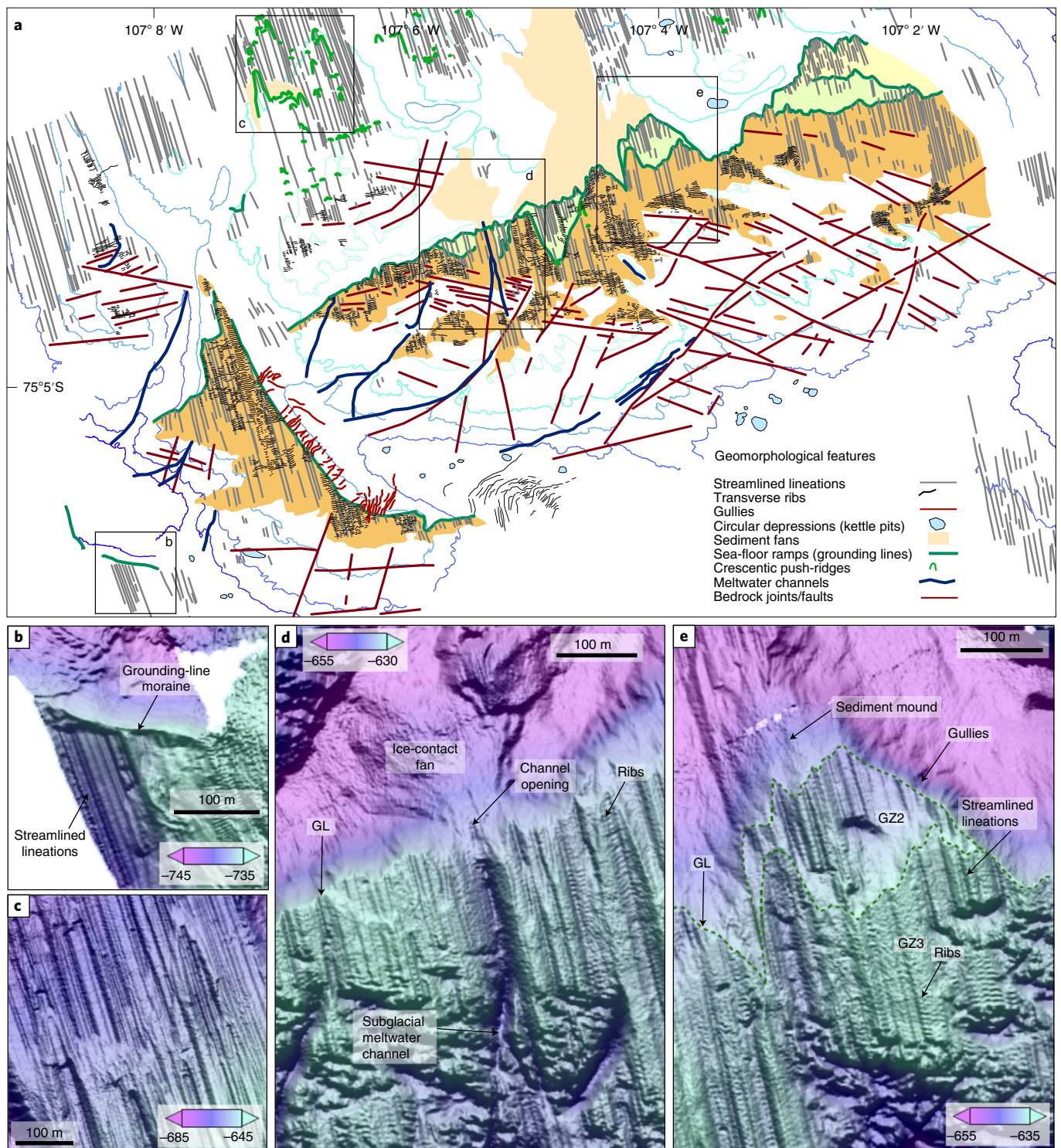


**Fig. 2 | Sedimentary grounding zone system mapped on ‘the bump’ seaward of Thwaites ice shelf. a**, Geomorphological map of features on and seaward of the bump. Coloured regions are successive sedimentary tops of former grounding zones (GZ 1–3). **b**, AUV multibeam bathymetry showing a grounding-line moraine marking the edge of a flat-topped lineated ramp. **c**, Examples of connecting crescentic push-ridges formed on downward-dipping slopes in the northern part of the study area. **d**, Subglacial meltwater channel and a connected ice-contact fan system. **e**, Examples of multiple back-stepping grounding lines (small ramps: green, dashed lines), lineations and overprinting ribs shown in more detail in subsequent figures.

### Observations from a former West Antarctic grounding zone

Sea-floor imagery reveals that the bump is a former grounding zone of Thwaites Glacier (Fig. 1d and Supplementary Fig. 1). From geomorphological mapping of the main promontories and northern half of the survey, we identify landforms that character-

ize a sedimentary grounding zone system<sup>26</sup> (Fig. 2). This sedimentary landscape is contrasted to the south and on smaller up-ice slopes of sea-floor highs by exposed and heavily jointed bedrock (Figs. 1d and 2a, Supplementary Fig. 2 and Supplementary Text). Three former grounding-zone fronts are identifiable, traceable as



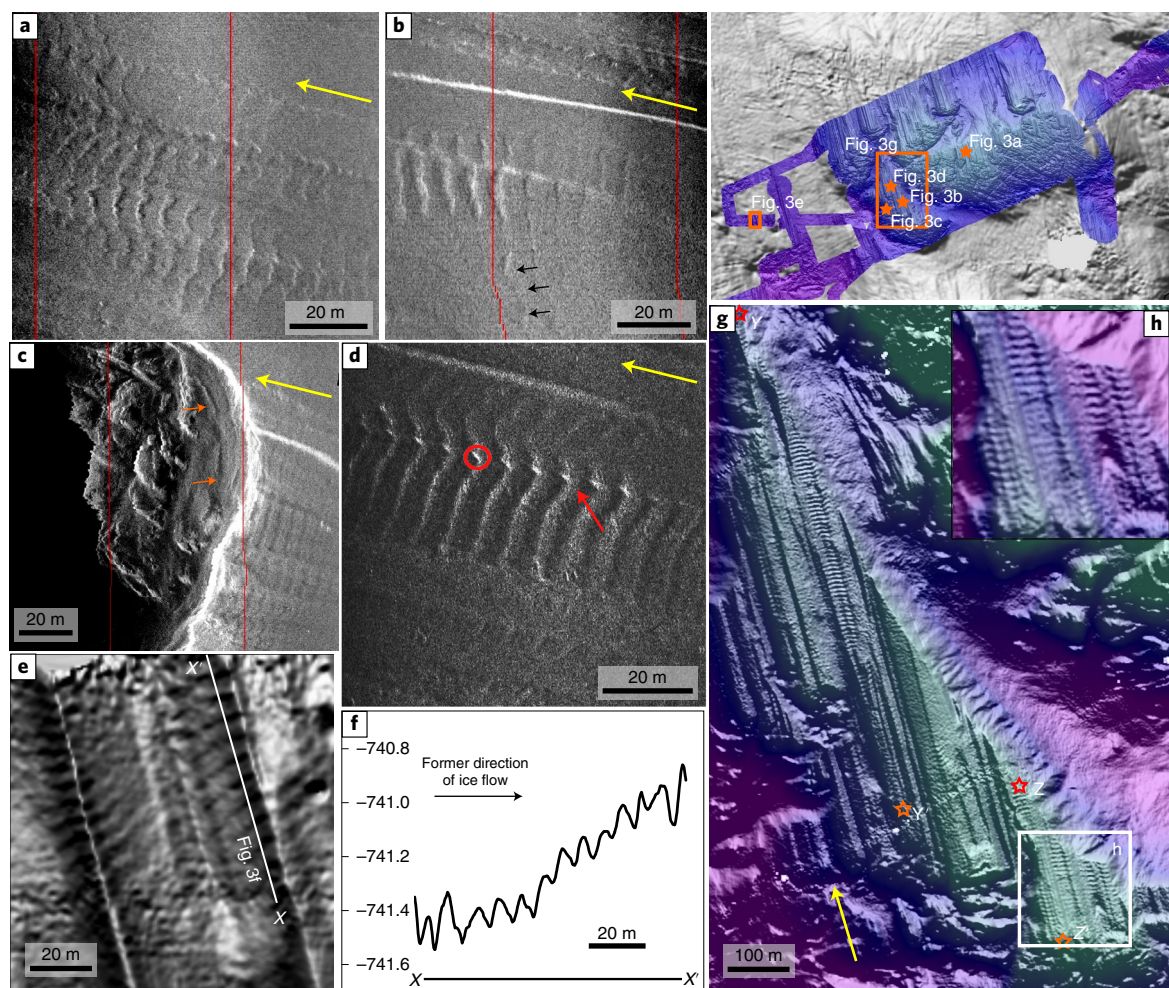


**Fig. 3 | Details of sea-floor ribs on high-resolution AUV sidescan and multibeam data. a–d**, Examples of high-frequency sidescan imagery illustrating the back-stepping conformity of ridge shape (**a**), non-alignment of ribs to underlying lineations (**b**), rib formation on terraces (**c**) and the ‘beading’ (red circle) and overprinting (red arrow) of existing subglacial features (**d**). **e**, Multibeam hillshade showing fine-scale landforms, <20 cm high, crossing lineation ridges and grooves. **f**, Corresponding profile X–X’, demonstrating the subtle geometries of some of the landforms (5–20 cm) and their surprising depth (>740 m). **g, h**, Multibeam swath bathymetry covering the longest series of ribs (profile Y–Y’ and Z–Z’ combined; stars mark start and end of profile sections). Inset shows close-up example of lateral continuity in the southern portion of the ribs. Black arrows in ‘b’ mark lateral continuation of one oblique ridge. Yellow arrows in each image show ice flow direction inferred from lineations.

tortuous, steep, 0.5–2 m-high ramps that can be mapped west to east, in some cases for approximately 2 km (Fig. 2a). The ramps are leading edges of till sheets laid down by grounded ice in contact with the sea floor, each marking successive steps of ice-sheet retreat southwards (Fig. 2a, GZ1–3; Supplementary Fig. 3). Straight and parallel sets of subglacial lineations characterize the sea bed between the ramps, becoming younger landward. The most extensive grounding zone (Fig. 2a,e, ‘GZ3’) is also the most recent, meaning the sea-bed record on top of the bump mainly relates to a single grounding period.

Multiple linear channels that shoal northwards cut through the lineated surfaces (Fig. 2a). One of these—a 6 m deep and 75 m wide channel—terminates in an ice-proximal fan, clearly showing the emergence of a subglacial meltwater conduit at the former grounding line (Fig. 2d and Supplementary Fig. 4). Gullies on slopes that coincide with former grounding-line positions, fans and meltwater features, together, indicate that Thwaites Glacier was fully grounded through its present-day ice-shelf cavity and possessed an active sediment and subglacial meltwater system when the grounding line retreated onto the bump, leaving landforms preserved as the glacier receded.

On seaward dipping, shallow (~660 m) portions of the sea bed, high-frequency sidescan data reveal tracks of parallel ribs transverse to former ice flow direction (Fig. 3a–d). The ribs relate dominantly to the most recent grounding surface, GZ3 (Fig. 2a). They are similar to regularly spaced ‘rungs’ recently observed in the Weddell Sea<sup>21</sup>. Ribs overprint and are traceable across multiple underlying lineations and form ‘beaded’ features at lineation ridge crests where they obliterate the pre-existing subglacial signature (Fig. 3d and Supplementary Fig. 7). Some ridges sit obliquely across the underlying lineations, distinguishing them from the processes that created the subglacial bedforms (Fig. 3b). The ribs are subtle—70% of them are <20 cm in height—but widespread through the study region ( $n > 1,500$ ; Fig. 2a).

To assess the processes that formed the ridges, we analysed the geometry of the longest series of ribs comprising 164 individual landforms (Figs. 2e, 3g and 4a). Amplitudes of the 0.1–0.7 m high ribs show clear along-flow modulation, with a 13–15 ridge periodicity repeating over ten cycles (Fig. 4b). Spectral analysis of the along-flow variance in rib heights shows a dominant frequency peak at 14.9 ridges (Fig. 4c, orange). The overall peak amplitude of each

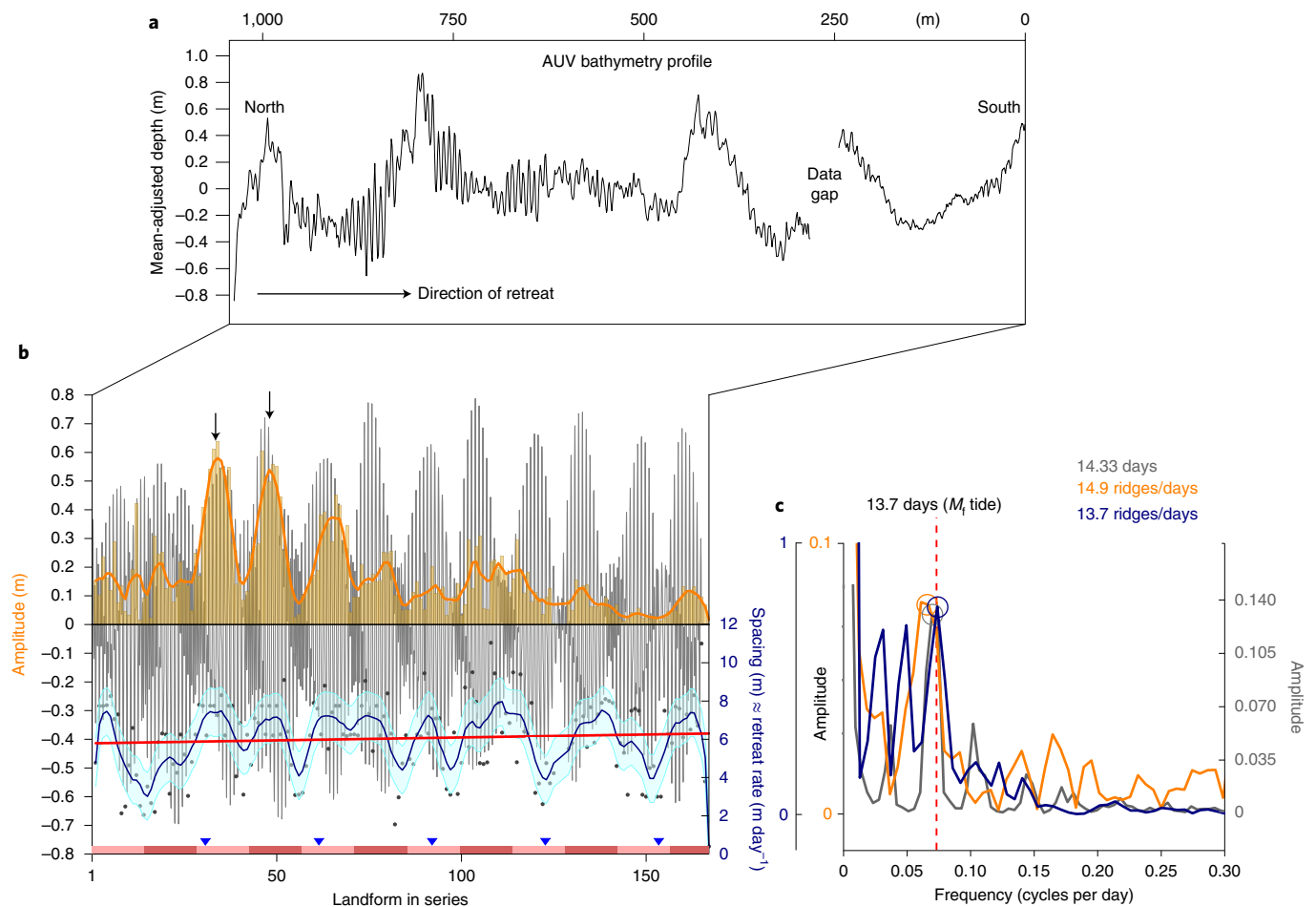


**Fig. 4 | Geometries and analysis of the longest series of ribs from the top of the bump.** **a**, Mean-adjusted composite topographic profile through the longest series of sea-floor ridges (see profile Y-Z' in Fig. 3h for location). **b**, Extracted geometries (Methods) from **a** showing the longitudinal variability in height (orange) and spacing (blue) of 164 ribs plotted together with the output from the tide model<sup>28</sup> (black; Methods). Alternating pink bars are 14-day periods, with blue triangles marking monthly intervals in the series (30.4 days). **c**, Periodograms (fast Fourier transforms) of the datasets in **b** showing the significance of frequencies in the series (cycles per day). Coloured circles mark the dominant peaks in the frequency spectra of the tidal model (grey), ridge amplitude data (orange) and ridge spacing data (blue), respectively. The tidal periodicity of 14.33 days in the tide model is the recurrence interval for spring and neap tides due to the interaction of principal lunar and principal solar semidiurnal tides. Red dashed line marks the  $M_2$  (lunar fortnightly) constituent.

cycle decreases gradually southwards. The periodicity is not unique to one series and is preserved in adjacent sequences of ribs found at different depths. This cyclic variability is mirrored in the spacing of the ribs along flow, and the two parameters co-vary (Fig. 4b and Supplementary Fig. 8). Ten cycles occur over the 1,050 m long profile. Between 0 m and 420 m along profile, the peak interval is about 21–23 ridges. From 420 m to 1,050 m along profile, peak intervals range from 12 to 16 ridges. The dominant period is calculated at 13.7 ridges (Fig. 4c, blue). The largest spacing between ridges correlates with higher peaks in ridge amplitude, showing that, generally, ribs are further apart when the ribs are taller (Supplementary Fig. 8d). Rib spacing is typically 6.6–7.6 m but ranges overall from ~1.6 m to 10.5 m (Supplementary Fig. 8b).

The amplitude, spacing and the 13–15 cycle amplitude variation match with present-day tides in this region<sup>27</sup> (Fig. 4 and Methods) that are predominantly diurnal (that is, one high and one low tide per day). The amplitude reaches  $\pm 0.8$  m, and there is a pronounced 14-day spring–neap cycle (grey, Fig. 4b). This suggests that tides modulate the ridges in both amplitude and spacing (Figs. 4b,c, and Supplementary Fig. 8), and that the ribs are imprints of a feature at the bottom of the ice (such as in the grounding zone). When

plotted together with the tide model predictions for the Thwaites region<sup>28,29</sup> (Methods), there is a strong coherence between the variability in the amplitudes of the ribs and daily tidal heights (Fig. 4b and Supplementary Fig. 8;  $R^2 = 0.57$ ). The 13–15 cycle periodicity is particularly clear in the peak-to-peak spacing and amplitude in the northern and central parts of the profile (arrowed, Fig. 4b; Fig. 4c). The spatial sequence of ribs therefore represents a series in time, and diurnal and spring–neap tidal constituents are the strongest influence over their geometry (Fig. 4c).

#### Ribs formed by tidally modulated grounding-line retreat

What process could create the distinct ribs? Forming in series, one per day, the ribs could relate either to the forward motion by grounded ice (that is, ice shelf/ice mélange keels<sup>30</sup>) or to its inland migration (Supplementary Information). Tidal flexure and fast, steady retreat of the grounding line—first lifting during high water, and then settling on the sea bed during low tide—can best explain the unusual rib features (Fig. 5; cf. ref. <sup>21</sup>). Sediment, extruded each time the grounding line settles on its substrate, forms a chain of ridges in the narrow accommodation space of the sub-ice shelf cavity (Fig. 5). The shape, regularity and periodicity of the ribs imply

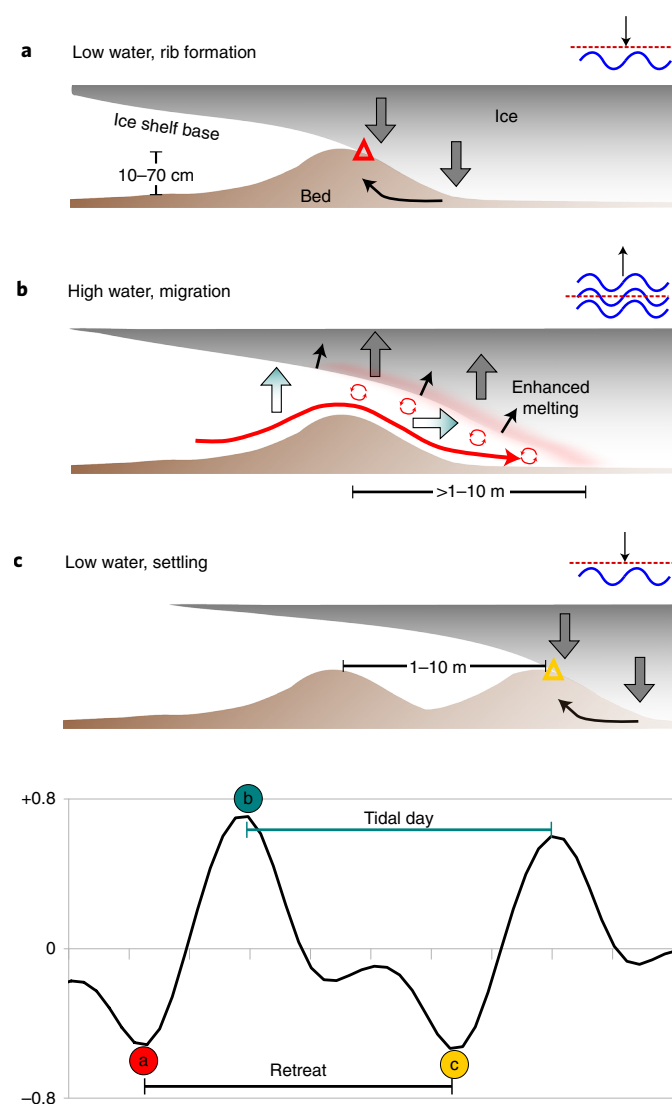


**Fig. 5 | Conceptual model for the formation of ribs by tidally modulated grounding-line migration.** **a**, Grounding at low water forms a rib by settling and sediment bulging/extrusion at the grounding line ahead of an ice plain. **b**, Subsequent grounding-line migration occurs during high water with the ice-shelf base displaced upwards and landwards by the tide, allowing contact with warm ocean water. Basal melting is enhanced by tidal mixing in the narrow cavity. **c**, Grounding line settles at new position on the next low water, creating a second rib in series. The amplitude and spacing of ribs is a function of tidal amplitude, which modulates the distance of retreat from ridge to ridge. Bottom: plot depicting typical diurnal tide cycle for a 48 h period at Thwaites Glacier. Intervals on x-axis correspond to 0.2 days (4.8 hours). **a–c** relate to positions on the tidal cycle. Triangles denote successive grounding-line positions. Note exaggerated vertical scale in all images; the true sea-floor expression of the ridges is subtle, with sea bed and ice bottom slopes only fractions of a degree.

vertical displacement at the grounding zone with grounding-line retreat proceeding at many metres per day.

The present study provides a rare example where the clear influence of tides has left geological markers of their interaction with the ice sheet on the sea bed (Fig. 4b)<sup>31</sup>. The rapid retreat documented by the ribs suggests an ice-dynamic response, but ocean-forced melting may also have played a key role. On the basis of the common amplitude of the ribs (approximately 0.1–0.4 m) and assuming daily rates of recession of 6–8 m per day, we estimate the daily ice loss

rate to exceed 1,000 kg per day per metre of the grounding zone (Supplementary Information and Supplementary Fig. 11). A heat flux exceeding  $600 \text{ W m}^{-2}$  is required to melt that quantity of ice. This compares to the  $300\text{--}900 \text{ W m}^{-2}$  that can be delivered to the ice by  $\sim 1.2^\circ\text{C}$  water ( $3.1^\circ\text{C}$  above in situ freezing point), if there is a fully turbulent ice–ocean boundary layer, and to the  $0.9\text{TW}$  (or  $300 \text{ W m}^{-2}$  for an ice shelf with an area of  $3,000 \text{ km}^2$ ) that is delivered through one of the deep troughs leading into the cavity from the north<sup>25</sup>. The distances between sequential ribs (Fig. 4b) show grounding-line migration ranged from  $\sim 4 \text{ m}$  per day during neap tides to  $\sim 8 \text{ m}$  per day during spring tides, and an explanation for this variation may be the increased turbulence during spring tides<sup>32</sup> (Supplementary Information).

Ribs are not found everywhere despite the grounding line having retreated through the study area. We suggest that low angle bed and ice slopes (that is, low gradients in height above buoyancy) are essential for the ribs to form. This configuration favours rapid migration of the grounding line, and low topographic variability allows ridges with a ‘pure’ tidal signal to be deposited sequentially. Regions of low-gradient ice surface and bed are ice plains; weakly grounded regions of ice streams immediately upstream of their grounding lines with low basal shear stress and small elevations above buoyancy<sup>33</sup>. An important implication is that when Thwaites Glacier grounding line sits on such high points even small amounts of ice-shelf thinning could instigate phases of rapid retreat.

### Pulses of rapid retreat at Thwaites Glacier

A second major implication of the formation mechanism is that the spacing of the ribs enables reconstruction of the rate of grounding-line recession of Thwaites Glacier in the past. The average spacing of the rib series increases upstream from 5.8 m to 6.3 m (Fig. 4b, red line). Converted to retreat rate, this corresponds to an 8% increase with time. Over a 5.5 month period, Thwaites Glacier retreated across the bump at an accelerated rate: from 2.12 km per year to 2.3 km per year. It has been suggested<sup>9</sup> that retreat from Thwaites Glacier’s offshore pinning points, across the deep inner cavity to its present-day position, was probably rapid. Our results indicate that the rate of retreat from the bump was double the average estimated for the period 1996 to 2009, and about three times faster than a location immediately inland of the bump between 2011 and 2017 (0.6–0.8 km per year (ref. 7)). The majority of observations for Amundsen Sea glaciers covering the past 30 years have shown retreat rates to not exceed 1–2 km per year<sup>34</sup>. For example, the Smith/Kohler Glaciers retreated 35 km between 1992 and 2011 at an average rate of approximately 1.8 km per year<sup>2</sup>, while Smith Glacier West retreated at a rate of 2 km per year between 2016 and 2018<sup>34</sup>. These rates—lower than those recorded on the bump—underscore the exceptionally fast retreat phase uncovered by our data. One notable study at nearby Pope Glacier observed almost 4 km of grounding-line retreat over a period of just under 4 months in 2017<sup>34</sup>, equivalent to a retreat rate  $>11 \text{ km per year}$ . Taken together with our results, long-term retreat rates obtained by satellites or airborne geophysical missions (on the order of 0.35–1 km per year over decades<sup>7</sup>) and derived from the offshore geological record (approximately 0.01–0.2 km per year over millennia<sup>35</sup>) may, therefore, hide temporal variability in grounding-line behaviour, including rapid, punctuated retreat phases that exceed the typically documented upper bounds on the pace of West Antarctic Ice Sheet recession.

Fast retreat from flat-topped ridges may be a process that is already occurring in several places at Thwaites Glacier today<sup>9</sup>. In previous work, the process of sediment removal from offshore sea-bed highs was suggested to have made the Thwaites Ice Shelf more sensitive to thinning in the past by lowering sea-bed topography<sup>18</sup>. Our results show that, in addition to increasing bathymetric depth, the process of flattening sea-bed highs during grounding may have also increased the likelihood of rapid retreat at Thwaites Glacier by



promoting the development of ice plains at which rapid inland tidal migration of the grounding line occurred. Erosion from the tops of analogous highs on which the grounding line sits today may have broadened the modern grounding zone. In doing so, this process may expose wider regions of intermittently grounded ice to melting through delivery of oceanic heat through a narrow cavity, thereby increasing the sensitivity of Thwaites Glacier to tidal forcing (Fig. 5b). Coupled ice–ocean finite element models of Thwaites Glacier have highlighted that wider grounding zones are more susceptible to faster rates of retreat<sup>16</sup>. Thus, we suggest that bed modification by erosion at the base of streaming ice may have pre-conditioned Thwaites Glacier to rapid recession. Moreover, in the presence of relatively unchanging external forcing (that is, persistent basal melting), non-linear phases of fast retreat can be expected as a result of fundamental grounding-zone processes.

Establishing the timing of retreat across the bump and, as a consequence, the age of the ribs on its surface remains to be resolved by direct sampling. The ice shelf was intact above the bump until the past decade<sup>11</sup>, and as recently as 1992 and 2011, TGT was ephemerally in contact with a pinning point, at shallow depths of approximately 300 m<sup>2</sup>. In airborne radar data from 1978, the grounding line was already situated southward of the bump<sup>36</sup>. Assuming current retreat rates of 0.8 km per year persisted back through time, and a monotonic retreat from the bump to the present-day grounding line, the ribs almost certainly pre-date the 1950s, and may be several centuries old if a slower average rate of retreat is invoked (for example, they would be approximately 180 years old, if the retreat rate was 0.3 km per year<sup>7</sup>).

Irrespective of the exact age of the landforms, the results shown here form a direct analogue for the glacier's current grounding zone, which is situated on elevated sea-floor ridges at similar water depths to the bump. Our landform evidence showing rapid retreat from a sea-bed ridge adjacent to the ice shelf suggests that major changes in flow dynamics could be initiated within months should the grounding line start to detach from high points in the sub-ice landscape.

The data described in this paper are unique in several aspects. They provide a rare example where the influence of tides is clear and has left imprints on the sea bed. The rates of retreat inferred from the landforms resolve daily grounding line motion for a key West Antarctic ice stream over nearly half a year, from a time period in which observations were not possible. We show one of probably many pulses of rapid retreat that characterized Thwaites Glacier's inland migration where the ice lost contact with topographic stabilizing highs. Rapid thinning and retreat will shorten the recurrence interval between such events, and in the context of recent observations, thinning and progressive grounding-line retreat at Thwaites Glacier increases the probability of such a pulse occurring in coming decades. The challenge for models predicting ice-sheet evolution is to now replicate the precise sequence of grounding-line movements across the bump, and to include processes of tidal migration and ice-plain formation in their physics. By evaluating models against our new high-resolution palaeo-data, it will be possible to gain a better understanding of Thwaites Glacier's ongoing retreat trajectory and its contributions to sea-level rise, which could threaten coastal communities and ecosystems in the next few human lifetimes.

### Online content

Any methods, additional references, Nature Research reporting summaries, source data, extended data, supplementary information, acknowledgements, peer review information; details of author contributions and competing interests; and statements of data and code availability are available at <https://doi.org/10.1038/s41561-022-01019-9>.

Received: 4 August 2021; Accepted: 27 July 2022;  
Published online: 5 September 2022

### References

- Joughin, I., Smith, B. E. & Medley, B. Marine ice sheet collapse potentially under way for the Thwaites Glacier Basin, West Antarctica. *Science* **344**, 735–738 (2014).
- Rignot, E., Mouginot, J., Morlighem, M., Seroussi, H. & Scheuchl, B. Widespread, rapid grounding line retreat of Pine Island, Thwaites, Smith, and Kohler glaciers, West Antarctica, from 1992 to 2011. *Geophys. Res. Lett.* **41**, 3502–3509 (2014).
- Sutterley, T. C. *et al.* Mass loss of the Amundsen Sea Embayment of West Antarctica from four independent techniques. *Geophys. Res. Lett.* **41**, 8421–8428 (2014).
- Holt, J. W. *et al.* New boundary conditions for the West Antarctic Ice Sheet: subglacial topography of the Thwaites and Smith glacier catchments. *Geophys. Res. Lett.* **33**, L09502 (2006).
- Pritchard, H. D. *et al.* Antarctic ice-sheet loss driven by basal melting of ice shelves. *Nature* **484**, 502–505 (2012).
- Shepherd, A., Wingham, D. & Rignot, E. Warm ocean is eroding West Antarctic Ice Sheet. *Geophys. Res. Lett.* **31**, L23402 (2004).
- Milillo, P. *et al.* Heterogeneous retreat and ice melt of Thwaites Glacier, West Antarctica. *Sci. Adv.* **5**, eaau3433 (2019).
- Wild, C. T. *et al.* Weakening of the pinning point buttressing Thwaites Glacier, West Antarctica. *Cryosphere* **16**, 397–417 (2022).
- Tinto, K. J. & Bell, R. E. Progressive unpinning of Thwaites Glacier from newly identified offshore ridge: constraints from aerogravity. *Geophys. Res. Lett.* **38**, L20503 (2011).
- Mouginot, J., Rignot, E. & Scheuchl, B. Sustained increase in ice discharge from the Amundsen Sea Embayment, West Antarctica, from 1973 to 2013. *Geophys. Res. Lett.* **41**, 1576–1584 (2014).
- Miles, B. W. J. *et al.* Intermittent structural weakening and acceleration of the Thwaites Glacier Tongue between 2000 and 2018. *J. Glaciol.* **66**, 485–495 (2020).
- Alley, K. E. *et al.* Two decades of dynamic change and progressive destabilization on the Thwaites Eastern Ice Shelf. *Cryosphere* **15**, 5187–5203 (2021).
- Alley, R. B., Anandakrishnan, S., Dupont, T. K., Parizek, B. R. & Pollard, D. Effect of sedimentation on ice-sheet grounding-line stability. *Science* **315**, 1838–1841 (2007).
- Jamieson, S. S. R. *et al.* Understanding controls on rapid ice-stream retreat during the last deglaciation of Marguerite Bay, Antarctica, using a numerical model. *J. Geophys. Res. Earth Surf.* **119**, 247–263 (2014).
- Yu, H., Rignot, E., Seroussi, H. & Morlighem, M. Retreat of Thwaites Glacier, West Antarctica, over the next 100 years using various ice flow models, ice shelf melt scenarios and basal friction laws. *Cryosphere* **12**, 3861–3876 (2018).
- Parizek, B. R. *et al.* Dynamic (in)stability of Thwaites Glacier, West Antarctica. *J. Geophys. Res. Earth Surf.* **118**, 638–655 (2013).
- Bevan, S. L., Luckman, A. J., Benn, D. I., Adusumilli, S. & Crawford, A. Brief communication: Thwaites Glacier cavity evolution. *Cryosphere* **15**, 3317–3328 (2021).
- Hogan, K. A. *et al.* Revealing the former bed of Thwaites Glacier using sea-floor bathymetry. *Cryosphere* **14**, 2883–2908 (2020).
- Jenkins, A. *et al.* West Antarctic Ice Sheet retreat in the Amundsen Sea driven by decadal oceanic variability. *Nat. Geosci.* **11**, 733–738 (2018).
- Hillenbrand, C. D. *et al.* Grounding-line retreat of the West Antarctic Ice Sheet from inner Pine Island Bay. *Geology* **41**, 35–38 (2013).
- Dowdeswell, J. *et al.* Delicate seafloor landforms reveal past Antarctic grounding-line retreat of kilometers per year. *Science* **68**, 1020–1024 (2020).
- Mackintosh, A. *et al.* Retreat of the East Antarctic ice sheet during the last glacial termination. *Nat. Geosci.* **4**, 195–202 (2011).
- Friedl, P., Weiser, F., Fluhrer, A. & Braun, M. H. Remote sensing of glacier and ice sheet grounding lines: a review. *Earth Sci. Rev.* **201**, 102948 (2020).
- Dowdeswell, J. A. & Bamber, J. L. Keel depths of modern Antarctic icebergs and implications for sea-floor scouring in the geological record. *Mar. Geol.* **243**, 120–131 (2007).
- Wählin, A. K. *et al.* Pathways and modification of warm water flowing beneath Thwaites Ice Shelf, West Antarctica. *Sci. Adv.* **7**, eabd7524 (2021).
- Dowdeswell, J. A., Ottesen, D., Evans, J., Cofaigh, C. Ó. & Anderson, J. B. Submarine glacial landforms and rates of ice-stream collapse. *Geology* **36**, 819–822 (2008).
- Padman, L., Siegfried, M. R. & Fricker, H. A. Ocean tide influences on the Antarctic and Greenland Ice Sheets. *Rev. Geophys.* **56**, 142–184 (2018).
- Egbert, G. D., Erofeeva, S. Y., Egbert, G. D. & Erofeeva, S. Y. Efficient inverse modeling of barotropic ocean tides. *J. Atmos. Ocean. Technol.* **19**, 183–204 (2002).
- Padman, L., Erofeeva, S. Y. & Fricker, H. A. Improving Antarctic tide models by assimilation of ICESat laser altimetry over ice shelves. *Geophys. Res. Lett.* **35**, L22504 (2008).
- Jakobsson, M. *et al.* Geological record of ice shelf break-up and grounding line retreat, Pine Island Bay, West Antarctica. *Geology* **39**, 691–694 (2011).



31. Batchelor, C. L. et al. New insights into the formation of submarine glacial landforms from high-resolution autonomous underwater vehicle data. *Geomorphology* **370**, 107396 (2020).
32. Galton-Fenzi, B. K., Hunter, J. R., Coleman, R., Marsland, S. J. & Warner, R. C. Modeling the basal melting and marine ice accretion of the Amery Ice Shelf. *J. Geophys. Res. Oceans* **117**, 9031 (2012).
33. Bindschadler, R., Vornberger, P. & Gray, L. Changes in the ice plain of Whillans Ice Stream, West Antarctica. *J. Glaciol.* **51**, 620–636 (2005).
34. Milillo, P. et al. Rapid glacier retreat rates observed in West Antarctica. *Nat. Geosci.* **15**, 48–53 (2022).
35. Smith, J. A. et al. New constraints on the timing of West Antarctic Ice Sheet retreat in the eastern Amundsen Sea since the Last Glacial Maximum. *Glob. Planet. Change* **122**, 224–237 (2014).
36. Schroeder, D. M. et al. Multidecadal observations of the Antarctic ice sheet from restored analog radar records. *Proc. Natl Acad. Sci. USA* **116**, 18867–18873 (2019).
37. Jordan, T. et al. New gravity-derived bathymetry for the Thwaites, Crosson and Dotson ice shelves revealing two ice shelf populations. *Cryosphere* **14**, 2869–2882 (2020).

**Publisher's note** Springer Nature remains neutral with regard to jurisdictional claims in published maps and institutional affiliations.



**Open Access** This article is licensed under a Creative Commons Attribution 4.0 International License, which permits use, sharing, adaptation, distribution and reproduction in any medium or format, as long as you give appropriate credit to the original author(s) and the source, provide a link to the Creative Commons license, and indicate if changes were made. The images or other third party material in this article are included in the article's Creative Commons license, unless indicated otherwise in a credit line to the material. If material is not included in the article's Creative Commons license and your intended use is not permitted by statutory regulation or exceeds the permitted use, you will need to obtain permission directly from the copyright holder. To view a copy of this license, visit <http://creativecommons.org/licenses/by/4.0/>.

© The Author(s) 2022

## Methods

**Data acquisition and processing.** Cruise NBP19-02 took place between January and March 2019 on the United States Antarctic Program icebreaking vessel RV *Nathaniel B. Palmer* as part of the wider National Science Foundation–Natural Environment Research Council funded International Thwaites Glacier Collaboration involving UK, US and multi-national affiliates. Onboard, we collected underway multibeam swath bathymetry, sub-bottom profiler data and recovered marine sediment cores to improve our understanding of Thwaites Glacier history. For this paper, we focus on datasets collected by the deployment of a 6,000-m-depth-rated free-swimming Kongsberg HUGIN AUV. The AUV, operated by the Swedish Research Council and maintained by the University of Gothenburg, was trialled and underwent first deployments in polar waters during the cruise. ‘Ran’ is equipped with a variety of oceanographic sensors, as well as a full suite of geophysical instrumentation. Here we show data collected using an AUV-mounted single-head Kongsberg EM2040 multibeam echo-sounder and a dual-frequency Edgetech 2205 sidescan sonar. Both sonars enabled the collection of high-resolution images of the sea bed at a resolution unrivalled for shelf regions around the West Antarctic Ice Sheet.

AUV mission 009 deployed the HUGIN at 75° 04.21′ S, 106° 58.89′ W, at 22:07h on 28 February 2019. Recovery occurred at 15:33h on 1 March 2019 at 75° 05.409′ S, 107° 10.925′ W. The total mission time was 17h 26min. Navigation was achieved by coupling an onboard INS (inertial navigation system consisting of accelerometers and gyros) with two 12kHz Universal Transponder Positioning (UTP; cNODES) units deployed at known locations that served as call and response range-positioning for the vehicle. In addition, the vehicle operated using a Doppler velocity log whereby it tracked the sea floor or sea surface via dead reckoning. Acquisition heights varied during the survey between 50 m and 95 m. Processing of navigation data was undertaken onboard in Kongsberg proprietary NavLab software. However, owing to noise from the first UTP station, the filtered navigation required further processing subsequent to the cruise by Kongsberg engineers in Norway.

Processing of the AUV multibeam swath bathymetry data using a first-pass cleaned navigation was undertaken in MB system while onboard the *Palmer*. The steps involved (1) extraction of navigational and attitude data, (2) bathymetry data conversion, (3) ping editing to remove spurious soundings and (4) gridding. Because of the varied flying height, an onboard gridded dataset was produced at a conservative 1.5 m grid cell size, which formed the basis of most bathymetric analysis in this paper. We gridded using a Gaussian-weighted mean algorithm in the mbgrid program, adopting a spline interpolation to fill grid cells not filled by swath data for gaps up to six grid cells in size. The grid was exported in an ESRI ASCII format for manipulation in a geographic information system. The 1.5 m grid was used for the majority of observations made in our analyses.

Post-processing of the AUV data by Kongsberg technicians removed noise problems associated with the first of the two UTPs that hampered processing of the vehicle’s navigation onboard. In post-processing, we removed fixes from the first UTP entirely. Consequently, for the start of the mission, the AUV ran on dead reckoning with GPS fix until the second UTP was encountered after which navigation was determined by UTP-INS. A cleaned and filtered real-time navigation using a best-fit solution was output via NavLab. Loops (avoidance turns) in the vehicle track, of which there were several, were removed, and a static shift of 95 m at 130° was applied. A second grid with improved resolution of 0.7 m was produced for subsequent visualization and verification of our analyses from the coarser, 1.5 m gridded dataset.

Images of the sea floor acquired by the AUV’s sidescan sonar were replayed and exported using Kongsberg reflection post-acquisition visualization software, isolating the high-frequency channel (400 kHz). Each image was slant-range corrected and processed with a pixel size of 0.05 × 0.05 m.

**Geomorphological mapping of landforms.** Glacial landforms were mapped from the gridded multibeam datasets in a geographic information system using associated hillshade surfaces and corresponding sidescan sonar imagery for guidance. All mapping was undertaken at horizontal scales between 1:500 and 1:5,000. We used the original 1.5 m multibeam grid for the majority of feature mapping but updated the map with subsequent mapping work in selected areas using digitized landforms from the later post-processed 70 cm grid. Any updates to the map at this second stage were geo-located to be consistent with the original mapping using an XY shift. As the landform map was generated before secondary post-processing of the AUV data, it should be noted that the completed map has a small XY offset of approximately 95 m at 130°. However, the data as a whole are internally consistent, meaning the interpretations and subsequent geometric analysis of the ribs are not subject to any appreciable change. Landforms were classified by geometry, independent of their genetic interpretation following best practices described in a variety of glacial geomorphological literature. Extended descriptions of the landforms and their genetic classification are included in Supplementary Section A2.

To extract landform statistics from the bathymetric data, we employed a semi-automated picking approach. Profiles were extracted from the bathymetry along the sets of ribs of interest, sampled at a horizontal resolution of 10 cm. The extracted long profiles were detrended and mean-adjusted by removing a

least-squares regression from the profile. Subsequently, the data were filtered by subtracting a 100-point adjacent averaging smooth of the detrended data, which served to remove long-wavelength features in the bathymetry profile while retaining the finer details and geometry of smaller-scale landforms of interest. From the filtered and detrended data, a manual baseline was digitized that assigned nodes to the troughs between ribs and interpolated between them. We subtracted the baseline from the data so that the ribs in series were levelled to a zero horizon. A peak analysis tool was then used to identify rib crests in the processed profiles from which height from baseline (amplitude) and peak-to-peak spacing were automatically derived.

**Tidal model.** To investigate the potential role of tides in forming sea-floor landforms, we extracted predicted tidal amplitudes from a tidal model of the global ocean for a location seaward of the Thwaites Glacier front (108° W, 74° S). This was carried out to provide a handle on the expected modern-day tidal amplitudes at the ice-shelf margin and to establish the dominant tidal constituents driving ice-shelf and grounding-line flexure on both short and long timescales. We used the Oregon State University TPXO-9 Global Tidal Model for analysis<sup>38</sup>. The model includes complex amplitudes of relative sea-surface elevations for eight primary (M2, S2, N2, K2, K1, O1, P1 and Q1), two long-period (Mf and Mm) and five non-linear (M4, MS4, MN4, 2N2 and S1) harmonic constituents.

The time window chosen for comparison covered the period 22 March 2020 to 4 September 2020 and was sampled at hourly intervals encompassing nearly 12 spring–neap cycles (166 days on plotted axis in Fig. 4). The dates selected for the tidal record comparison began at the end of the austral summer, and were forecast through to the end of the following austral spring. The late March start date for the time series reflects an attempt to correlate the landform record with a time period in which West Antarctica is generally at its warmest, and sea ice is at a minimum in the Amundsen Sea. Although investigations of the seasonal variability in the properties of CDW in the easternmost Amundsen Sea embayment generally indicate a thicker and slightly warmer deep water layer during winter<sup>38</sup>, we view the end of summer as the most likely time interval in which rapid ice sheet retreat events might be triggered. Modelling studies indicate that the largest southward transport of heat and the thickest CDW layer peaks in the March–May period. For guiding our choice, other rapid changes in Antarctic glaciers have typically been observed to have initiated in the late summer period: for example, the Larsen A Ice Shelf disintegrated in January 1995, while Larsen B collapsed during the period 31 January to March 2002, and Wilkins Ice Shelf underwent partial collapse through February and March of 2008. Whereas collapses of the Antarctic Peninsula ice shelves have mainly been triggered by surface melting and hydrofracture as a result of atmospheric warmth, changes at Thwaites Glacier are likely to be ocean or sea-level instigated. Although there is no explicit link between the timing of major calving events and grounding-zone retreat, we note observations of major changes in Thwaites Glacier in March of previous years: Thwaites had a partial outburst of its western mélange in the period immediately following our AUV survey in early March 2019, while the large iceberg B-22 previously calved from the Thwaites Ice Tongue in mid-March 2002.

**Analysis of rib landforms.** The periodograms in Fig. 4 of the main manuscript investigate the dominant periods (frequencies) in the series of ribs compared with the frequency content of the tidal series. The dominant frequencies describe important periodicities in the data. The periodograms were produced using a fast Fourier transform implemented in OriginLab. Frequency corresponds to cycles per unit of time. In this case, the unit of time was set to 1 calendar day so that periods equate to 1/peak frequency. For the tidal model, we filtered the hourly modelled tidal amplitude outputs from the TPXO-9 model using a 24-point percentile filter with a percentile value set at 99 (Supplementary Fig. 13). This corresponded to replacing the signal point with the 99th percentile value of the data points in the moving data window. The resultant filtered dataset removes the 24, 12 and 6 h tidal periodicities that dominate the full-resolution tidal dataset (Supplementary Fig. 13b), preserving and tracking closely the daily peak tidal height. We compared this approach with a method that decimated the data to a single time per day. Both achieve similar results in emphasizing the dominance of a fortnightly spring–neap cyclicity in the daily tidal values.

For the ribs, we analysed the dominant frequencies in the amplitude data as a series. Since the amplitude data are already detrended and extracted from the initial topography, they represent an appropriate way of investigating periods in the data. However, periodograms of the filtered and mean-adjusted topography produce results with no discernible differences. In each FFT (Fast Fourier Transform) analysis, we carried out the routine using a Hanning window and display the amplitude as a function of frequency.

## Data availability

All data needed to evaluate the conclusions in the paper are present in the paper and/or Supplementary Information. A high-resolution multibeam raster grid from AUV mission 009, on which the majority of the analyses in this paper were based, is available for download from the PANGAEA database (<https://pangaea.de>) and figshare (<https://doi.org/10.6084/m9.figshare.6025748.v1>).

## References

38. Heywood, K. et al. Between the devil and the deep blue sea: the role of the Amundsen Sea continental shelf in exchanges between ocean and ice shelves. *Oceanography* **29**, 118–129 (2016).

## Acknowledgements

We thank the captain, officers, support staff and science party of the RV *Nathaniel B. Palmer* for their valuable contributions to cruise NBP19-02. J. Andersson and J. Rolandsson, and MMT, are thanked for their technical expertise and vital support with AUV operations. C. Wallace and Kongsberg Maritime are thanked for technical assistance in post-processing AUV navigation and multibeam data. This work was supported by grants NE/S006206/1 (A.G.), NE/S006641/1 (R.D.L., C.-D.H., J.A.S. and K.A.H.), and NE/S006419/1 (K.J.H.) from the Natural Environment Research Council, by grant 1738942 (J.S.W., F.O.N., R.L.T., L.M.S. and J.B.A.) from NSF, Office of Polar Programs, and by grant 2017-04257 (A.W.) from Vetenskapsrådet, as well as funding from the SSF project SMARC (A.W.). ITGC Contribution No. ITGC-079.

## Author contributions

Conceptualization: A.G.C.G., A.W. and R.D.L. Field investigation: A.G.C.G., A.W., K.A.H., R.D.L. and R.L.T. Methodology, processing and analysis: A.G.C.G., A.W., K.A.H.

and R.D.L. Visualization: A.G.C.G. Writing—original draft: A.G.C.G., A.W., K.A.H. and R.D.L. Writing—review and editing: F.O.N., K.J.H., R.L.T., J.A.S., C.-D.H., L.M.S., J.B.A. and J.S.W. Funding acquisition: all authors.

## Competing interests

The authors declare no competing interests.

## Additional information

**Supplementary information** The online version contains supplementary material available at <https://doi.org/10.1038/s41561-022-01019-9>.

**Correspondence and requests for materials** should be addressed to Alastair G. C. Graham.

**Peer review information** *Nature Geoscience* thanks Andrew Mackintosh, Kiya Riverman and the other, anonymous, reviewer(s) for their contribution to the peer review of this work. Primary Handling Editor Tom Richardson, in collaboration with the Nature Geoscience team.

**Reprints and permissions information** is available at [www.nature.com/reprints](http://www.nature.com/reprints).

Seafloor images explain Thwaites Glacier retreat.

British Antarctic Survey

# Seafloor images explain Thwaites Glacier retreat

5 September, 2022 News stories

New high resolution images of the the seafloor in West Antarctica show past retreat of Thwaites Glacier. They reveal that at times in its past, retreat of the massive Thwaites Glacier was even quicker than it is today, heightening concerns for its future. The results are published today (Monday 5 September) in the journal Nature Geoscience.

The Thwaites Glacier in West Antarctica – about the size of the UK or Florida – has been an elephant in the room for scientists trying to make global sea level rise predictions. This massive ice shelf is already in a phase of fast retreat (a “collapse” when viewed on geological timescales) leading to widespread concern about exactly how much, or how fast, it may give up its ice to the ocean. The potential impact of Thwaites’ retreat could be up to 65 cms of global sea-level rise.

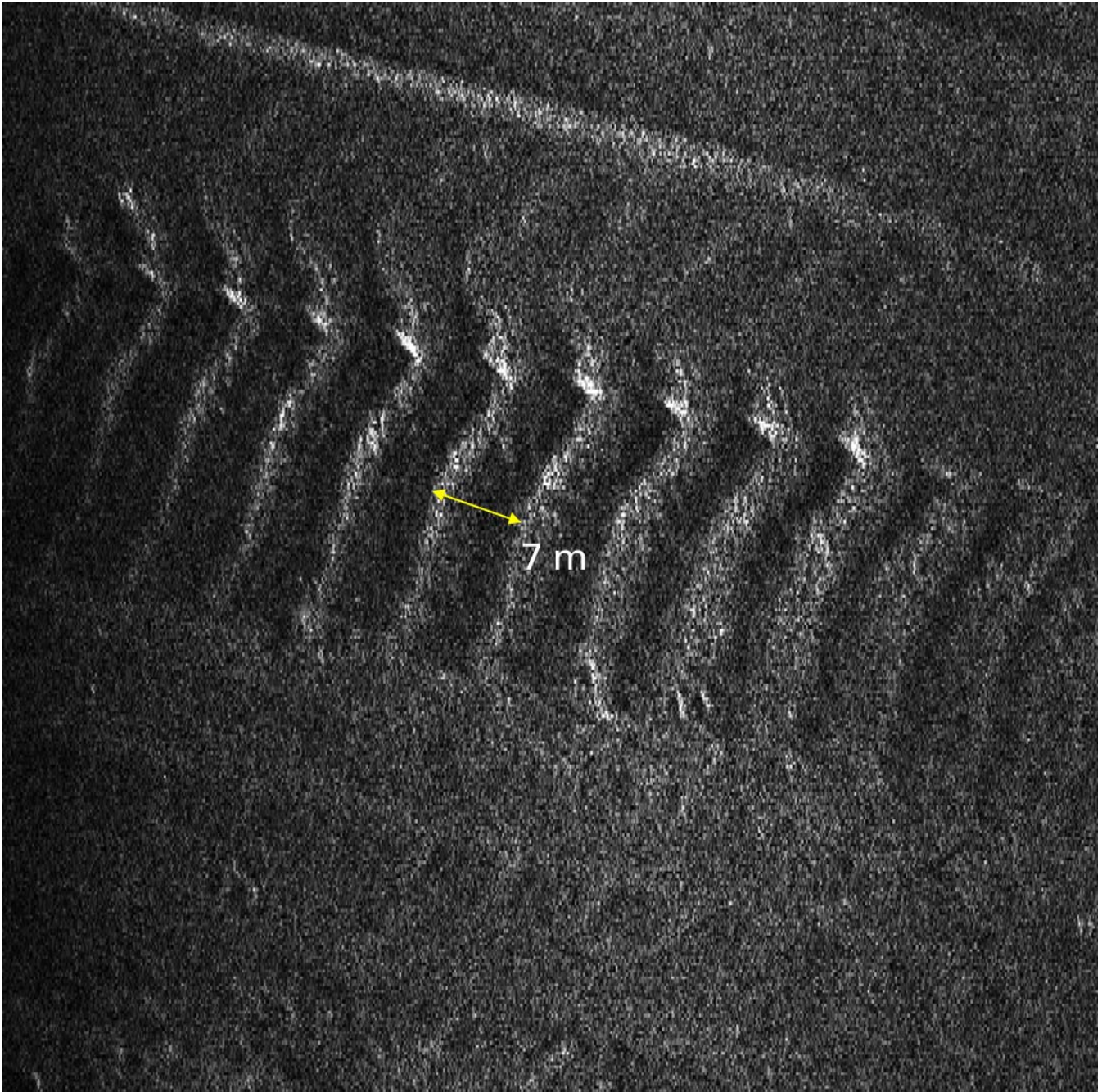


The underwater robot Ran operated at the ice front of Thwaites Glacier from the RV Nathaniel B Palmer. Photo credit\_Ali Graham.



For the first time, scientists mapped in high-resolution a critical area of the seafloor in front of the glacier that gives them a window into how fast Thwaites retreated in the past. The stunning imagery shows geologic features that are new to science, and also provides a kind of crystal ball to see into Thwaites' future.

The team documented more than 160 parallel ridges that were created, like a footprint, as the glacier's leading edge retreated and bobbed up and down with the daily tides.



A side scan shows the ridges detected by Ran. Image credit\_Ali Graham.

“It’s as if you are looking at a tide gauge on the seafloor,” says lead author Dr Ali Graham from Florida University. “It really blows my mind how beautiful the data are.”

Beauty aside, what’s alarming is that the rate of Thwaites’ retreat that scientists have documented more recently are small compared to the fastest rates of change in its past, said Graham.

To understand Thwaites’ past retreat, the team analysed the rib-like formations submerged 700 meters (just under half a mile) beneath the polar ocean. They factored in the tidal cycle for the region, as predicted by computer models, to show that one ‘rib’ must have been formed every single day.

At some point in the last 200 years, over a duration of less than six months, the front of the glacier lost contact with a seabed ridge and retreated at a rate of more than 2.1 kilometres per year (1.3 miles per year) — twice the rate documented using satellites between 2011 and 2019.

Graham continues:

“Our results suggest that pulses of very rapid retreat have occurred at Thwaites Glacier in the last two centuries, and possibly as recently as the mid-20<sup>th</sup> Century.”

Marine geophysicist and study co-author, Dr Robert Larter, from British Antarctic Survey, says:

“Thwaites is really holding on today by its fingernails, and we should expect to see big changes over small timescales in the future – even from one year to the next – once the glacier retreats beyond a shallow ridge in its bed.”



Rob Larter from BAS (left) with lead author Ali Graham at the ice front of Thwaites Glacier in 2019.

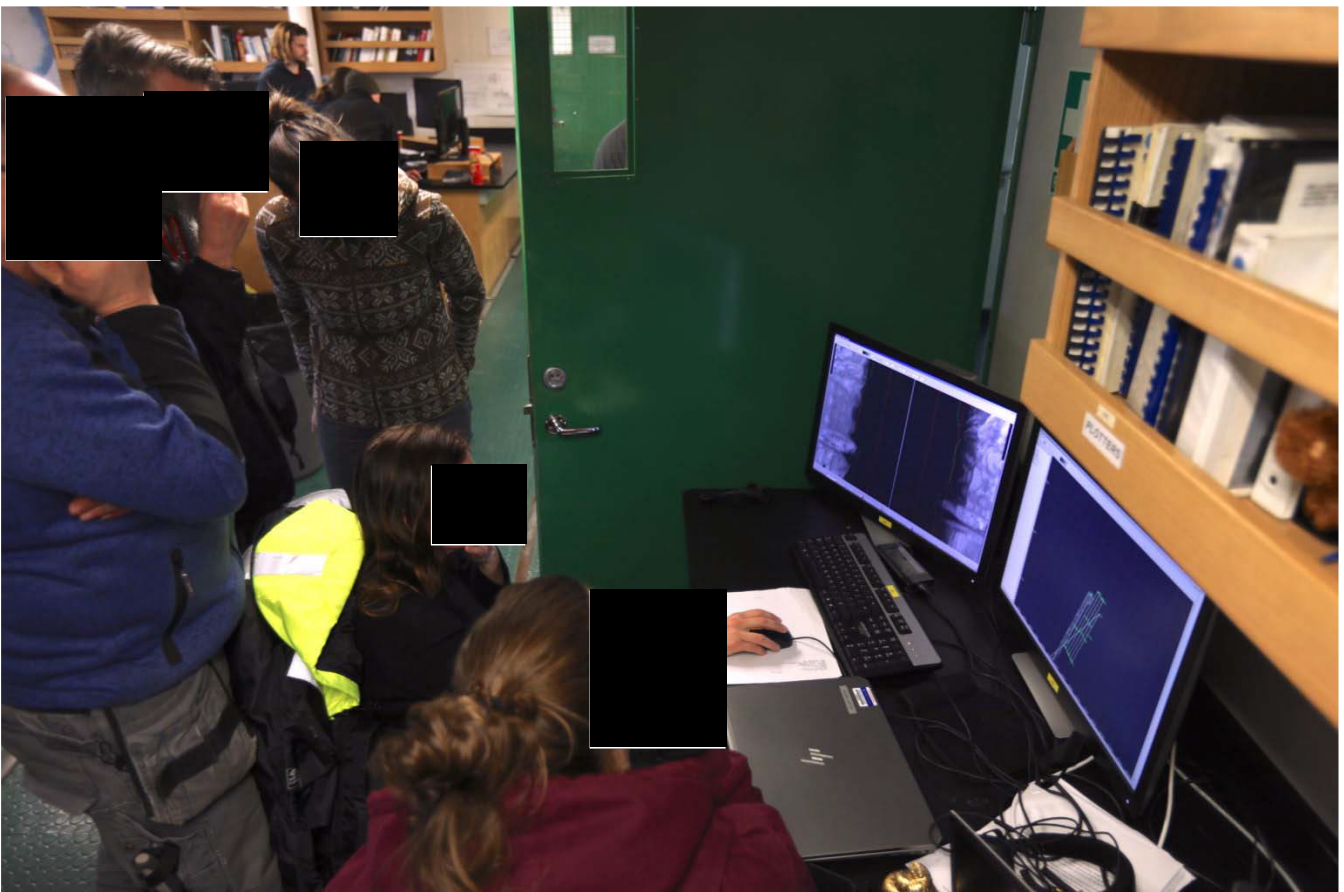
To collect the imagery and supporting geophysical data, the team, which included scientists from the United States, the United Kingdom, and Sweden, launched 'Rán', a state-of-the-art orange robotic vehicle loaded with imaging sensors, from the *R/V Nathaniel B. Palmer* during an expedition in 2019. Rán, operated by scientists at the University of Gothenburg in Sweden, embarked on a 20-hour mission that was as risky as it was serendipitous, Graham said. It mapped an area of the seabed in front of the glacier about the size of Houston, during an unusual summer notable for its lack of sea ice, allowing the team to access the glacier front for the first time in history.



Anna Wåhlin, a physical oceanographer from the University of Gothenburg who deployed Rán at Thwaites, says:

“This was a pioneering study of the ocean floor, made possible by recent technological advancements in autonomous ocean mapping and a bold decision by the Wallenberg Foundation to invest into this research infrastructure. The images Rán collected give us vital insights into the processes happening at the critical junction between the glacier and the ocean today.”

“It was truly a once in a lifetime mission,” said Graham, who said the team would like to sample the seabed sediments directly so they can more accurately date the ridge-like features. “But the ice closed in on us pretty quickly and we had to leave before we could do that on this expedition,” he said.



Scientists on the RV Nathaniel B Palmer analyse the side view of scans collected by Rán. Photo credit\_Ali Graham.

While many questions remain, one thing's for sure: it used to be that scientists thought of the Antarctic ice sheets as sluggish and slow to respond, but that's simply not true, said Graham.

"Just a small kick to Thwaites could lead to a big response," he said.

According to the United Nations, roughly 40 percent of the human population lives within 60 miles of the coast. "This study is part of a cross-disciplinary collective effort to understand the Thwaites Glacier system better," said Tom Frazer, dean of the College of Marine Science, University of South Florida, "and just because it's out of sight, we can't have Thwaites out of mind. This study is an important step forward in providing essential information to inform global planning efforts."

The study was supported by the National Science Foundation and the UK Natural Environment Research Council through the International Thwaites Glacier Collaboration (ITGC). The 2019 expedition was the first in a 5-year project dubbed THOR, which stands for Thwaites Offshore Research, and also included team members from a sister project called the Thwaites-Amundsen Regional Survey and Network Integrating Atmosphere-Ice-Ocean Processes, or TARSAN.

For more information, read this companion story authored by Graham and the team.

*Rapid retreat of Thwaites Glacier in the pre-satellite era* by Alastair G.C. Graham<sup>1\*</sup>, Anna Wåhlin<sup>2</sup>, Kelly A. Hogan<sup>3</sup>, Frank O. Nitsche<sup>4</sup>, Karen J. Heywood<sup>5</sup>, Rebecca L. Totten<sup>6</sup>, James A. Smith<sup>3</sup>, Claus-Dieter Hillenbrand<sup>3</sup>, Lauren M. Simkins<sup>7</sup>, John B. Anderson<sup>8</sup>, Julia S. Wellner<sup>9</sup>, Robert D. Larter<sup>3</sup>.

Scientists expose vulnerabilities of critical Antarctic ice shelf.

British Antarctic Survey

# Scientists expose vulnerabilities of critical Antarctic ice shelf

21 September, 2022 Press releases

Pine Island Ice Shelf in West Antarctica, which holds back enough ice to raise sea levels by 0.5 metres, could be more vulnerable to complete disintegration than previously thought. A new study led by British Antarctic Survey (BAS) scientists shows two processes, whose recent enhancement already threatens the stability of the shelf can interact to increase the likelihood of collapse.

This large ice shelf (the section of the glacier that floats on the sea) controls the flow of ice from Pine Island Glacier, roughly the size of England, into the Amundsen Sea. This is a crucial role as the glacier is one of the world's largest and fastest changing and is responsible for approximately 25% of ice loss from Antarctica. This equivalent to the amount of water in 13,000 Olympic swimming pools.



The present day ice front of Pine Island Glacier, which stands approximately 50-60 metres above the

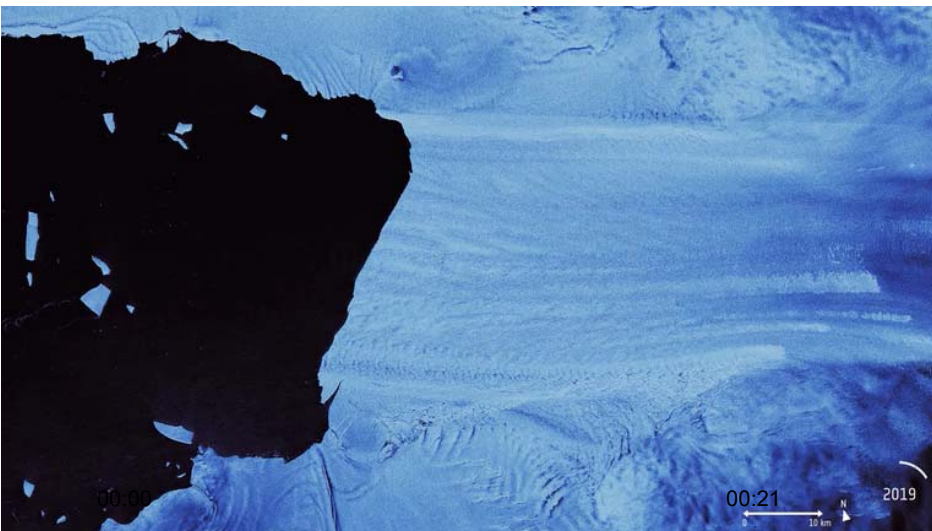
water. Photo credit: Robert Larter.

Scientists have previously observed that Pine Island Ice Shelf is becoming increasingly fragile due to two processes: enhanced thinning, as a result of an increase in ice shelf melting into the sea, and an increase in calving events in which masses of ice break off into icebergs.

Now, a team of researchers has shown that the combination of calving and melting will likely make an even greater contribution to melting of Pine Island Ice Shelf than was assumed.

Dr Alex Bradley, an ocean modeller at BAS and lead author on the study, says:

“This study highlights the extreme sensitivity of ice shelves to climate change. It shows the interplay between calving and melting can promote disintegration of the Pine Island Ice Shelf, which we already thought was vulnerable to collapse.”

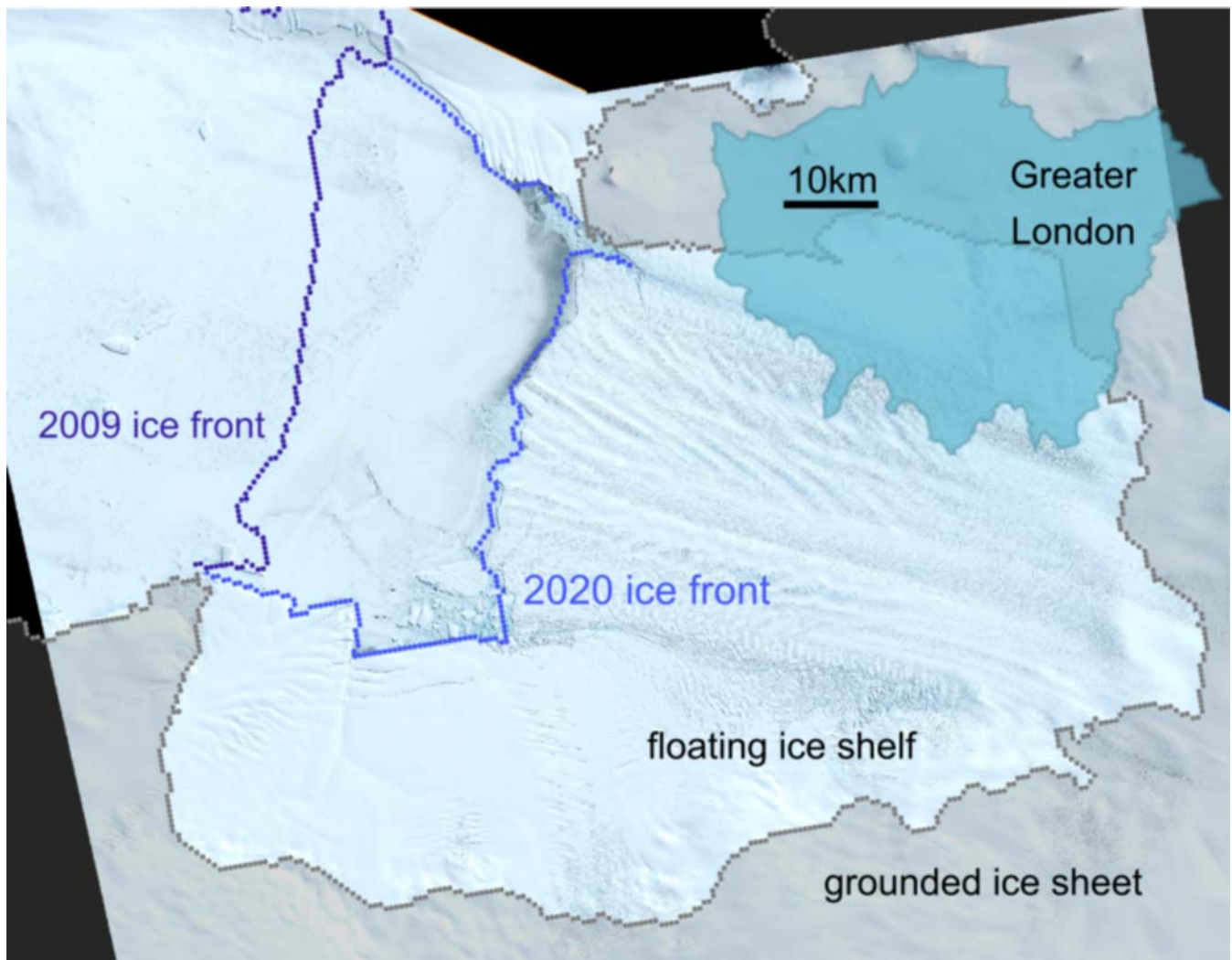


[Animation credit ESA (distributed under CC BY-SA 3.0 IGO)]

The team used advanced ocean modelling techniques to simulate the effects of continued calving events to see how this would impact melt rate. Their simulations show that calving events could result in further thinning of the ice shelf, which will in turn make the ice shelf more vulnerable to calving. This suggests that a feedback loop between the two processes could exist and expedite the complete disintegration of the ice shelf. This would reduce its ability to stem the flow of ice from Pine Island Glacier into the sea and increase its contribution to global sea-level rise.



Bradley continues: "Complete disintegration of the Pine Island Ice Shelf will have profound consequences not only for the glacier but all of West Antarctica as it is thought to play an integral role in maintaining the stability of the West Antarctic Ice Sheet."



Graphic shows how the ice front of the Pine Island Glacier ice front has retreated.

In a warming climate, calving events are likely to become more frequent and so this study further signals the urgent need to reduce emissions and mitigate the worst effects of climate change.

**The influence of Pine Island Ice Shelf calving on basal melting** by Alex Bradley, David Bett, Pierre Dutrioux, Jan de Rydt and Paul Holland is published in the *Journal of Geophysical Research: Oceans*.

Sea Level Rise: Implications for International Peace and Security.

UN Secretary General





**United  
Nations**

**Secretary-  
General**

**New York**

**14 February 2023**

## **Secretary-General's remarks to the Security Council Debate on "Sea-level Rise: Implications for International Peace and Security"**

**[Bilingual, as delivered; scroll further down for all-English]**

Mr. President, Dr. Ian Borg, Minister for Foreign and European Affairs and Trade of Malta, Excellencies,

I thank the government of Malta for shining a light on the dramatic implications of rising sea levels on global peace and security.

Rising seas are sinking futures.

Sea-level rise is not only a threat in itself.

It is a threat-multiplier.

For the hundreds of millions of people living in small island developing states and other low-lying coastal areas around the world, sea-level rise is a torrent of trouble.

Rising seas threaten lives, and jeopardize access to water, food and healthcare.

Saltwater intrusion can decimate jobs and entire economies in key industries like agriculture, fisheries and tourism.

It can damage or destroy vital infrastructure – including transportation systems, hospitals and schools, especially when combined with extreme weather events linked to the climate crisis.

And rising seas threaten the very existence of some low-lying communities and even countries.

The World Meteorological Organization has just released a new compilation of data that spells out the grave danger of rising seas.

Global average sea levels have risen faster since 1900 than over any preceding century in the last 3,000 years.

The global ocean has warmed faster over the past century than at any time in the past 11,000 years.

Meanwhile, the WMO tells us that even if global heating is miraculously limited to 1.5 degrees, there will still be a sizeable sea level rise.

But every fraction of a degree counts. If temperatures rise by 2 degrees, that level rise could double, with further temperature increases bringing exponential sea level increases.

Under any scenario, countries like Bangladesh, China, India and the Netherlands are all at risk.

Mega-cities on every continent will face serious impacts including Lagos, Maputo, Bangkok, Dhaka, Jakarta, Mumbai, Shanghai, Copenhagen, London, Los Angeles, New York, Buenos Aires and Santiago.

The danger is especially acute for nearly 900 million people who live in coastal zones at low elevations – that's one out of ten people on earth.

Some coastlines have already seen triple the average rate of sea-level rise.

I have seen with my own eyes how people in Small Island Developing States in the Western Pacific are facing sea-rise levels up to four times the global average.

In the Caribbean, rising seas have contributed to the devastation of local livelihoods in the tourism and agriculture sectors.

Rising seas and other climate impacts are already forcing some relocations in Fiji, Vanuatu, the Solomon Islands and elsewhere.

Flooding and coastal erosion in West Africa are damaging infrastructure and communities, undermining farming and often costing lives.

In North Africa, saltwater intrusion is contaminating land and freshwater resources, destroying crops and livelihoods alike.

Somalia is also grappling with saltwater intrusion, contributing to competition over scarce freshwater resources.

And around the world, a hotter planet is melting glaciers and ice sheets.

According to NASA, Antarctica is losing an average of 150 billion tons of ice mass annually.

The Greenland ice cap is melting even faster – losing 270 billion tons per year.

And consider the hundreds of millions of people living in the river basins of the Himalayas.

We have already seen how Himalayan melts have worsened flooding in Pakistan.

But as these glaciers recede over the coming decades, over time, the Indus, Ganges and Brahmaputra rivers will shrink.

And rising sea levels combined with a deep intrusion of saltwater will make large parts of their huge deltas simply uninhabitable.

We see similar threats in the Mekong Delta and beyond.

The consequences of all of this are unthinkable.

Low-lying communities and entire countries could disappear forever.

We would witness a mass exodus of entire populations on a biblical scale.

And we would see ever-fiercer competition for fresh water, land and other resources.

So, Excellencies, the impact of rising seas is already creating new sources of instability and conflict.

We must meet this rising tide of insecurity with action across three areas.

First – we must address the root cause of rising seas, the climate crisis.

Our world is hurtling past the 1.5-degree warming limit that a livable future requires, and with present policies, is careening towards 2.8 degrees – a death sentence for vulnerable countries.

We urgently need more concerted action to reduce emissions and ensure climate justice.

Developing countries must have the resources to adapt and build resilience against climate disaster.

Among other things, this means delivering on the loss and damage fund, making good on the \$100-billion climate finance commitment to developing countries, doubling adaptation finance, and leveraging massive private financing at a reasonable cost.

Second – we must broaden our understanding of the root causes of insecurity.

That means identifying and addressing a much wider range of factors that undermine security – from poverty, discrimination and inequality, violations of human rights, to environmental disasters like rising sea levels.

That is why, for example, the Peacebuilding Fund is actively supporting grassroots resilience efforts against the effects of climate change.

We must also improve foresight and early warnings to prepare and protect vulnerable communities.

One prime example is our plan to ensure that early warning systems against natural disasters protect every person on earth within five years.

Troisièmement, nous devons aborder les conséquences de la montée des eaux sur les cadres juridiques et les droits humains.

L'élévation du niveau de la mer provoque – littéralement – un rétrécissement des masses terrestres, entraînant de possibles litiges liés à l'intégrité territoriale et aux espaces maritimes.

Le régime juridique actuel doit être tourné vers l'avenir et combler les lacunes des cadres existants.



Oui, cela inclut le droit international des réfugiés.

Mais il s'agit également de mettre en place des solutions juridiques et pratiques innovantes, pour faire face aux impacts de l'élévation du niveau de la mer sur les déplacements forcés de populations et sur l'existence même du territoire terrestre de certains États.

Les droits humains des personnes ne disparaissent pas lorsque leurs foyers disparaissent.

L'an dernier, la Commission du droit international a examiné cette question et exploré, pour y remédier, une série d'options qui consisteraient notamment à préserver le statut d'État malgré la perte de territoire, à céder ou à attribuer des portions de territoire à un État touché, voire à créer des confédérations d'États.

C'est essentiel de tenir ces débats pour trouver des solutions, et je salue les délégations de la Sixième Commission qui se penchent activement sur ces questions.

Nous devons continuer à œuvrer pour protéger les populations touchées et garantir leurs droits humains essentiels.

Le Conseil de sécurité a un rôle essentiel à jouer pour mobiliser la volonté politique nécessaire afin de relever les défis de sécurité dévastateurs que pose la montée des eaux.

Nous devons tous continuer de donner à cette question toute la visibilité qu'elle mérite, et à soutenir les vies, les moyens de subsistance et les communautés vivant en première ligne de cette crise.

Je vous remercie.

\*\*\*\*\*

**[all-English]**

Mr. President, Dr. Ian Borg, Minister for Foreign and European Affairs and Trade of Malta, Excellencies,

I thank the government of Malta for shining a light on the dramatic implications of rising sea levels on global peace and security.

Rising seas are sinking futures.

Sea-level rise is not only a threat in itself.

It is a threat-multiplier.

For the hundreds of millions of people living in small island developing states and other low-lying coastal areas around the world, sea-level rise is a torrent of trouble.

Rising seas threaten lives, and jeopardize access to water, food and healthcare.

Saltwater intrusion can decimate jobs and entire economies in key industries like agriculture, fisheries

and tourism.

It can damage or destroy vital infrastructure – including transportation systems, hospitals and schools, especially when combined with extreme weather events linked to the climate crisis.

And rising seas threaten the very existence of some low-lying communities and even countries.

The World Meteorological Organization has just released a new compilation of data that spells out the grave danger of rising seas.

Global average sea levels have risen faster since 1900 than over any preceding century in the last 3,000 years.

The global ocean has warmed faster over the past century than at any time in the past 11,000 years.

Meanwhile, the WMO tells us that even if global heating is miraculously limited to 1.5 degrees, there will still be a sizeable sea level rise.

But every fraction of a degree counts. If temperatures rise by 2 degrees, that level rise could double, with further temperature increases bringing exponential sea level increases.

Under any scenario, countries like Bangladesh, China, India and the Netherlands are all at risk.

Mega-cities on every continent will face serious impacts including Lagos, Maputo, Bangkok, Dhaka, Jakarta, Mumbai, Shanghai, Copenhagen, London, Los Angeles, New York, Buenos Aires and Santiago.

The danger is especially acute for nearly 900 million people who live in coastal zones at low elevations – that's one out of ten people on earth.

Some coastlines have already seen triple the average rate of sea-level rise.

I have seen with my own eyes how people in Small Island Developing States in the Western Pacific are facing sea-rise levels up to four times the global average.

In the Caribbean, rising seas have contributed to the devastation of local livelihoods in the tourism and agriculture sectors.

Rising seas and other climate impacts are already forcing some relocations in Fiji, Vanuatu, the Solomon Islands and elsewhere.

Flooding and coastal erosion in West Africa are damaging infrastructure and communities, undermining farming and often costing lives.

In North Africa, saltwater intrusion is contaminating land and freshwater resources, destroying crops and livelihoods alike.

Somalia is also grappling with saltwater intrusion, contributing to competition over scarce freshwater resources.

And around the world, a hotter planet is melting glaciers and ice sheets.

According to NASA, Antarctica is losing an average of 150 billion tons of ice mass annually.

The Greenland ice cap is melting even faster — losing 270 billion tons per year.

And consider the hundreds of millions of people living in the river basins of the Himalayas.

We have already seen how Himalayan melts have worsened flooding in Pakistan.

But as these glaciers recede over the coming decades, over time, the Indus, Ganges and Brahmaputra rivers will shrink.

And rising sea levels combined with a deep intrusion of saltwater will make large parts of their huge deltas simply uninhabitable.

We see similar threats in the Mekong Delta and beyond.

The consequences of all of this are unthinkable.

Low-lying communities and entire countries could disappear forever.

We would witness a mass exodus of entire populations on a biblical scale.

And we would see ever-fiercer competition for fresh water, land and other resources.

So, Excellencies, the impact of rising seas is already creating new sources of instability and conflict.

We must meet this rising tide of insecurity with action across three areas.

First — we must address the root cause of rising seas, the climate crisis.

Our world is hurtling past the 1.5-degree warming limit that a livable future requires, and with present policies, is careening towards 2.8 degrees — a death sentence for vulnerable countries.

We urgently need more concerted action to reduce emissions and ensure climate justice.

Developing countries must have the resources to adapt and build resilience against climate disaster.

Among other things, this means delivering on the loss and damage fund, making good on the \$100-billion climate finance commitment to developing countries, doubling adaptation finance, and leveraging massive private financing at a reasonable cost.

Second — we must broaden our understanding of the root causes of insecurity.

That means identifying and addressing a much wider range of factors that undermine security — from



poverty, discrimination and inequality, violations of human rights, to environmental disasters like rising sea levels.

That is why, for example, the Peacebuilding Fund is actively supporting grassroots resilience efforts against the effects of climate change.

We must also improve foresight and early warnings to prepare and protect vulnerable communities.

One prime example is our plan to ensure that early warning systems against natural disasters protect every person on earth within five years.

Third – we must address the impacts of rising seas across legal and human rights frameworks.

Rising sea levels are – literally – shrinking landmasses, a cause of possible disputes related to territorial integrity and maritime spaces.

The current legal regime must look to the future and address any gaps in existing frameworks.

Yes, this means international refugee law.

But it also means innovative legal and practical solutions to address the impact of rising sea levels on forced human displacement and on the very existence of the land territory of some states.

People's human rights do not disappear because their homes do.

Last year, the International Law Commission considered this issue and explored a range of potential solutions.

This includes continuing statehood despite loss of territory, ceding or assigning portions of territory to an affected state, or even establishing confederations of states.

These discussions are critical to finding solutions, and I appreciate the active consideration by delegations in the Sixth Committee.

We must keep working to protect affected populations and secure their essential human rights.

Excellencies,

The Security Council has a critical role to play in building the political will required to address the devastating security challenges arising from rising seas.

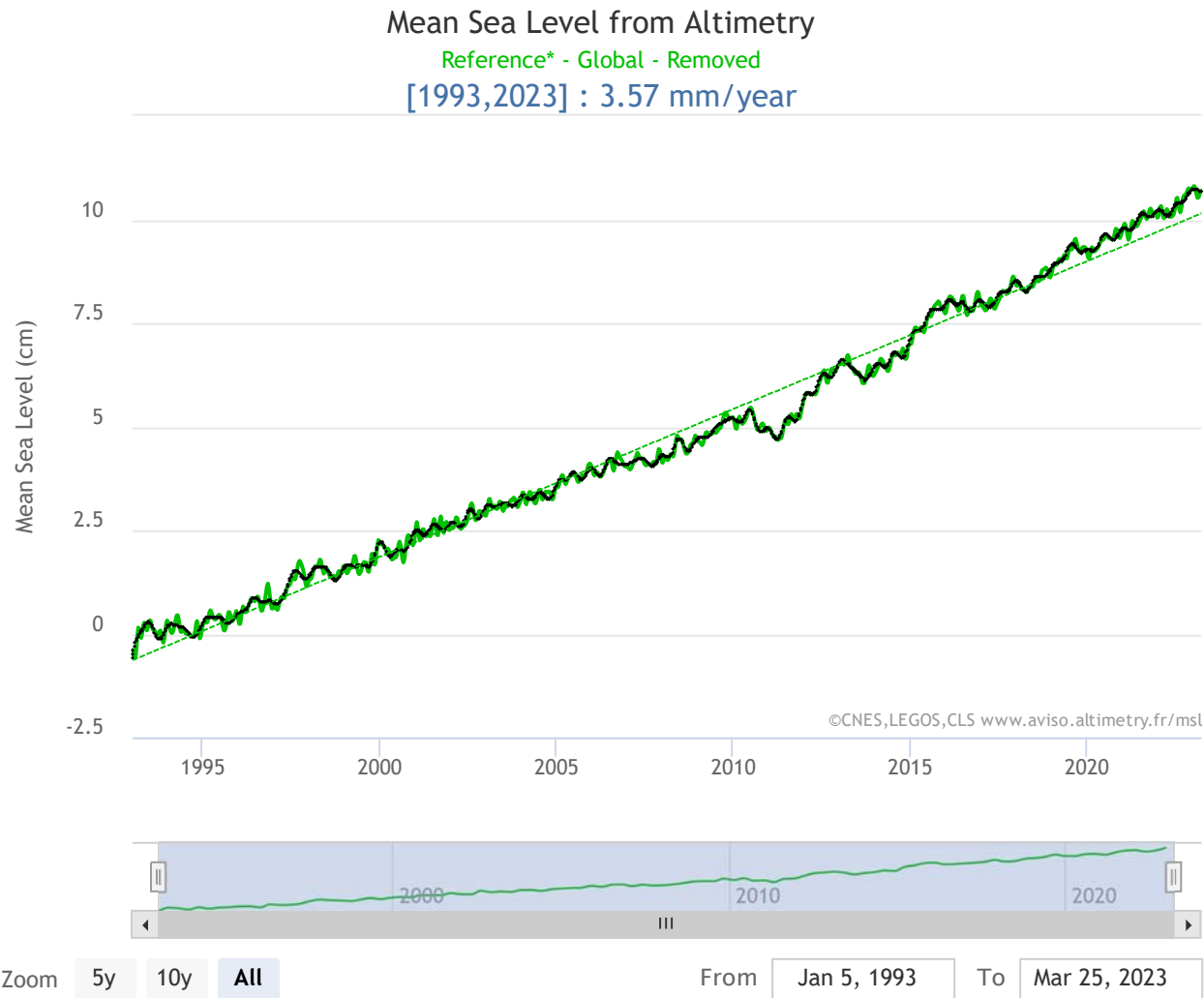
We must all work to continue turning up the volume on this critical issue, and supporting the lives, livelihoods and communities of people living on the front lines of this crisis.

Thank you.



Aviso Satellite Altimetry Website Extract.  
May 2023      Aviso

# Mean Sea Level products



Plot Type ⚙️

Time Serie

Missions 🌐

Reference\*

Zone 🌐

Global

Seasonal signal 📉

Removed

Trend Line

Show

6-month filtered data 📄

Show

Download 📄

image (PNG)

Help ([https://www.aviso.altimetry.fr/en/news/front-page-news/news-detail.html?tx\\_ttnews%5Btt\\_news%5D=2035](https://www.aviso.altimetry.fr/en/news/front-page-news/news-detail.html?tx_ttnews%5Btt_news%5D=2035)) and Tutorials

## Global and Regional MSL products

Manage services

The following products are available:

- GMSL timeseries for reference missions (TopEx-Poseidon, Jason-1,-2,-3, Sentinel-6MF) and auxiliary missions (Saral/Altika, ERS-1,-2, Envisat, GFO)
- Mono-mission regional maps of sea level trends (1x3 degrees)
- Ssalto/DUACS regional map of sea level trends (0.25x0.25 degrees)

The product can be downloaded in open access on the HTTPS server (<https://data.aviso.altimetry.fr/aviso-gateway/data/indicators/msl/>) or via the non authenticated FTP download (<ftp://ftp.aviso.altimetry.fr/pub/oceano/AVISO/indicators/msl/>) (if the FTP protocol is not supported by your browsers, see this note (</en/data/data-access/ftp.html>)).

The product is available free of charge for any project or study, and delivered as stated in the licence agreement ([/fileadmin/documents/data/License\\_Aviso\\_ini.pdf](/fileadmin/documents/data/License_Aviso_ini.pdf)).

### Documentation

- GMSL timeseries products are based on reprocessed AVISO L2P along-track V03\_00 (</en/data/products/sea-surface-height-products/global/along-track-sea-level-anomalies-l2p.html>)
- Regional map of sea level trends are based on reprocessed L4 C3S SSALTO/DUACS data (<https://cds.climate.copernicus.eu/cdsapp#!/dataset/satellite-sea-level-global?tab=overview>)

### Download

- Through the interactive visualisation interface
- AVISO+ product data portal (</en/data/data-access/registration-form.html>)

# Updates

## **January 2023**

- Introduction of Sentinel-6MF

## **September 2021**

- Data reprocessing and updates (</en/data/products/ocean-indicators-products/mean-sea-level/processing-and-corrections.html>) of the geophysical standards
- Regional maps for Jason-3 and Saral/Alti-Ka

## **March 2017**

- Integration of Jason-3

## **October 2016**

- Data reprocessing and updates ([/fileadmin/documents/data/products/indic/msl/MSL\\_reprocessing\\_Aviso\\_201610.pdf](/fileadmin/documents/data/products/indic/msl/MSL_reprocessing_Aviso_201610.pdf)) of the geophysical standards

## **July 2014**

- Integration of Saral/Alti-Ka mission

January 2014

- Data reprocessing and updates (/fileadmin/documents/data/products/indic/msl/MSL\_reprocessing\_201402.pdf) of the geophysical standards

April 2012

- Use of ENVISAT V2.1 GDR reprocessed data - Ollivier et al, 2012 (<https://www.tandfonline.com/doi/full/10.1080/01490419.2012.721632?scroll=top&needAccess=true&>)

# Tutorials










## YouTube is disabled.

Video sharing services help to add rich media on the site and increase its visibility.

By allowing these third party services, you accept their cookies and the use of tracking technologies necessary for their proper functioning.

Allow YouTube

## Data (/en/data.html)

- Products guide (/en/data/products-guide.html)
-  Products (/en/data/products.html)
  -  Sea surface height products (/en/data/products/sea-surface-height-products.html)
  -  Value-added products (/en/data/products/value-added-products.html)
  -  Wind/wave products (/en/data/products/windwave-products.html)
  -  Auxiliary products (/en/data/products/auxiliary-products.html)
  -  Ice products (/en/data/products/ice-products.html)
  -  Ocean indicators products (/en/data/products/ocean-indicators-products.html)
    -  El Niño bulletin (/en/data/products/ocean-indicators-products/el-nino-bulletin.html)
    -  Mean Sea Level (/en/data/products/ocean-indicators-products/mean-sea-level.html)
      - **Data access**

- [Processing & corrections \(/en/data/products/ocean-indicators-products/mean-sea-level/processing-and-corrections.html\)](/en/data/products/ocean-indicators-products/mean-sea-level/processing-and-corrections.html)
- [Other techniques \(/en/data/products/ocean-indicators-products/mean-sea-level/other-techniques.html\)](/en/data/products/ocean-indicators-products/mean-sea-level/other-techniques.html)
- [Validation \(/en/data/products/ocean-indicators-products/mean-sea-level/validation.html\)](/en/data/products/ocean-indicators-products/mean-sea-level/validation.html)
- [MSL Science issues \(/en/data/products/ocean-indicators-products/mean-sea-level/science-issues.html\)](/en/data/products/ocean-indicators-products/mean-sea-level/science-issues.html)
- [References \(/en/data/products/ocean-indicators-products/mean-sea-level/references.html\)](/en/data/products/ocean-indicators-products/mean-sea-level/references.html)
- [Kuroshio \(/en/data/products/ocean-indicators-products/kuroshio.html\)](/en/data/products/ocean-indicators-products/kuroshio.html)
- [Ocean Heat Content and Earth Energy Imbalance \(/en/data/products/ocean-indicators-products/ocean-heat-content-and-earth-energy-imbalance.html\)](/en/data/products/ocean-indicators-products/ocean-heat-content-and-earth-energy-imbalance.html)
- [Ionian Sea circulation \(/en/data/products/ocean-indicators-products/ionian-sea-circulation.html\)](/en/data/products/ocean-indicators-products/ionian-sea-circulation.html)
- [Ocean data challenges \(/en/data/products/ocean-data-challenges.html\)](/en/data/products/ocean-data-challenges.html)
- [In-situ products \(/en/data/products/in-situ-products.html\)](/en/data/products/in-situ-products.html)
- [Data access \(/en/data/data-access.html\)](/en/data/data-access.html)
- [Tools \(/en/data/tools.html\)](/en/data/tools.html)
- [Product information \(/en/data/product-information.html\)](/en/data/product-information.html)
- [CALVAL \(/en/data/calval.html\)](/en/data/calval.html)
- [Operational information \(/en/news/operational-news-and-status.html\)](/en/news/operational-news-and-status.html)

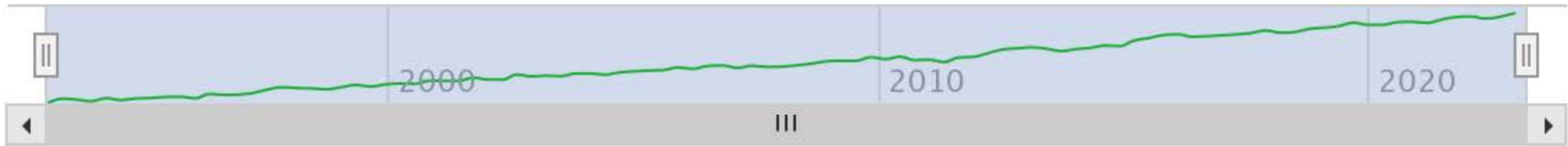
Aviso Satellite Altimetry – Graph of Rate of Sea Level Rise.

May 2023      Aviso

# Mean Sea Level from Altimetry

Reference\* - Global - Removed

[1993,2023] : 3.57 mm/year



Zoom **5y** **10y** **All**

From **Jan 5, 1993** To **Mar 25, 2023**



Crustal motions in Great Britain: evidence from continuous GPS, absolute gravity and Holocene sea level data.

Teferle et al

# Crustal motions in Great Britain: evidence from continuous GPS, absolute gravity and Holocene sea level data

F. N. Teferle,<sup>1</sup> R. M. Bingley,<sup>1</sup> E. J. Orliac,<sup>1</sup> S. D. P. Williams,<sup>2</sup> P. L. Woodworth,<sup>2</sup> D. McLaughlin,<sup>2</sup> T. F. Baker,<sup>2</sup> I. Shennan,<sup>3</sup> G. A. Milne,<sup>4,\*</sup> S. L. Bradley<sup>4</sup> and D. N. Hansen<sup>1</sup>

<sup>1</sup>Institute of Engineering Surveying and Space Geodesy, University of Nottingham, Nottingham, UK. E-mail: norman.teferle@nottingham.ac.uk

<sup>2</sup>Proudman Oceanographic Laboratory, Liverpool, UK

<sup>3</sup>Department of Geography, Durham University, Durham, UK

<sup>4</sup>Department of Earth Sciences, Durham University, Durham, UK

Accepted 2009 March 19. Received 2009 March 18; in original form 2008 July 16

## SUMMARY

Two independent continuous global positioning system (CGPS) processing strategies, based on a double-difference regional network and a globally transformed precise point positioning solution, provide horizontal and vertical crustal motion estimates for Great Britain. Absolute gravity and geological information from late Holocene sea level data further constrain the vertical motion estimates. For 40 CGPS stations we estimate station velocities and associated uncertainties using maximum likelihood estimation, assuming the presence of white and coloured noise. Horizontal station velocity estimates agree to  $<1 \text{ mm yr}^{-1}$  between the two CGPS processing strategies and closely follow predicted plate motions. Residual velocities, generally  $<1 \text{ mm yr}^{-1}$ , follow no regular pattern, that is, there is no discernible internal deformation, nor any dependence on station monumentation or time-series length. Vertical station velocity estimates for the two CGPS processing strategies agree to  $\sim 1 \text{ mm yr}^{-1}$ , but show an offset of  $\sim 1 \text{ mm yr}^{-1}$  with respect to the absolute gravity (AG) estimates. We attribute this offset to a bias related to known issues in current CGPS results and correct for it by AG-alignment of our CGPS estimates of vertical station velocity. Both CGPS estimates and AG-aligned CGPS estimates of present-day vertical crustal motions confirm the pattern of subsidence and uplift in Great Britain derived from Holocene sea level data for the last few thousand years: ongoing subsidence on Shetland, uplift in most areas of Scotland, and subsidence in large areas of England and Wales.

**Key words:** Time series analysis; Satellite geodesy; Time variable gravity; Plate motions; Europe.

## 1 INTRODUCTION

### 1.1 Context

There are two large-scale geophysical processes known to cause crustal motions in Great Britain. The first, the motion of the Eurasian plate due to plate tectonics, predominantly acts on the horizontal coordinate components with negligible effect on the vertical. The second, known as glacial isostatic adjustment (GIA), is the on-going viscous response of the solid Earth to past changes in ice sheets and sea level. This process contributes a signal in both the vertical and horizontal components (e.g. Mitrovica *et al.* 1994; Milne *et al.* 2001, 2006).

The plate tectonics signal in Great Britain, a rotation along with the Eurasian plate, is seen as motion in a northeasterly direction of approximately  $23 \text{ mm yr}^{-1}$ . Great Britain is considered part of the rigid interior of the Eurasian plate, although some residual motion of southeast England with respect to central Europe has been reported previously (Nocquet *et al.* 2001; Nocquet & Calais 2003). Apart from this, there have been few studies concerned with the plate motion signal or the stability of the plate within Great Britain due to a lack of geodetic data.

In contrast to plate motions, the GIA signal has been studied in great detail in the area of Great Britain. The majority of studies to date have considered only the sea level aspect of the GIA signal (e.g. Lambeck 1993a,b; Lambeck *et al.* 1996; Peltier *et al.* 2002; Shennan *et al.* 2002). As the precision of geodetic constraints from continuous global positioning system (CGPS) measurements have improved, these data have been employed more recently in GIA modelling studies (e.g. Milne *et al.* 2006). With regard to the

\*Now at: Department of Earth Sciences, University of Ottawa, Canada.

crustal motion signal recorded by CGPS, the data provide a good test of the models through the summation of both the near and far-field effects. In general, the signal manifests itself as a combination of the effects related to the deglaciation of the Laurentide, Fennoscandian and the British–Irish ice sheets (Milne *et al.* 2006). For the horizontal components, the dominant signal is associated with the Laurentide ice sheet and is predicted to be in a northwesterly direction. The magnitude of the horizontal GIA signal varies across the region and is thought to be of the order of  $1\text{--}2\text{ mm yr}^{-1}$  (Milne *et al.* 2006). For the vertical component, the dominant signal is associated with the British–Irish ice sheet and the adjacent, significantly larger Fennoscandian ice sheet, resulting in subsidence on Shetland, uplift in most areas of Scotland, and subsidence in large areas of England and Wales. Prior to the availability of CGPS measurements, vertical crustal motion was inferred from geological information of relative sea level change, inverted to form maps of Holocene crustal movements (Shennan 1989; Shennan & Horton 2002; Shennan *et al.* 2006). As changes in sea level around Great Britain are of major concern, it is this geological information which has so far been used to correct tide gauge (TG) records for changes in land levels (e.g. Woodward *et al.* 1999).

On a local scale, past crustal motions occurred along the main fault systems in Scotland (e.g. Curry 1986; Canning *et al.* 1998; Stewart *et al.* 2001), but these motions are believed to have largely ceased. Whereas, more recent neotectonic crustal motions have been reported for London in southeast England (Ellison *et al.* 2004). Similarly, in some areas we may also expect to see subsidence associated with sediment compaction (e.g. Zong & Tooley 1996; Shennan & Horton 2002; Edwards 2006; Hill *et al.* 2007) and the extended deep mining activities throughout the Anthropocene (e.g. Humphries 2001; Bell *et al.* 2005; Donnelly 2006). Although it is worth noting that most deep mining ended in the 1980s and the current geodetic monitoring network of CGPS and absolute gravity (AG) stations were established in the late 1990s.

For many years the only CGPS station in Great Britain was located at Herstmonceux in southeast England. In the late 1990s other CGPS stations were established, predominantly at sites of the national TG network. The main objective of these was to measure the vertical land motions directly at the TG sites (Teferle *et al.* 2002, 2006; Teferle 2003). We note here that such CGPS@TG stations may not only be affected by large-scale vertical crustal motions and local scale subsidence, but also by local instabilities, as these stations are often founded on structures such as piers and quays of varying age and foundations.

Initially the CGPS network grew slowly, as expansion was mainly driven by various scientific objectives, similar to those in Scandinavia (e.g. Milne *et al.* 2001; Johansson *et al.* 2002; Lidberg *et al.* 2007). However, since the year 2000, a larger number of CGPS stations were established as network real-time kinematic (RTK) CGPS stations, but mainly located on buildings.

To advance sea level research, in the late 1990s three AG stations were also established near TGs (Williams *et al.* 2001). In contrast to the CGPS@TG stations, these were located in buildings believed to be founded on bedrock, thus providing estimates of vertical crustal motions. That AG is an essential technique when investigating such motions has been shown previously (e.g. Larson & van Dam 2000; Lambert *et al.* 2001; Mazzotti *et al.* 2007). In terms of accuracy, the role of AG is also becoming critical for the vertical component, as a geodetic technique independent of the International Terrestrial Reference Frame (ITRF), namely ITRF2000 (Altamimi *et al.* 2002) and its update ITRF2005 (Altamimi *et al.* 2007).

Although much work has been undertaken to improve the precision of vertical crustal motions from CGPS, the absolute accuracy of these is currently still limited by the accuracy of the ITRF, which is  $\sim 2\text{ mm yr}^{-1}$  in the vertical. This limitation stems from difficulties in the accurate determination of the geocentre of the ITRF and its long-term motion with respect to the centre of mass (CM) of the Earth system (e.g. Wu *et al.* 2002; Blewitt 2003; Dong *et al.* 2003; Argus 2007).

In recent discussions, the accuracy of horizontal crustal motions from CGPS has also been questioned. These may only be accurate at the  $1\text{--}2\text{ mm yr}^{-1}$  level due to the implementation of the no-net rotation condition in ITRF2000 and ITRF2005 (Kreemer *et al.* 2006; Altamimi *et al.* 2007). Additionally, estimates from regional realizations of the terrestrial reference frame, still implemented in many studies, may be biased/offset, depending on the subset of reference frame sites used for the regional reference frame implementation (Dong *et al.* 2003; Mazzotti *et al.* 2008).

In response to these issues, Aoki & Scholz (2003) computed absolute vertical station velocities by alignment of their CGPS estimates to those estimated at 18 TGs in the Japanese Islands, assuming a global averaged sea level rise of  $1.8\text{ mm yr}^{-1}$ . Caccamise *et al.* (2005) reported only relative and not absolute vertical station velocity estimates between several CGPS stations in Hawaii, and Bennett & Hreinsdóttir (2007) determined a local vertical reference frame using Holocene and Late Pleistocene geological evidence of vertical crustal motions. A similar, but alternative approach has been advocated for the CGPS@TG stations in Great Britain based on an alignment of the CGPS vertical station velocity estimates to those from AG (Teferle 2003; Teferle *et al.* 2006). The advantage of this approach lies in the nature of these two complementary geodetic techniques giving independent estimates over a comparable time span if operated in parallel.

In addition to problems with the terrestrial reference frame, it is well known that CGPS coordinate solutions suffer from residual errors due to inaccurate models of systematic biases both directly, when these are applied by the user, and indirectly through the use of GPS satellite orbit and clock, and Earth rotation products. For example, significant effects on the vertical coordinate component have been reported due to inadequate modelling of satellite and receiver antenna phase centres (e.g. Ge *et al.* 2005; Cardellach *et al.* 2007), the neglecting of higher-order ionospheric terms (Kedar *et al.* 2003; Fritsche *et al.* 2005; Hernández-Pajares *et al.* 2007), the inadequate modelling of the tropospheric delay (e.g. Böhm *et al.* 2006; Vey *et al.* 2006), and the effect of different loading processes (e.g. van Dam *et al.* 2001; Tregoning & Van Dam 2005). The benefits of improved models from some of this recent research have been demonstrated in a re-analysis of global CGPS data set for the period between 1994 and 2005 (Steigenberger *et al.* 2006). However, such improved models are not always readily available to users of different GPS software, or accounted for in the current GPS satellite orbit and clock, and Earth rotation products available from the International GNSS (Global Navigation Satellite System) Service (IGS; Beutler *et al.* 1999).

All of these biases are in part responsible for the increased day-to-day scatter in the vertical component of CGPS coordinate solutions and lead to a loss in precision and accuracy. However, as some of these effects have similar magnitudes over large areas, they can often be identified as common mode biases (Wdowinski *et al.* 1997). Hence, by using spatial filtering the common mode can successfully be removed, reducing the day-to-day scatter and improving the error bounds of parameter estimates (e.g. Wdowinski *et al.* 1997; Johansson *et al.* 2002; Nikolaidis 2002; Dong *et al.* 2006). Although,

spatial filtering may also de-couple station velocity estimates from the reference frame of the coordinate solutions (Wdowinski *et al.* 1997, 2004).

Besides obtaining highly accurate station velocity estimates, it is essential that a realistic uncertainty is assigned to any estimate. For example, several authors (Langbein & Johnson 1997; Zhang *et al.* 1997; Mao *et al.* 1999; Williams 2003; Williams *et al.* 2004) have shown that CGPS coordinate time-series contain both white and coloured noise, that is, time-independent and time-correlated noise, and if coloured noise is not accounted for station velocity uncertainties may be underestimated by an order of magnitude.

## 1.2 Aims

Teferle *et al.* (2006) compared the CGPS estimates of vertical land motions obtained for seven CGPS@TG stations to those from AG, geological information, sea level records, and GIA models, and found the CGPS estimates to be offset. Their CGPS estimates were too positive, or less negative, than the other estimates ergo they used a combination of CGPS and AG to align the CGPS estimates to their AG estimates at Newlyn and Lerwick. This study is partly an update of the work of Williams *et al.* (2001) and Teferle *et al.* (2006), but more so an expansion of it in four different ways.

(i) We introduce a second and independent CGPS processing strategy using the Bernese GPS software version 5.0 (Dach *et al.* 2007) in precise point positioning mode (Teferle *et al.* 2007).

(ii) We expand our reference frame implementation from regional (European) to global.

(iii) We include more CGPS stations in Great Britain, to get better coverage.

(iv) We make improvements to the spatial filtering used in Teferle *et al.* (2006) to avoid, as much as possible, a de-coupling of our station velocity estimates from our reference frame implementations.

Through this expansion and the inclusion of more recent data we present the followings:

(i) Updated vertical station velocity estimates from the expanded CGPS network and AG.

(ii) Horizontal station velocity estimates (and residual velocities) for the expanded CGPS network.

(iii) AG-aligned CGPS estimates of vertical crustal motions for the expanded CGPS network, and a comparison of these with estimates from geological information.

(iv) Initial maps of vertical crustal motion for Great Britain based on geodetic data.

The expansion of the CGPS network brought about the inclusion of stations with very different monumentation, often *a priori* deemed inappropriate for geophysical interpretation. Here we follow the approach of previous studies (e.g. Calais *et al.* 2006) and include such stations, then look at their suitability *a posteriori*. In this way, we provide the horizontal and vertical station velocity estimates which form the basis for the studies of Woodworth *et al.* (2009) to update the trends in sea level changes around Great Britain, and of Bradley *et al.* (2009), who investigate the modelling of the GIA processes observed in this region.

## 1.3 Method

In the following section we discuss the available data sets, that is, from CGPS, AG, and geological information. This is followed by

a description of the processing and analysis of the CGPS, AG and geological data before we present our results. For CGPS, we compare our horizontal and vertical station velocity estimates in order to quantify the effects of our two independent CGPS processing strategies, spatial filtering, and reference frame implementations. For AG, we show our best estimates for the change in gravity and derive AG estimates of vertical station velocities from them. The velocity estimates from both geodetic techniques are then interpreted as crustal motions under the assumption that no other local displacement has occurred. For the horizontal component, we then investigate which CGPS stations seem promising for future geophysical interpretations. For the vertical component, we compare our CGPS estimates to those from AG, compute AG-aligned CGPS estimates of vertical crustal motions, and compare these to the latest geological information. Through this process we establish sets of stations for which we have confidence that their station velocity estimates represent present-day crustal motions in Great Britain.

## 2 DATA SETS

### 2.1 Continuous GPS

The CGPS stations in Great Britain can be divided into two categories: scientific and network RTK. Data for all of these are archived in the Natural Environment Research Council funded British Isles continuous GNSS Facility (BIGF; <http://www.bigf.ac.uk>). All of the CGPS stations we considered in this study are shown in Fig. 1.

Four scientific CGPS stations, HERS and HERT at Herstmonceux in southeast England, MORP at Morpeth in northeast England, and

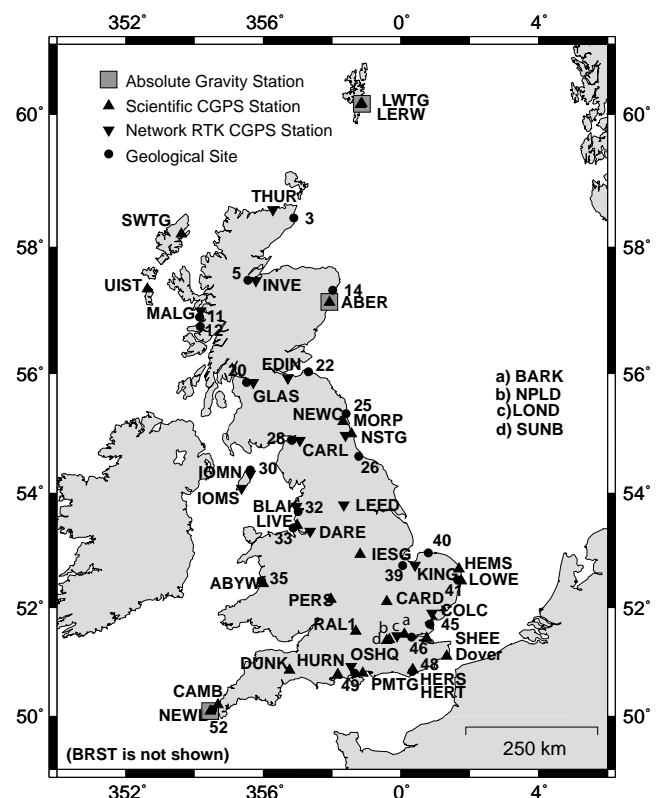


**Figure 1.** Locations of the scientific CGPS stations, network real-time kinematic (RTK) CGPS stations, absolute gravity (AG) stations, and geological sites (from Shennan & Horton 2002) used in this study.

NPLD at the National Physical Laboratory in Teddington, west of London, contribute to both the IGS and the European Reference Frame Permanent Network (EPN; Bruyninx *et al.* 2001). The scientific CGPS station NEWL in Newlyn, southwest England and ABER in Aberdeen, eastern Scotland, contribute to the IGS TG Benchmark Monitoring (TIGA) Pilot-Project and the European Sea Level Service (ESEAS). NEWL and the two network RTK stations INVE in Inverness, northern Scotland and DARE in Daresbury, northwest England, also contribute to the EPN.

Established in 1992, HERS is the longest operating CGPS station in Great Britain, but its data quality suffered during the 1990s and we regard this station to be of highest quality only after 2001. MORP is certainly an interesting CGPS station within the IGS network due to its unique monumentation, a 4.5 tonne carved monolith that rests directly on top of the underlying bedrock (Blewitt *et al.* 1997). Again, this station suffered from poor data quality in the late 1990s (Teferle 2003), which improved only after modifications in 2002 (IGSMail-4222 (2002), see <http://igsceb.jpl.nasa.gov/mail/igsmail/igsmail.html>).

Within BIGF the scientific CGPS stations include those established at ten of the 44 TGs which form the national TG network as part of the National Tidal and Sea Level Facility (<http://www.pol.ac.uk/ntsif>), 12 others established at sites of the UK Meteorological Office (UKMO) or the Environment Agency (EA), and one at the University of Nottingham. All of these were established during the period from 1997 to 2005 (Table 1).

The CGPS@TG stations have GPS receivers housed in the same building as the TG equipment and the GPS antennas mounted on monuments, sited as close as possible to the TG, i.e. within a few meters of the TG itself; to fulfil the requirement for site-specific, direct estimates of the changes in land level. Teferle (2003) gives further details of these CGPS@TG stations. Due to our interest in sea level studies, we have also included the IGS/EPN station BRST located close to the TG at Brest, France, in our analysis, and we will list it along with the ten CGPS@TG stations located in Great Britain.

The network RTK CGPS stations in Great Britain that are archived in BIGF belong to the Ordnance Survey of Great Britain (OSGB), who have established over 120 such stations since 2000, with larger numbers in more recent years. In this study we only include the 16 stations that were established before 2003 and that have a sufficient and consistent enough data span to warrant any scientific analysis. If they are founded on a stable structure connected to solid rock, then they can provide a series of CGPS stations that densifies the sparse network of scientific stations (Fig. 1 and Table 1).

Overall, we do not consider the CGPS network used in this study as homogeneous. However, we point out elements of homogeneity in the groups of the scientific CGPS stations and the network RTK CGPS stations, which relate to the GPS equipment (Table 1) and the station-specific monumentation (Table 2).

From Table 2 it can be seen that most scientific CGPS stations use IESSG-designed carbon-fibre poles with stainless steel ends that have been attached to either a solid structure or a submerged concrete block that rests directly on top of bedrock, whereas almost all network RTK CGPS stations are located on brick buildings with varying number of storeys. For these stations the monument normally consists of a stainless steel tripod on the roof, or a bracket, which has been mounted on the roof or onto a wall, with the antenna reaching above the roof.

Although HEMS was used for scientific investigations in the past (Teferle *et al.* 2002), the station was decommissioned in 2001 and is mentioned here only for completeness. As DVTG, LWTG, SWTG

and UIST were only established in 2005, their coordinate time-series are still too short and we do not discuss these sites further.

## 2.2 Absolute gravity

AG measurements near TGs began in 1995 at Newlyn and Aberdeen and in 1996 at Lerwick (Williams *et al.* 2001). Given the complexity in making AG measurements we decided to focus our attention on three TG sites. The sites were selected based on their geographical distribution and their representation of the expected changes in land level due to GIA, that is, subsidence at Newlyn in southwest England, uplift or no movement at Aberdeen in eastern Scotland and subsidence at Lerwick on Shetland. Newlyn and Lerwick TGs contribute to the Global Sea Level Observing System (GLOSS) coordinated by the Intergovernmental Oceanographic Commission (IOC) and Newlyn and Aberdeen both have some of the longest and highest quality mean sea level time-series in the country (Williams *et al.* 2001).

At each TG a detailed reconnaissance was carried out to identify potential sites for the establishment of an AG station considered suitable for the long-term monitoring of vertical crustal motion. The main criterion for an AG station is location within a building (for a stable and protected environment) that is likely to have a secure future, with little or no change to its surrounding environment over a sufficient period of time, and built on a bedrock foundation. There are certain effects that restrict the station from being placed at the TG or close to the coastline. The direct gravitational attraction of the ocean mass changes (tidal and non-tidal) close to the TG would impart unwanted noise into the measurements if they are not modelled sufficiently, and it would be difficult to interpret the gravity changes as such. For example, the conversion factor to apply depends on the source of the land movements, that is, free-air for a subsiding pier or Bouguer for a GIA signal. The AG station was, therefore, established sufficiently far from the coastline to minimize these effects while still representing the motion at the TG.

Lerwick AG station is located in the basement of a school, about 0.5 km from the TG and the CGPS@TG station LWTG and 5 km from the scientific CGPS station LERW; Aberdeen AG station is located in a church, about 3.2 km from the TG and the CGPS@TG station ABER; and Newlyn AG station is located in the church at Paul about 1.5 km from the TG and the CGPS@TG station NEWL. We show the locations of AG stations used in this study in Fig. 1.

AG measurements are made by dropping a mass in a vacuum and using an Iodine stabilized He–Ne laser interferometer and rubidium atomic clock to obtain distance–time pairs and solve the equations of motion to obtain the acceleration (Niebauer *et al.* 1995). We use the POL absolute gravimeter (FG5-103), produced commercially by Micro-g LaCoste Inc., USA, to make our measurements. Measurement campaigns at each station are made approximately annually over duration of three to four days. The instrument is set up at the start of each day and the measurements consist of 24 hourly sets of 200 drops spaced 10 s apart. Occasionally, if the measurements do not go as planned, a second trip to the station is organized. Prior to and after each field visit, measurements are made at the gravity station in the laboratory and compared with measurements from our second instrument (FG5-222), to ensure the measurements are consistent. In addition, both instruments are regularly intercompared with other instruments in Europe and the USA to ensure that they are in agreement at the 1–2  $\mu\text{Gal}$  level (Williams *et al.* 2001; Vitushkin *et al.* 2002; Francis *et al.* 2005). A summary of the data availability for the AG stations is given in Table 3.



**Table 1.** Continuous GPS (CGPS) station information for scientific stations co-located with tide gauges (TG), other scientific and network real-time kinematic (RTK) stations in Great Britain used in this study.

Station ID	Domes number	Location	Operator	Longitude (°)	Latitude (°)	Start date	Span (yr)	Current GPS equipment (on 31 December 2005) receiver	Antenna	Radome
CGPS@TG stations										
ABER	13231M001	Aberdeen	POL <sup>a</sup> /UNT <sup>b</sup>	357.92	57.14	1998-09-18	7.3	ASHTECH Z-XII3	ASH700936F_C	SNOW
BRST	10004M004	Brest, France	IGN <sup>c</sup>	355.50	48.38	1998-10-31	7.2	TRIMBLE 5700	TRM29659.00	NONE
DVTG		Dover	UNT	1.32	51.11	2005-11-24	0.0	ASHTECH UZ-12	ASH701945C_M	SNOW
LIVE	13233M001	Liverpool	UNT	356.98	53.45	1999-02-04	6.9	ASHTECH Z-XII3	ASH700936D_M	SNOW
LOWE	13232M001	Lowestoft	UNT	1.75	52.47	1999-02-13	6.9	ASHTECH Z-XII3	ASH700936F_C	SNOW
LWTG		Lerwick	POL/UNT	358.86	60.15	2005-08-19	0.4	ASHTECH UZ-12	ASH701945C_M	SNOW
NEWL	13273M001	Newlyn	UNT	354.46	50.10	1998-09-30	7.3	ASHTECH Z-XII3	ASH700936D_M	SNOW
NSTG	13216M001	North Shields	NCL <sup>d</sup> /UNT	358.56	55.01	2001-05-15	6.1	ASHTECH Z-XII3	ASH700936B_M	SNOW
PMTG	13289M003	Portsmouth	UNT	358.89	50.80	2001-09-25	4.3	ASHTECH UZ-12	ASH701945C_M	SNOW
SHEE	13236M001	Sheerness	EA <sup>e</sup> /UNT	0.74	51.45	1997-03-26	8.7	TRIMBLE 4000SSI	TRM29659.00	NONE
SWTG		Stornoway	POL/UNT	353.61	58.21	2005-09-02	0.0	ASHTECH UZ-12	ASH701945C_M	SNOW
Other scientific CGPS stations										
ABYW		Aberystwyth	UKMO <sup>f</sup>	356.00	52.42	1998-04-04	7.7	ASHTECH UZ-12	ASH700936D_M	SNOW
BARK		Barking Barrier	EA/OSGB <sup>g</sup>	0.10	51.52	1997-04-25	8.7	TRIMBLE 4000SSI	TRM29659.00	NONE
CAMB		Camborne	UKMO/OSGB	354.67	50.22	1998-04-03	7.7	ASHTECH UZ-12	ASH700936D_M	SNOW
CARD		Cardington	UKMO	359.58	52.10	2003-01-12	2.9	ASHTECH UZ-12	ASH700936D_M	SNOW
DUNK		Dunkeswell	UKMO	356.76	50.86	2000-02-05	5.9	ASHTECH UZ-12	ASH700936F_C	SNOW
HEMS		Hemsby	UKMO/UNT	1.69	52.69	1998-04-10	2.8	ASHTECH Z-XII3	ASH700936D_M	SNOW
HERS	13212M007	Herstmonceux	NSGF <sup>h</sup>	0.34	50.87	1992-03-24	8.7	ASHTECH Z-XII3	ASH700936E	NONE
HERT	13212M010	Herstmonceux	NSGF	0.33	50.87	2003-03-12	2.8	ASHTECH Z18	ASH701946.2	NONE
HURN		Hurn	UKMO/UNT	358.16	50.78	2000-09-13	5.3	ASHTECH Z-XII3	ASH700936F_C	SNOW
IESG	13220M001	Nottingham	UNT	358.81	52.94	1997-04-27	8.7	ASHTECH Z-XII3	ASH700936D_M	SNOW
LERW		Lerwick	UKMO/OSGB	358.82	60.14	1998-04-18	7.7	ASHTECH Z-XII3	ASH700936D_M	SNOW
MORP	13299S001	Morpeth	NCL	358.31	55.21	1996-10-31	8.7	ASHTECH Z-XII3	AOAD/M.T	NONE
NPLD	13234M003	Teddington	NPL <sup>i</sup>	359.66	51.42	2000-08-16	4.9	ASHTECH Z-XII3T	AOAD/M.T	NONE
PERS		Pershore	UKMO/UNT	357.96	52.15	2001-05-09	4.6	ASHTECH Z-XII3	ASH700936F_C	SNOW
RAL1		Chilton	UKMO	358.69	51.57	2003-03-11	2.8	ASHTECH UZ-12	ASH700936F_C	SNOW
SUNB		Sunbury Yard	EA/UNT	359.58	51.40	1997-04-08	8.7	TRIMBLE 4000SSI	TRM29659.00	NONE
UIST		Uist	UKMO	352.63	57.35	2005-01-21	0.9	ASHTECH UZ-12	ASH700936D_M	SNOW
Network RTK CGPS stations										
BLAK		Blackpool	OSGB	356.97	53.78	2002-01-02	4.0	LEICA RS500	LEIAT504	LEIS
CARL	13205S001	Carlisle	OSGB	357.06	54.90	2000-04-12	5.7	LEICA RS500	LEIAT504	LEIS
COLC	13207S001	Colchester	OSGB	0.90	51.89	2000-04-27	5.7	LEICA RS500	LEIAT504	LEIS
DARE	13208S001	Daresbury	OSGB	357.36	53.34	2001-12-03	5.7	LEICA RS500	LEIAT504	LEIS
EDIN	13217S001	Edinburgh	OSGB	356.71	55.92	2000-03-16	5.8	LEICA RS500	LEIAT504	LEIS
GLAS	13219S001	Glasgow	OSGB	355.70	55.85	2000-03-15	5.8	LEICA RS500	LEIAT504	LEIS
INVE	13221S001	Inverness	OSGB	355.78	57.49	2002-07-05	6.0	LEICA SR530	ASH700936E	SNOW
IOMN	13222S001	Ramsay	OSGB	355.61	54.33	2001-03-21	4.8	LEICA RS500	LEIAT504	LEIS
IOMS	13224S001	Ronaldsway	OSGB	355.37	54.09	2001-03-20	4.8	LEICA RS500	LEIAT504	LEIS
KING	13225S001	King's Lynn	OSGB	0.40	52.75	2000-01-02	6.0	LEICA SR530	ASH700936E	SNOW
LEED	13215S001	Leeds	OSGB	358.34	53.80	2000-01-02	6.0	LEICA SR530	ASH700936E	SNOW
LOND		London	OSGB	359.88	51.49	2000-01-02	6.0	LEICA SR530	ASH700936E	SNOW
MALG	13226S001	Mallaig	OSGB	354.17	57.01	2000-05-31	5.6	LEICA RS500	LEIAT504	LEIS
NEWC	13227S001	Newcastle	OSGB	358.38	54.98	2000-01-02	6.0	LEICA SR530	ASH700936E	SNOW
OSHQ	13274S002	Southampton	OSGB	358.55	50.93	2000-01-02	6.0	LEICA SR530	ASH700936E	SNOW
THUR	13230S001	Thurso	OSGB	356.27	58.58	2000-05-09	5.6	LEICA RS500	LEIAT504	LEIS

Notes: Start date either depicts the point in time of the actual station installation or for some sites, the point in time from which data is available from in the British Isles continuous GNSS Facility (BIGF). Span depicts the maximum theoretical period for which data were available in the archive up to 2005 December 31.

<sup>a</sup>Proudman Oceanographic Laboratory (POL).

<sup>b</sup>University of Nottingham (UNT).

<sup>c</sup>Institut Géographique National (IGN).

<sup>d</sup>Newcastle University (NCL).

<sup>e</sup>Environment Agency (EA).

<sup>f</sup>United Kingdom Meteorological Office (UKMO).

<sup>g</sup>Ordnance Survey of Great Britain (OSGB).

<sup>h</sup>National Space Geodetic Facility (NSGF).

<sup>i</sup>National Physical Laboratory (NPL).

**Table 2.** Monumentation information for CGPS stations in Great Britain used in this study.

Station ID	Domes	Location	Monumentation Information
CGPS@TG stations			
ABER	13231M001	Aberdeen	4 m high c/f pipe attached to s/s plate connected to concrete quay with piled foundations
BRST	10004M004	Brest, France	2 m high s/s mast connected to stone pier
DVTG		Dover	2 m high c/f pipe attached to s/s plate connected to stone pier
LIVE	13233M001	Liverpool	5 m high concrete pillar connected to stone pier with piled foundations
LOWE	13232M001	Lowestoft	0.8 m high c/f pipe attached to s/s bracket connected to side wall of 2-storey building on concrete quay with piled foundations
LWTG		Lerwick	3 m high c/f pipe attached to s/s plate connected to stone pier
NEWL	13273M001	Newlyn	3 m high c/f pipe attached to s/s plate connected to observation platform of steel lighthouse on stone pier
NSTG	13216M001	North Shields	4 m high aluminium pole connected to concrete quay with piled foundations
PMTG	13289M003	Portsmouth	1.5 m high s/s pole and bracket connected to side wall of 1-storey building on stone quay
SHEE	13236M001	Sheerness	0.2 m high s/s bracket connected to flat roof of 1-storey building on concrete jetty with piled foundations
SWTG		Stornoway	2 m high c/f pipe attached to s/s plate connected to concrete wharf with piled foundations
Other scientific CGPS stations			
ABYW		Aberystwyth	2 m high c/f pipe attached to s/s plate connected to ~3 m deep concrete block founded on bedrock
BARK		Barking Barrier	0.6 m high s/s pole and bracket connected to ~40 m high concrete structure founded on bedrock
CAMB		Camborne	2 m high c/f pipe attached to s/s plate connected to ~2 m deep concrete block founded on bedrock
CARD		Cardington	2 m high c/f pipe attached to s/s plate connected to ~1 m deep concrete block
DUNK		Dunkeswell	2 m high c/f pipe attached to s/s plate connected to ~2 m deep concrete block founded on bedrock
HEMS		Hemsby	2 m high c/f pipe attached to s/s plate connected to flat roof of 1-storey building with piled foundations
HERS	13212M007	Herstmonceux	8 m high steel mast connected to ~5 m deep concrete block
HERT	13212M010	Herstmonceux	0.5 m high brick/concrete pillar on top of water tower with ~5 m deep foundations
HURN		Hurn	2 m high c/f pipe attached to s/s plate connected to ~1 m deep concrete block
IESG	13220M001	Nottingham	0.6 m high s/s pole and bracket connected to ~13 m high brick turret founded on bedrock
LERW		Lerwick	2 m high c/f pipe attached to s/s plate connected to ~1 m deep concrete block founded on bedrock
MORP	13299S001	Morpeth	2.4 m high, 4.5 tonne quarried trapezoidal stone buried to ~2.4 m depth and founded on bedrock
NPLD	13234M003	Teddington	On roof of multistorey building
PERS		Pershore	2 m high c/f pipe attached to s/s plate connected to ~1 m deep concrete block
RAL1		Chilton	On roof of multi-storey building
SUNB		Sunbury Yard	0.6 m high c/f pipe attached to s/s bracket connected to side wall of 2-storey building
UIST		Uist	2 m high c/f pipe attached to s/s plate connected to ~1 m deep concrete block
Network RTK CGPS stations			
BLAK		Blackpool	~2 m high s/s pole connected to side wall of 1-storey brick building (~4 m tall)
CARL	13205S001	Carlisle	~1.8 m high s/s tripod connected to roof of 3-storey concrete building (~9 m tall)
COLC	13207S001	Colchester	~2 m high s/s pole connected to side wall of multi-storey brick and concrete building (~22 m tall)
DARE	13208S001	Daresbury	~2 m high s/s pole connected to side wall of 1-storey brick building (~5 m tall)
EDIN	13217S001	Edinburgh	~2 m high s/s pole connected to side wall of 1-storey brick building (~5 m tall)

**Table 2.** (Continued.)

Station ID	Domes	Location	Monumentation Information
GLAS	13219S001	Glasgow	~2 m high s/s pole connected to side wall of 2-storey brick building (~6 m tall)
INVE	13221S001	Inverness	~2 m high s/s pole connected to side wall of 2-storey block building (~8 m tall)
IOMN	13222S001	Ramsay	no information available
IOMS	13224S001	Ronaldsway	no information available
KING	13225S001	King's Lynn	~1.8 m high steel tripod connected to flat roof of multi-storey brick building (~13 m tall)
LEED	13215S001	Leeds	~1.8 m high steel tripod connected to flat roof of 3-storey building (~13 m tall)
LOND		London	~1.8 m high steel tripod connected to roof of multi-storey building
MALG	13226S001	Mallaig	~2 m high s/s pole connected to side wall of 2-storey brick building (~7 m tall)
NEWC	13227S001	Newcastle	~1.8 m high steel tripod connected to concrete block on flat roof of 4-storey brick building (~12 m tall)
OSHQ	13274S002	Southampton	~1.8 m high s/s tripod connected to flat roof of multi-storey re-inforced concrete building (~24 m tall)
THUR	13230S001	Thurso	~3 m high steel mast connected to flat roof of 2-storey concrete building (~6 m tall)

Notes: Information is given for scientific stations collocated with tide gauges (TG), other scientific, and network real-time kinematic (RTK) stations and was accurate as of 2005 December 31. c/f stands for carbon-fibre and s/s for stainless steel.

**Table 3.** Data availability for the absolute gravity (AG) stations in Great Britain used in this study.

Station	Start date	End date	# of campaigns	Data span
Lerwick	1996-09	2006-08	10	9.9
Aberdeen	1995-05	2006-08	13	11.3
Newlyn	1995-10	2006-09	12	10.9

### 2.3 Geological information

The database of Holocene sea level index points held at Durham University (Shennan 1989; Shennan & Horton 2002; Shennan *et al.* 2006) allows investigations of Holocene, and ongoing, land and sea level changes in Great Britain. Observations, with quantified uncertainty terms, of past changes in sea level relative to present come from sediments, both organic and minerogenic, and from morphological features whose origin was controlled by palaeo-sea level. In order to be useful, sediments must not have been eroded or transported since the time of accumulation and where such sediments and morphological features survive, they can be used as sea level index points by defining attributes such as location, age, altitude and tendency (Shennan *et al.* 2006). If no transportation of the sediments can be assumed, then the location attribute of a sea level index point is defined by its geographical coordinates. The age attribute is obtained from radiocarbon techniques with calibrated ages as 95 per cent confidence limits using Calib 4.4 (<http://depts.washington.edu/qil>). We wish to mention that most sea level index points in the database from Great Britain have at least one type of corroborating evidence to support the radiocarbon age and to demonstrate continuity of sedimentation. The ages of most sea level index points range between 3000 and 10 000 calibrated years before present (cal. yr BP), with some sites in northwest Scotland having the longest records dating back to up to 15 000 cal. yr BP. With very few locations worldwide providing such long (> 10 000 year) records of relative sea level change, these are key to determining changes in global ice volume (Shennan *et al.* 2006). We show the

sea level index points from Shennan & Horton (2002) used in this study in Fig. 1 and list associated information in Table 4.

## 3 PROCESSING AND ANALYSIS

### 3.1 Continuous GPS

We utilized two independent CGPS processing strategies during our analysis of the daily GPS observation data from Great Britain and our reference frame networks. Following the examples of Geirsson *et al.* (2006) and Kierulf *et al.* (2008), by having multiple independent solutions (softwares/strategies) we are able to better understand processing strategy specific issues which may be of station-specific or solution-specific character. As we will show, at this stage it is important for the investigations to be carried out separately as the specific effects may be diluted by a combination process.

In the first strategy, we used the IESSG's GPS Analysis Software version 2.4 (GAS2.4; Stewart *et al.* 2002) to produce a series of daily double-difference (DD) regional network (RN) solutions (Teferle 2003; Teferle *et al.* 2006), below denoted as DDRN, for the period from 1997 March to 2005 December. In this case, the reference frame definition was effected through the inclusion of four European IGS stations, with well-determined station coordinates and velocities in the ITRF2000, as reference stations (Fig. 2).

In the second strategy, we used the IESSG's GNSS processing tools to run the Bernese software version 5.0 (BSW5.0; Dach *et al.* 2007) to produce a series of daily precise point positioning (PPP) globally transformed (GT) solutions (Teferle *et al.* 2007), below denoted as PPPGT, for the period from 2000 January to 2005 December. In this case, the reference frame definition was effected by using the 99 IGS reference frame stations included in IGB00 [IGSMail-4748 (2003); IGSMail-4928 (2004) on <http://igsceb.jpl.nasa.gov/mail/igsmail/igsmail.html>], the IGS realization of ITRF2000, as reference stations when computing the transformation parameters (Fig. 2).

After the CGPS processing, we formed coordinate time-series in ITRF2000 from the daily position solutions from both processing

**Table 4.** Information on sites with geological evidence for vertical crustal motions in Great Britain from Shennan & Horton (2002).

Site number	Site name	Lon (°)	Lat (°)	Rate (mm yr <sup>-1</sup> )	CGPS station	Distance (km)
3	Wick	356.88	58.45	0.42	THUR	38
5	Moray Firth	355.54	57.49	1.11	INVE	14
14	Aberdeen	358.01	57.33	0.69	ABER	21
11	NW Scotland (Arisaig)	354.15	56.91	1.01	MALG	11
	NW Scotland (Kenra)	354.16	56.76	1.00	MALG	28
22	SE Scotland	357.31	56.03	1.15	EDIN	39
20	Clyde	355.51	55.86	1.53	GLAS	12
28	South Solway Firth	356.83	54.90	0.87	CARL	15
30	Isle of Man	355.61	54.40	0.45	IOMN	7
					IOMS	38
25	NE England (South)	358.40	55.34	0.17	MORP	15
					NEWC	40
					NSTG	38
26	Tees	358.77	54.63	-0.17	NEWC	46
					NSTG	44
32	Lancashire	357.01	53.69	0.47	BLAK	11
					LIVE	26
33	Mersey	356.86	53.40	-0.21	DARE	34
					LIVE	10
35	Mid Wales	355.94	52.47	-0.38	ABYW	7
39	Fens	0.04	52.74	-0.37	KING	24
40	Norfolk	0.79	52.97	-0.60	KING	35
41	East Anglia	1.64	52.49	-0.60	LOWE	7
45	Essex	0.83	51.70	-0.85	SHEE	28
					COLC	23
46	Thames	0.31	51.46	-0.74	BARK	16
					SHEE	30
48	Sussex	0.33	50.84	-0.42	HERS	3
					HERT	3
49	Hampshire	358.65	50.80	-0.58	PMTG	17
					OSHQ	17
52	SW England (Cornwall)	354.52	50.13	-1.12	CAMB	15
					NEWL	5

Notes: Site number and name are given as published, the rate is the best estimate from Shennan & Horton (2002) and each site has been assigned CGPS stations close-by, with distance given.

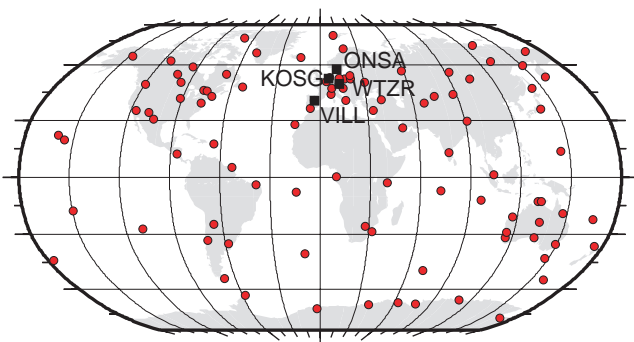


**Figure 2.** Reference frame stations used by the GAS2.4 DD regional network (squares) and the BSW5.0 globally transformed PPP (circles) solutions.

strategies for each of the CGPS stations. As such daily coordinate estimates have been shown to contain both temporal (e.g. Zhang *et al.* 1997; Mao *et al.* 1999; Williams 2003; Williams *et al.* 2004) and spatial (e.g. Wdowinski *et al.* 1997; Nikolaidis 2002; Dong *et al.* 2006) correlations we apply the following coordinate time-series analysis strategy.

To account for white and coloured noise (temporally correlated errors) in our coordinate time-series, we estimate, using the coor-

dinate time-series analysis software CATS (Williams 2008) which employs Maximum-Likelihood estimation (MLE), the parameters of a linear velocity, annual and semi-annual periodic terms, coordinate offset magnitudes, and the noise amplitudes for both white and coloured noise components. For the coloured noise component we choose flicker noise rather than another power-law process, as it has been shown to be widely present and a very appropriate model in CGPS coordinate time-series (Williams *et al.* 2004).

We use spatial filtering to reduce the spatially correlated features within the coordinate time-series, to improve the signal-to-noise ratio and station velocity uncertainties. Several spatial filtering methods involving simple unweighted and weighted stacking of daily residuals (e.g. Wdowinski *et al.* 1997; Nikolaidis 2002; Wdowinski *et al.* 2004) to more complex methods using Empirical Orthogonal Functions (Dong *et al.* 2006; Teferle *et al.* 2008) have been suggested. Following Teferle *et al.* (2006), we use the weighted stacking method to compute the daily common mode bias as the weighted mean coordinate residual from a selection of stations on a particular day and subtract this bias estimate from all unfiltered coordinate time-series, forming our filtered coordinate time-series.

It has been suggested that the coordinate time-series used for the computation of the common mode bias should be of high quality and not show any station-specific features (e.g. Wdowinski *et al.* 1997; Nikolaidis 2002; Teferle 2003). This ensures that the computed bias

only contains the common systematic variations of the coordinate time-series for a particular solution, as including a CGPS station behaving in an unusual manner, that is, due to large multipath or interference effects, would change the common mode estimate.

We argue that the effect of spatial filtering should merely be an improvement in the signal-to-noise ratio of the coordinate time-series and should not affect station velocity estimates such that a departure, that is, a de-coupling, from a given reference frame occurs (Wdowinski *et al.* 1997, 2004).

In previous studies (e.g. Nikolaidis 2002; Wdowinski *et al.* 1997, 2004), annual and semi-annual signals in the coordinate time-series were assumed to be part of the spatially correlated noise and hence were not modelled during the common mode bias computation, giving very smooth filtered coordinate time-series. Only Prawirodirdjo *et al.* (2006) argued to model both these signals when computing the daily common mode bias in order for the common mode to contain only noise and not predictable thermo-elastic signal.

It is also well known that annual and semi-annual signals in coordinate time-series can significantly bias station velocity estimates (Blewitt & Lavallée 2002). Assuming typical amplitudes of 2–4 and 1–2 mm for annual and semi-annual signals, Blewitt & Lavallée (2002) recommended that coordinate time-series with data time spans of less than 2.5 yr should not be considered for investigations and that for those with more than 2.5 yr the additional estimation of annual and semi-annual periodic terms would avoid the associated velocity bias. Furthermore, they stated that this simultaneous estimation may not be necessary, once time-series reached a span of more than 4.5 yr. With amplitudes of these signals often being significantly larger, it seems beneficial to continue to model these signals. Therefore, we argue that not including terms for these signals during the common mode bias computation may lead to a non-zero, artificial linear trend in the daily common mode bias time-series itself, which in turn will alter the trend of the filtered coordinate time-series thereby biasing station velocity estimates. Although we agree that as the velocity bias due to periodic signals reduces with increasing length of the time-series, this issue will become less prominent for spatial filtering of longer ones.

Another factor that can influence station velocity estimates of filtered coordinate time-series that has, so far, not been mentioned in the published literature and may thus be easily overlooked, is related to the way the station velocities are estimated in the common mode bias computation and thereafter in the analysis of the filtered coordinate time-series. Already Zhang *et al.* (1997) reported millimetre-level differences in their velocity estimates between those obtained from weighted least squares and more complex MLE. Similar differences between the two methods for computing station velocities were also reported in Teferle (2003) for some of the CGPS stations used in this study. As the station velocities are estimated several times during spatial filtering and the following analysis, it might seem convenient to mix both methods for computational efficiency and a faster analysis. Considering the above reported velocity differences, we argue that mixing of both methods potentially introduces a velocity bias. In order to avoid this bias, we consistently use MLE throughout the common mode bias estimation and the following analysis of the filtered coordinate time-series.

### 3.2 Absolute gravity

The processing and analysis of the AG measurements was carried out using the GAP (Gravity@POL) software developed at POL. The data from each drop were fit using least squares to an equation of

motion that includes a known a-priori vertical gravity gradient. The measurements of time were also corrected for the time delay due to the finite speed of light. The gravity gradients for Newlyn and Aberdeen have been measured using a relative spring gravimeter (Hopewell 2003). For Lerwick, a standard value equal to the free-air correction of  $-0.3086 \mu\text{Gal mm}^{-1}$  was used. Standard corrections were made for solid Earth tides, ocean tide loading, polar motion, and comparator response (Niebauer *et al.* 1995; Williams *et al.* 2001). Geophysical corrections were made for atmospheric loading using a single admittance factor and local pressure data. No attempt was made to correct for hydrological loading. Finally, the results were transferred from the height of observation to a common reference height. Data from each day were then combined into a single mean value. To estimate the AG rates and their uncertainties we used weighted least squares and assumed the gravity noise budget consisted of an instrumental set up error ( $1.6 \mu\text{Gal}$ ; Van Camp *et al.* 2005) that was common to all days during the measurement campaign, a statistical error based on the daily drop-to-drop standard deviations, and a long period noise that was modelled as a first-order Gauss Markov process (Van Camp *et al.* 2005). In an additional step, the error bars for each measurement campaign are scaled by the reduced chi-square fit to the mean value over those days in an attempt to reflect the short-term day-to-day scatter.

To obtain an estimate of the vertical station velocity and associated uncertainty we need to apply a gravity/uplift ratio. This ratio is dependent on many factors, not least the physical processes causing the deformation. Estimates from various models range from  $-0.15 \mu\text{Gal mm}^{-1}$  (Wahr *et al.* 1995) to  $-0.26 \mu\text{Gal mm}^{-1}$  (de Linage *et al.* 2007). Computed ratios from data range from  $-0.18 \pm 0.03 \mu\text{Gal mm}^{-1}$  (Lambert *et al.* 2006) through  $-0.20 \pm 0.06 \mu\text{Gal mm}^{-1}$  to  $-0.24 \pm 0.13 \mu\text{Gal mm}^{-1}$  (Mazzotti *et al.* 2007). We used a gravity/uplift ratio of  $-0.2 \mu\text{Gal mm}^{-1}$  or  $-5 \text{ mm } \mu\text{Gal}^{-1}$  which is the mean of all these estimates. We do not, as yet, propagate uncertainties of the ratio, into the vertical station velocities. Neither are we prepared, given the scale of the deformation expected in Great Britain compared to Fennoscandia or North America, to attempt to estimate a ratio from the GPS and AG data sets.

### 3.3 Geological information

We obtain an estimate of relative vertical crustal motion from the geological information by fitting a linear trend to relative sea level data from as early as 4000 cal. yr BP to the present day (Shennan 1989; Shennan & Horton 2002). In some cases the oldest data are younger than 4000 cal. yr BP and so the regression is over a shorter and more recent period. In applying this procedure, we assume that there has been a negligible secular height shift of the sea surface over the period for which data exist at a given locality. Specifically, we have assumed that there is no significant ocean surface height change due to contemporaneous mass changes in continental ice sheets and glaciers or due to ocean water density changes.

GIA can lead to ocean surface height changes in the UK through two processes. One is regional perturbations to the gravity field due to vertical land motion. The corresponding geoid height shift is spatially correlated with the land motion signal, but is more than an order of magnitude smaller (i.e.  $<0.1 \text{ mm yr}^{-1}$  at most sites) and so is not accounted for here. A second process that leads to a global-scale lowering of the ocean surface following the last glacial maximum is known as ocean siphoning (Mitrovica & Peltier 1991; Mitrovica & Milne 2002). This process is due to increasing ocean basin volume associated with vertical motion of the ocean



**Table 5.** GPS results related acronyms and definitions used throughout this study.

Acronym	Definition
GAS2.4	GPS Analysis Software Version 2.4
BSW5.0	Bernese GPS Software Version 5.0
DD	Double-difference
DDRN	GAS2.4 double-difference regional network
DDRNU	Unfiltered GAS2.4 DD regional network coordinate time-series
DDRNF	Filtered GAS2.4 DD regional network coordinate time-series
PPP	Precise point positioning
PPPGT	BSW5.0 globally transformed precise point positioning
PPPGTU	Unfiltered BSW5.0 globally transformed PPP coordinate time-series
PPPGTF	Filtered BSW5.0 globally transformed PPP coordinate time-series

floor. Current GIA models predict this lowering to be about  $0.2\text{--}0.4\text{ mm yr}^{-1}$  during the late Holocene (e.g. Peltier 2001) and so estimates of vertical crustal motions inferred from relative sea level data will be biased high (i.e. more positive) by this amount. Since the magnitude of this effect is relatively small, we do not explicitly revise the values of vertical crustal motion estimated from the relative sea level data. However, in the data comparisons that follow, we are mindful that the inferred estimates have a positive bias by a few tenths of a millimetres per year.

## 4 RESULTS

This section presents the horizontal and vertical station velocity estimates from CGPS. Using these estimates we carry out comparisons to quantify the effects of the two independent CGPS processing strategies, spatial filtering, and reference frame implementations. Following this we present the vertical station velocity estimates from AG and the geological information before we start the interpretation of the station velocity estimates as crustal motions. Based on our horizontal station velocity estimates we investigate the suitability of the current CGPS network to provide estimates of horizontal crustal motion for geophysical interpretations, i.e. plate motions or on a more demanding scale, the motions associated with GIA processes. Using the vertical station velocity estimates we carry out a comparison of these to those from AG, compute AG-aligned CGPS vertical station velocities, and compare these to vertical crustal motions from the geological evidence.

For convenience, we list the definitions of relevant acronyms which will be used extensively in the following sections in Table 5.

### 4.1 Continuous GPS

We used the daily coordinate estimates for both CGPS processing strategies to form coordinate time-series for 39 of the 44 CGPS stations in Table 1. As outlined above, we used spatial filtering based on weighted stacking to obtain filtered coordinate time-series for both independent CGPS processing strategies.<sup>1</sup> In this manner, we arrived at four different solutions, namely the unfiltered and filtered GAS2.4 DD regional network coordinate time-series solutions, below denoted as solutions DDRNU and DDRNF, and the unfiltered and filtered BSW5.0 globally transformed PPP coordinate time-series solutions, below denoted as solutions PPPGTU and PPPGTF.

All four solutions use data for the period up to 2005 December 31, but differ in their time span as outlined previously. For solutions

<sup>1</sup> Details on the particular implementation of spatial filtering can be found in Appendix A.

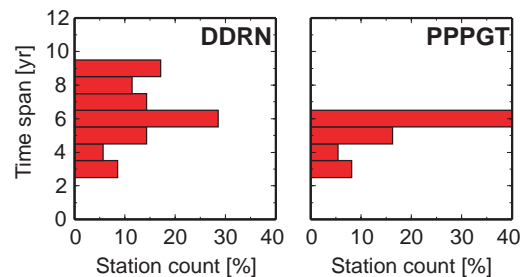


**Figure 3.** Distribution of coordinate time-series lengths for the GAS2.4 DD regional network (DDRN) and BSW5.0 globally transformed PPP (PPPGT) solutions.

PPPGTU and PPPGTF we considered the currently available satellite orbit and clock products to be of not good enough quality prior to 2000 (Teferle *et al.* 2007). From Fig. 3, it is clear that over 70 per cent of our coordinate time-series span a period of more than 5 yr.

We show the unfiltered and spatially filtered coordinate time-series for each CGPS station for solutions DDRNU, DDRNF, PPPGTU and PPPGTF, respectively, in Figs S1–S4 of the Supporting Information.

#### 4.1.1 Horizontal station velocities

We obtained horizontal station velocity estimates and associated uncertainties from the MLE for all four coordinate time-series solutions (Table 6 and Table S1 of the Supporting Information).

In the case of solutions DDRNU and DDRNF we excluded BLAK, COLC, HERT, LOND and OSHQ due to network size limitations in the GAS2.4 software while for the solutions PPPGTU and PPPGTF, BRST and RAL1 gave unreasonably noisy daily coordinate estimates. HEMS was excluded due to its short data span, as it was decommissioned in 2001.

We draw several general conclusions from Table 6. First of all, the four solutions show excellent overall agreement in their velocity estimates, well within their uncertainties (all uncertainties here and throughout this study are  $1\sigma$ ). Second, there is a reduction in the range of the velocity uncertainties for solutions DDRNF and PPPGTF compared to those of solutions DDRNU and PPPGTU, respectively, which is a first indication of the effectiveness of the spatial filter.

To investigate the effect of the CGPS processing strategy on the horizontal velocities we computed the mean of the velocity differences (and their corresponding standard deviations) between solutions DDRNU and PPPGTU to be  $-0.0 \pm 0.4$  and  $0.1 \pm 0.7\text{ mm yr}^{-1}$ , for north and east, respectively. Similarly, we computed the mean of the velocity differences (and their corresponding

**Table 6.** CGPS horizontal station velocity estimates for unfiltered GAS2.4 DD regional network (DDRNU), unfiltered BSW5.0 globally transformed PPP (PPPGTU), filtered GAS2.4 DD regional network (DDRNF) and filtered BSW5.0 globally transformed PPP (PPPGTF) coordinate time-series solutions. All values are in  $\text{mm yr}^{-1}$ . Uncertainties are  $1\sigma$ .

	DDRNU		PPPGTU		DDRNF		PPPGTF	
	North ( $\text{mm yr}^{-1}$ )	East ( $\text{mm yr}^{-1}$ )	North ( $\text{mm yr}^{-1}$ )	East ( $\text{mm yr}^{-1}$ )	North ( $\text{mm yr}^{-1}$ )	East ( $\text{mm yr}^{-1}$ )	North ( $\text{mm yr}^{-1}$ )	East ( $\text{mm yr}^{-1}$ )
CGPS@TG stations								
ABER	14.7 ± 0.3	15.3 ± 0.6	14.9 ± 0.3	15.1 ± 0.5	14.7 ± 0.2	15.1 ± 0.3	14.6 ± 0.2	15.4 ± 0.3
BRST	16.0 ± 0.4	17.6 ± 0.7	n/a	n/a	16.0 ± 0.4	17.7 ± 0.6	n/a	n/a
LIVE	13.6 ± 0.4	17.3 ± 0.7	13.3 ± 0.5	16.8 ± 0.7	13.5 ± 0.3	17.1 ± 0.3	13.3 ± 0.4	16.8 ± 0.3
LOWE	14.8 ± 0.2	18.4 ± 0.4	15.0 ± 0.2	18.0 ± 0.4	14.9 ± 0.2	18.6 ± 0.3	15.0 ± 0.1	18.0 ± 0.2
NEWL	16.1 ± 0.3	16.7 ± 0.5	15.7 ± 0.3	16.5 ± 0.4	16.0 ± 0.2	16.7 ± 0.4	15.7 ± 0.2	16.5 ± 0.2
NSTG	14.5 ± 0.3	17.3 ± 0.7	15.2 ± 0.4	16.3 ± 0.6	14.7 ± 0.2	17.4 ± 0.6	15.1 ± 0.2	16.3 ± 0.5
PMTG	17.4 ± 0.6	19.6 ± 0.6	16.1 ± 0.5	19.2 ± 0.5	17.5 ± 0.5	20.5 ± 0.4	16.3 ± 0.4	19.5 ± 0.3
SHEE	15.3 ± 0.3	18.0 ± 0.4	14.9 ± 0.4	17.1 ± 0.5	15.4 ± 0.3	17.9 ± 0.2	14.9 ± 0.4	17.1 ± 0.3
Other scientific CGPS stations								
ABYW	15.9 ± 0.2	17.9 ± 0.5	15.9 ± 0.3	17.2 ± 0.4	16.0 ± 0.1	17.8 ± 0.3	15.9 ± 0.1	17.1 ± 0.2
BARK	15.3 ± 0.5	17.7 ± 0.4	15.5 ± 0.6	16.8 ± 0.6	15.3 ± 0.5	17.7 ± 0.4	15.6 ± 0.6	16.9 ± 0.4
CAMB	16.0 ± 0.3	17.3 ± 0.5	15.9 ± 0.3	16.7 ± 0.4	15.9 ± 0.2	17.3 ± 0.2	15.8 ± 0.1	16.5 ± 0.2
CARD	15.4 ± 0.5	16.7 ± 1.0	16.1 ± 1.0	18.0 ± 2.4	15.6 ± 0.3	18.0 ± 0.6	14.7 ± 0.9	17.9 ± 2.1
DUNK	15.7 ± 0.6	17.4 ± 0.7	15.5 ± 0.3	17.3 ± 0.5	15.7 ± 0.4	17.9 ± 0.4	15.5 ± 0.1	17.1 ± 0.2
HEMS	14.3 ± 0.8	20.4 ± 1.0	n/a	n/a	14.2 ± 0.6	19.5 ± 0.6	n/a	n/a
HERS	14.4 ± 0.4	17.9 ± 0.6	15.0 ± 0.4	17.2 ± 0.6	14.4 ± 0.3	18.0 ± 0.5	15.0 ± 0.3	17.1 ± 0.3
HERT	n/a	n/a	14.9 ± 0.6	16.4 ± 1.1	n/a	n/a	14.8 ± 0.4	16.5 ± 0.9
HURN	14.8 ± 0.4	17.0 ± 0.9	14.6 ± 0.3	17.1 ± 0.4	15.1 ± 0.3	17.1 ± 0.3	14.3 ± 0.2	17.3 ± 0.1
IESG	14.5 ± 0.2	17.7 ± 0.3	14.8 ± 0.2	17.0 ± 0.4	14.5 ± 0.1	17.7 ± 0.2	14.8 ± 0.1	17.0 ± 0.1
LERW	16.0 ± 0.3	13.7 ± 0.6	16.0 ± 0.3	13.7 ± 0.3	16.0 ± 0.2	13.7 ± 0.3	15.9 ± 0.2	13.6 ± 0.2
MORP	16.1 ± 0.4	14.6 ± 0.6	16.5 ± 0.9	16.4 ± 1.1	16.0 ± 0.4	14.4 ± 0.5	16.7 ± 0.8	16.7 ± 0.9
NPLD	15.1 ± 0.4	17.2 ± 0.5	14.9 ± 0.4	17.0 ± 0.5	15.0 ± 0.2	17.2 ± 0.4	14.6 ± 0.2	17.0 ± 0.3
PERS	15.4 ± 0.3	16.0 ± 0.5	15.7 ± 0.4	15.8 ± 0.6	15.5 ± 0.1	16.6 ± 0.3	15.4 ± 0.2	16.0 ± 0.4
RAL1	15.0 ± 0.5	17.0 ± 0.7	n/a	n/a	15.2 ± 0.1	17.8 ± 0.4	n/a	n/a
SUNB	15.4 ± 0.3	18.1 ± 0.6	15.5 ± 0.4	16.6 ± 0.5	15.4 ± 0.2	18.1 ± 0.5	15.4 ± 0.3	16.5 ± 0.4
Network RTK CGPS stations								
BLAK	n/a	n/a	15.1 ± 0.4	16.6 ± 0.5	n/a	n/a	15.0 ± 0.2	16.4 ± 0.2
CARL	15.1 ± 0.4	15.5 ± 0.6	15.1 ± 0.3	15.8 ± 0.4	15.2 ± 0.1	16.2 ± 0.2	15.2 ± 0.1	15.9 ± 0.1
COLC	n/a	n/a	15.4 ± 0.3	17.3 ± 0.4	n/a	n/a	15.4 ± 0.1	17.6 ± 0.2
DARE	15.6 ± 0.3	16.5 ± 0.6	15.5 ± 0.3	16.5 ± 0.4	15.7 ± 0.1	16.8 ± 0.2	15.7 ± 0.1	16.4 ± 0.1
EDIN	15.4 ± 0.4	15.4 ± 0.6	15.3 ± 0.3	15.2 ± 0.4	15.4 ± 0.3	15.8 ± 0.2	15.5 ± 0.1	15.3 ± 0.1
GLAS	15.8 ± 0.3	14.3 ± 0.6	15.6 ± 0.3	14.9 ± 0.4	15.8 ± 0.2	14.8 ± 0.3	15.8 ± 0.1	14.9 ± 0.2
INVE	15.4 ± 0.4	15.7 ± 0.7	15.6 ± 0.3	15.1 ± 0.4	15.4 ± 0.3	15.7 ± 0.4	15.5 ± 0.1	15.2 ± 0.3
IOMN	15.2 ± 0.6	14.7 ± 0.8	15.6 ± 0.5	15.6 ± 0.5	15.1 ± 0.6	15.8 ± 0.4	15.3 ± 0.4	15.6 ± 0.2
IOMS	15.6 ± 0.4	14.4 ± 0.7	15.7 ± 0.3	15.7 ± 0.5	15.6 ± 0.3	15.8 ± 0.2	15.5 ± 0.1	15.8 ± 0.2
KING	15.2 ± 0.2	17.5 ± 0.4	15.2 ± 0.2	17.1 ± 0.4	15.2 ± 0.1	17.7 ± 0.2	15.2 ± 0.1	17.2 ± 0.1
LEED	15.4 ± 0.3	16.8 ± 0.5	15.3 ± 0.2	16.3 ± 0.4	15.3 ± 0.1	16.9 ± 0.1	15.3 ± 0.1	16.4 ± 0.1
LOND	n/a	n/a	15.0 ± 0.3	18.2 ± 0.6	n/a	n/a	15.0 ± 0.3	18.3 ± 0.5
MALG	15.0 ± 0.6	13.5 ± 1.0	15.7 ± 0.3	14.5 ± 0.4	15.2 ± 0.3	14.4 ± 0.5	15.7 ± 0.1	14.1 ± 0.2
NEWC	15.2 ± 0.3	16.2 ± 0.5	15.2 ± 0.3	15.8 ± 0.4	15.2 ± 0.1	16.3 ± 0.2	15.1 ± 0.1	15.9 ± 0.2
OSHQ	n/a	n/a	15.1 ± 0.3	17.2 ± 0.4	n/a	n/a	15.1 ± 0.1	17.2 ± 0.2
THUR	15.8 ± 0.4	14.0 ± 0.7	15.6 ± 0.3	14.6 ± 0.4	15.7 ± 0.2	14.4 ± 0.3	15.7 ± 0.2	14.5 ± 0.2

standard deviations) between solutions DDRNF and PPPGTF to be  $0.1 \pm 0.4$  and  $0.4 \pm 0.7 \text{ mm yr}^{-1}$ , for north and east, respectively. Again, we find excellent overall agreement between the different solutions, that is, the CGPS processing strategies.

We further investigated the effect of spatial filtering on the horizontal velocities by computing the mean of the velocity differences (and their corresponding standard deviations) between solutions DDRNU and DDRNF to be  $-0.0 \pm 0.1$  and  $-0.3 \pm 0.5 \text{ mm yr}^{-1}$ , for north and east, respectively, and between solutions PPPGTU and PPPGTF to be  $0.1 \pm 0.3$  and  $-0.0 \pm 0.1 \text{ mm yr}^{-1}$ , for north and east, respectively. We find excellent overall agreement between the velocity estimates of the unfiltered and filtered coordinate time-series. Therefore, we conclude that we have largely avoided de-coupling

our horizontal station velocity estimates from their given reference frames.

Although we have shown excellent agreements between the four coordinate time-series solutions, with standard deviations in the velocity differences of less than  $0.4 \text{ mm yr}^{-1}$  for the north and less than  $0.7 \text{ mm yr}^{-1}$  for the east component, there are several stations for which the velocity differences are greater than  $1.0 \text{ mm yr}^{-1}$  in at least one comparison. We can list those stations to be CARD, IOMN, IOMS, MORP, NSTG, PMTG and SUNB. In almost all cases the large velocity differences are in the east component of the involved station. We associate the discrepancies for CARD with a shorter coordinate time-series of only 2.9 yr and a data gap in early 2005; for IOMN and IOMS with their east velocity estimate in

solution DDRNU, which might be affected by data gaps during 2005; for MORP and NSTG with their general data quality issues (Teferle 2003); for PMTG potentially due to a shorter coordinate time-series and/or our modelling, and for SUNB with the significantly different data span used by both CGPS processing strategies, that is, solutions DDRNU and DDRNF were based on 8.7 yr whereas solutions PPPGTU and PPPGTF were based on only 6 yr. Considering these findings we will concentrate on solutions DDRNF and PPPGTF in our discussions of the horizontal crustal motions in Section 4.4.

#### 4.1.2 Vertical station velocities

It is generally accepted that the vertical component of CGPS coordinate time-series is less well determined than the horizontal components, hence we do not expect the excellent agreements found in the north and east velocity estimates between the four solutions to be repeated in our vertical station velocity estimates. Additionally, the data time span will have a more significant effect on the estimates and as the coordinate time-series for solutions PPPGTU and PPPGTF are capped at 5 yr, this will affect the comparison between the two CGPS processing strategies. Furthermore, any other CGPS processing strategy-specific effects may be more pronounced in the vertical component and affect our station velocity estimates.

We obtained the vertical station velocity estimates and their associated uncertainties from the MLE for all four coordinate time-series solutions (Table 7 and Table S2 of the Supporting Information).

The velocities range from  $-2.8$  to  $3.3$ ,  $-2.0$  to  $1.5$ ,  $-2.6$  to  $2.3$  and  $-1.7$  to  $1.6$   $\text{mm yr}^{-1}$  for solutions DDRNU, PPPGTU, DDRNF and PPPGTF, respectively. This suggests not only that the spread is somewhat processing strategy dependent, but also that spatial filtering reduces the spread for both strategies. Similarly, we show the vertical station velocity uncertainties for solutions DDRNU, PPPGTU, DDRNF and PPPGTF to range from  $\pm 0.5$  to  $\pm 2.4$ ,  $\pm 0.7$  to  $\pm 5.5$ ,  $\pm 0.4$  to  $\pm 1.9$  and  $\pm 0.2$  to  $\pm 5.1$   $\text{mm yr}^{-1}$ , respectively. Although these ranges appear to be quite large, it is shown that the upper bounds in all ranges are related to station CARD. We compute the mean of the velocity uncertainties (and their corresponding standard deviations) for solutions DDRNU, PPPGTU, DDRNF and PPPGTF to be  $0.9 \pm 0.4$ ,  $1.1 \pm 0.8$ ,  $0.6 \pm 0.3$  and  $0.7 \pm 0.8$   $\text{mm yr}^{-1}$ , respectively. We point out that, first, solutions DDRNU and DDRNF seem to be more homogeneous than solutions PPPGTU and PPPGTF, as both the mean velocity uncertainties and their standard deviations are smaller, and, secondly, that spatial filtering clearly improved the homogeneity of solutions DDRNF and PPPGTF by reducing the mean velocity uncertainties.

Considering the mean of the vertical station velocity differences (and their corresponding standard deviations) between solutions DDRNU and DDRNF, and solutions PPPGTU and PPPGTF, we compute these to be  $0.2 \pm 0.6$  and  $-0.1 \pm 0.5$   $\text{mm yr}^{-1}$ , respectively, confirming that the effect of spatial filtering on the vertical station velocity estimates is negligible, and that we have again avoided a de-coupling from the given reference frame. However, when considering the mean of the velocity differences (and their corresponding standard deviations) between solutions DDRNU and PPPGTU and solutions DDRNF and PPPGTF, we compute these to be  $1.1 \pm 1.1$  and  $0.7 \pm 0.6$   $\text{mm yr}^{-1}$ , respectively, which suggests a systematic bias in the vertical station velocity estimates between the regional and global solutions for both the unfiltered and filtered cases. Similar biases between different solutions and/or their

**Table 7.** CGPS vertical station velocity estimates for unfiltered GAS2.4 DD regional network (DDRNU), unfiltered BSW5.0 globally transformed PPP (PPPGTU), filtered GAS2.4 DD regional network (DDRNF) and filtered BSW5.0 globally transformed PPP (PPPGTF) coordinate time-series solutions. All values are in  $\text{mm yr}^{-1}$ . Uncertainties are  $1\sigma$ .

	DDRNU ( $\text{mm yr}^{-1}$ )	PPPGTU ( $\text{mm yr}^{-1}$ )	DDRNF ( $\text{mm yr}^{-1}$ )	PPPGTF ( $\text{mm yr}^{-1}$ )
CGPS@TG stations				
ABER	$1.6 \pm 0.7$	$-0.9 \pm 1.0$	$1.3 \pm 0.3$	$-0.3 \pm 0.4$
BRST	$1.5 \pm 0.8$	n/a	$1.3 \pm 0.6$	n/a
LIVE	$0.1 \pm 0.9$	$0.8 \pm 1.1$	$1.1 \pm 0.3$	$1.1 \pm 0.4$
LOWE	$0.0 \pm 0.6$	$-0.6 \pm 0.7$	$0.0 \pm 0.5$	$-0.6 \pm 0.3$
NEWL	$1.1 \pm 1.1$	$0.1 \pm 0.8$	$0.6 \pm 0.9$	$0.1 \pm 0.7$
NSTG	$0.5 \pm 1.0$	$0.1 \pm 1.1$	$0.1 \pm 0.8$	$0.3 \pm 0.5$
PMTG	$0.7 \pm 1.0$	$-0.6 \pm 0.9$	$0.5 \pm 0.7$	$-0.6 \pm 0.4$
SHEE	$0.4 \pm 0.6$	$-0.2 \pm 0.9$	$0.5 \pm 0.5$	$-0.2 \pm 0.6$
Other scientific CGPS stations				
ABYW	$0.6 \pm 0.9$	$-0.5 \pm 0.8$	$0.9 \pm 0.6$	$-0.7 \pm 0.4$
BARK	$-0.2 \pm 0.5$	$-0.6 \pm 0.9$	$-0.1 \pm 0.5$	$-0.6 \pm 0.5$
CAMB	$0.8 \pm 0.8$	$-1.5 \pm 0.9$	$0.5 \pm 0.4$	$-0.8 \pm 0.6$
CARD	$2.2 \pm 2.4$	$-1.4 \pm 5.5$	$0.1 \pm 1.9$	$-1.5 \pm 5.1$
DUNK	$0.5 \pm 0.6$	$-0.2 \pm 1.5$	$0.2 \pm 0.4$	$-0.8 \pm 1.1$
HEMS	$0.4 \pm 1.5$	n/a	$1.7 \pm 1.2$	n/a
HERS	$-0.4 \pm 0.9$	$0.4 \pm 1.0$	$-0.3 \pm 0.8$	$0.1 \pm 0.6$
HERT	n/a	$1.4 \pm 1.8$	n/a	$0.4 \pm 1.1$
HURN	$0.7 \pm 0.8$	$-0.2 \pm 0.9$	$0.3 \pm 0.5$	$-0.1 \pm 0.4$
IESG	$-0.9 \pm 0.6$	$-0.6 \pm 0.7$	$-0.8 \pm 0.3$	$-0.6 \pm 0.2$
LERW	$0.9 \pm 0.8$	$-0.1 \pm 0.7$	$0.8 \pm 0.5$	$-0.1 \pm 0.5$
MORP	$0.6 \pm 1.4$	$-2.0 \pm 2.5$	$0.3 \pm 1.1$	$-1.7 \pm 2.0$
NPLD	$0.9 \pm 0.7$	$-1.8 \pm 1.0$	$0.1 \pm 0.5$	$-0.3 \pm 0.4$
PERS	$0.2 \pm 0.7$	$-1.3 \pm 1.0$	$0.0 \pm 0.4$	$-0.5 \pm 0.3$
RAL1	$-2.8 \pm 1.6$	n/a	$-2.6 \pm 1.1$	n/a
SUNB	$-0.9 \pm 0.7$	$-1.0 \pm 0.9$	$-0.8 \pm 0.6$	$-1.2 \pm 0.6$
Network RTK CGPS stations				
BLAK	n/a	$0.9 \pm 1.2$	n/a	$0.5 \pm 0.4$
CARL	$1.8 \pm 0.8$	$0.3 \pm 0.8$	$1.2 \pm 0.4$	$0.7 \pm 0.3$
COLC	n/a	$-0.7 \pm 0.8$	n/a	$-0.1 \pm 0.3$
DARE	$1.5 \pm 0.7$	$0.0 \pm 0.8$	$1.0 \pm 0.5$	$0.5 \pm 0.3$
EDIN	$2.3 \pm 0.8$	$1.5 \pm 0.7$	$2.2 \pm 0.5$	$1.6 \pm 0.3$
GLAS	$2.5 \pm 0.7$	$1.0 \pm 0.8$	$2.3 \pm 0.4$	$1.0 \pm 0.3$
INVE	$0.9 \pm 0.8$	$0.1 \pm 0.8$	$1.0 \pm 0.5$	$0.1 \pm 0.5$
IOMN	$2.2 \pm 1.3$	$0.8 \pm 1.2$	$1.7 \pm 0.9$	$1.2 \pm 0.8$
IOMS	$1.5 \pm 1.0$	$0.0 \pm 0.8$	$0.9 \pm 0.6$	$0.4 \pm 0.3$
KING	$-0.3 \pm 0.6$	$-0.3 \pm 0.7$	$-0.3 \pm 0.4$	$-0.5 \pm 0.2$
LEED	$-0.3 \pm 0.5$	$0.0 \pm 0.7$	$0.0 \pm 0.3$	$-0.3 \pm 0.2$
LOND	n/a	$-0.9 \pm 1.4$	n/a	$-0.4 \pm 1.1$
MALG	$3.2 \pm 1.8$	$0.7 \pm 0.8$	$2.2 \pm 1.0$	$0.9 \pm 0.4$
NEWC	$0.5 \pm 0.7$	$1.4 \pm 1.0$	$0.8 \pm 0.4$	$0.9 \pm 0.6$
OSHQ	n/a	$-0.1 \pm 0.7$	n/a	$-0.3 \pm 0.4$
THUR	$2.2 \pm 0.9$	$0.2 \pm 0.9$	$1.7 \pm 0.4$	$0.4 \pm 0.5$

reference frame implementations have previously been reported on (e.g. Mazzotti *et al.* 2008; Teferle *et al.* 2008).

Considering the vertical station velocity estimates and their uncertainties in Table 7 on a station-by-station basis, then we can say that for CARD, HEMS, HERT and RAL1, and potentially also for BLAK, IOMN, IOMS and MALG the velocity estimates are affected by the shorter data time span. Besides this, there have been issues with data quality for ABER, MORP and NSTG (Teferle 2003; Teferle *et al.* 2003). In addition to the stations already mentioned, there are two CGPS stations which exhibit velocity differences of greater than  $1$   $\text{mm yr}^{-1}$  between one of their unfiltered and filtered solutions, these are LIVE and NPLD.

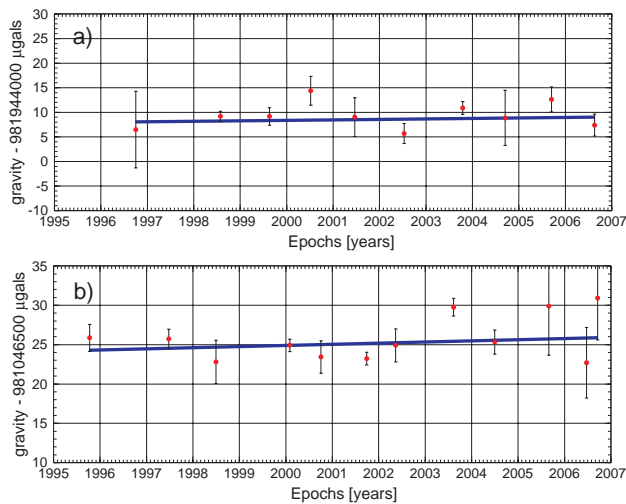


**Figure 4.** Absolute gravity time-series for Lerwick (a), and Newlyn (b) AG stations used in this study. The red dots show the AG estimates of absolute gravity and the blue line represents the best-fitting linear trend in the absolute gravity estimates.

Based on the results presented in this section, we conclude that parallel processing with two or more independent CGPS processing strategies is essential in order to make the best use of stations that have data of varying quality. We note that when considered together with the vertical crustal motion estimates from the geological information (below), it is suggested that the more realistic solutions for ABER, DUNK and NPLD might be DDRNU and DDRNF whereas the more realistic solutions for MALG, NSTG and LIVE might be PPPGTU and PPPGTF.

#### 4.2 Absolute gravity

The AG time-series for Newlyn and Aberdeen are shown in Fig. 4. A visual inspection shows that there appears to be a positive change in AG at both Lerwick and Newlyn AG stations, which would equate to subsidence at those sites. We do not show the time-series for the AG station in Aberdeen in Fig. 4 as we see a very bimodal distribution in the results. This could be a result of local hydrological conditions at the site. The church in which the AG measurements are made, is at the edge of the granitic bedrock in Aberdeen on a sliver of conglomerate and situated next to alluvial sediments in the valley of the river Don. We assume that due to local hydrological conditions, our current AG results for this station are not reliable and would need to be treated with extreme caution. In the future, we may need to locate a new AG site in Aberdeen or perhaps measure in winter when the soil may become completely saturated giving a more constant gravity effect (Lambert *et al.* 2006). Therefore, we did not include the estimated changes in AG or vertical station velocity for the AG station in Aberdeen in our further analysis.

As stated in above, we have not attempted to correct for any hydrological variations. At Newlyn and Lerwick we are confident that the hydrological conditions produce only minimal annual variations that are further limited by the fact that we measure annually at nearly the same time each year. The church at Newlyn is built on solid granite bedrock with minimal soil cover and the basement of the school in Lerwick is surrounded by a concrete cap, which should minimize rainfall infiltration into the soil in the nearby vicinity. However, we do intend to study the hydrological conditions at all three sites in the future. For Lerwick and Newlyn, we estimate changes in AG and

their uncertainties of  $+0.10 \pm 0.19$  and  $+0.14 \pm 0.14 \mu\text{Gal yr}^{-1}$ , and of vertical station velocities and their uncertainties of  $-0.5 \pm 1.0$  and  $-0.7 \pm 0.7 \text{ mm yr}^{-1}$ , respectively. The increased noise in the last few Newlyn campaigns reflects an increase in day-to-day scatter of those data sets. This can be partly explained by a noticeable increase in the scatter of the superspring in FG5-103 over the last few years. However, since no comparable increase is evident in the results at Lerwick another, so far unexplained, factor must also be involved that is perhaps local to Newlyn.

At this stage, we point to Appendix B which discusses the levelling ties between the AG station and the TG benchmarks at Newlyn, and serves to validate the AG-alignment procedure carried out later.

#### 4.3 Geological information

Shennan & Horton (2002) and Shennan *et al.* (2006) obtained estimates of vertical crustal motions based on Holocene sea level data for over 50 locations in Great Britain to form a map. For completeness we list a subset of these sites, which are of interest for this study owing to their proximity to the CGPS and AG stations, in Table 4 together with their estimates of vertical crustal motion.

#### 4.4 Horizontal crustal motions

We obtain estimates of horizontal crustal motions for Great Britain from our horizontal CGPS station velocity estimates if we assume that the apparent station displacement is solely due to motion of the Earth's crust and does not include any movement associated with the location or monumentation of the CGPS station. In this case Figs 5(a) and (b) show the absolute horizontal station velocity estimates for solutions DDRNF and PPPGTF, respectively. Also shown are velocities computed for the CGPS stations in Great Britain based on the ITRF2000 plate motion model (Altamimi *et al.* 2002, Table S3 of the Supporting Information).

From Figs 5(a) and (b), we can see that there is generally good agreement in both direction and magnitude of the velocity vectors between both solutions and the model. However, a better impression of the agreement at a particular CGPS station is gained by looking at the residual velocities, i.e. after subtracting the ITRF2000 plate motion model velocities (Altamimi *et al.* 2002). The residual velocities will show to what extent the CGPS stations move according to the plate motion model, but also, more importantly at this stage, will show which stations do not behave in an expected manner. As mentioned previously, we expect a horizontal GIA signal at the  $1\text{--}2 \text{ mm yr}^{-1}$  level (Bradley *et al.* 2009) to be superimposed onto the observed plate motion. In addition, since only a few CGPS stations in Great Britain are believed to have appropriate geodetic-quality monumentation, we cannot ignore the possibility of additional movements due to local factors.

Since we do not estimate integer ambiguities in either solution, we would expect the east component velocities to be somewhat biased (e.g. Johansson *et al.* 2002). Therefore, we do not investigate the plate motion signal in Great Britain any further at this stage, but instead try to identify those stations that seem to behave in a consistent manner, ensuring their use in our investigations into the horizontal component of the GIA signal.

Figs 5(c) and (d) show the residual velocity vectors for solutions DDRNF and PPPGTF given in Table 8. Comparing the horizontal velocity vectors from both solutions, there are a number of stations, which show excellent agreement with the ITRF2000 plate motion

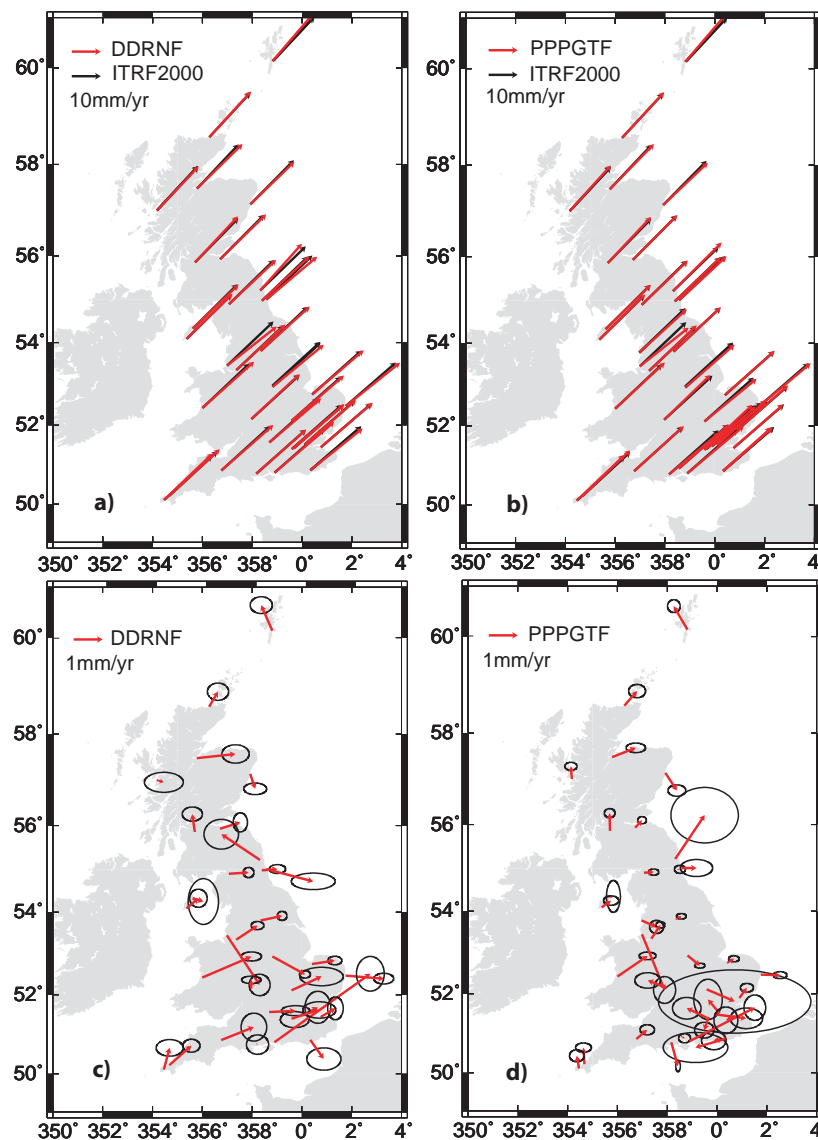


**Figure 5.** Absolute and residual horizontal station velocities for filtered GAS2.4 DD regional network (DDRNF) and BSW5.0 globally transformed PPP (PPPGTF) time-series solutions. Computed horizontal station velocities are compared to the ITRF2000 plate motion model velocities and residual velocities have been computed by subtracting the ITRF2000 plate motion model velocities from the computed velocities. Note the change in scale for the residual velocities. Error ellipses are at the 95 per cent confidence level and their scale is that of the residual velocities.

model. There are obviously also stations with fewer similarities to the plate motion model in their residuals and some showing much larger residuals. Stations with residuals visibly larger than  $1 \text{ mm yr}^{-1}$  in both solutions are ABYW, LIVE, MORP and PMTG, while NSTG shows a large residual only for solution DDRNF. However, it is important to note that we have already identified these CGPS stations as likely to give unreliable results based on their data quality.

From Figs 5(c) and (d) as well as Table 8 it is noticeable that for a number of stations there are large differences in their error ellipses and uncertainties, respectively. Primarily, these depend on the length of the coordinate time-series and magnitude of their day-to-day scatter, which is a reflection of the amount of noise and the ratio of its white and coloured noise components. Ultimately, the uncertainties will also depend on how well a particular coordinate time-series can be modelled, as velocity, offsets, periodic signals, and noise, and on how much spatial filtering improves the time-series and subsequently the final model fit. A more detailed investigation of

the stochastic properties of the coordinate time-series on station-specific and solution-specific effects would go beyond the scope of this study.

From a geophysical perspective, the estimates of absolute and residual horizontal crustal motion confirm that overall Great Britain behaves in a consistent manner with Eurasia plate motion and that there is, with the current resolution, no discernible internal deformation in the horizontal velocity field over the area investigated. Contrary to previous studies (Nocquet *et al.* 2001; Nocquet & Calais 2003), our results do not confirm any residual motion of southeast England with respect to Eurasia.

Further investigation reveals a distribution depending on two categories of monumentation used. We can separate stations believed to be sufficiently connected to bedrock (either via a carbon-fibre pole with stainless steel ends attached to a submerged concrete block that rests directly on top of bedrock, or via a large structure, i.e. Barking Barrier) from those mounted on roofs or walls of single to

**Table 8.** Residual horizontal station velocity estimates computed for the filtered GAS2.4 DD regional network (DDRNF) and filtered BSW5.0 globally transformed PPP (PPPGTF) coordinate time-series solutions by subtracting ITRF2000 plate motion model estimates for each CGPS station. All values are in  $\text{mm yr}^{-1}$ . Uncertainties are  $1\sigma$ .

	DDRNF			PPPGTF		
	North ( $\text{mm yr}^{-1}$ )	East ( $\text{mm yr}^{-1}$ )	horiz. ( $\text{mm yr}^{-1}$ )	North ( $\text{mm yr}^{-1}$ )	East ( $\text{mm yr}^{-1}$ )	horiz. ( $\text{mm yr}^{-1}$ )
CGPS@TG stations						
ABER	$-0.5 \pm 0.2$	$0.2 \pm 0.3$	0.5	$-0.6 \pm 0.2$	$0.4 \pm 0.3$	0.7
LIVE	$-1.7 \pm 0.3$	$1.1 \pm 0.3$	2.1	$-1.9 \pm 0.4$	$0.8 \pm 0.3$	2.1
LOWE	$-0.1 \pm 0.2$	$1.3 \pm 0.3$	1.3	$0.0 \pm 0.1$	$0.7 \pm 0.2$	0.7
NEWL	$0.8 \pm 0.2$	$0.2 \pm 0.4$	0.8	$0.4 \pm 0.2$	$-0.1 \pm 0.2$	0.5
NSTG	$-0.4 \pm 0.2$	$1.6 \pm 0.6$	1.7	$0.0 \pm 0.2$	$0.5 \pm 0.5$	0.5
PMTG	$2.4 \pm 0.5$	$3.3 \pm 0.4$	4.1	$1.2 \pm 0.4$	$2.3 \pm 0.3$	2.5
SHEE	$0.3 \pm 0.3$	$0.5 \pm 0.2$	0.6	$-0.2 \pm 0.4$	$-0.3 \pm 0.3$	0.4
Other scientific CGPS stations						
ABYW	$0.7 \pm 0.1$	$1.7 \pm 0.3$	1.8	$0.7 \pm 0.1$	$1.0 \pm 0.2$	1.3
BARK	$0.2 \pm 0.5$	$0.5 \pm 0.4$	0.5	$0.5 \pm 0.6$	$-0.4 \pm 0.4$	0.6
CAMB	$0.7 \pm 0.2$	$0.8 \pm 0.2$	1.0	$0.6 \pm 0.1$	$0.0 \pm 0.2$	0.6
CARD	$0.5 \pm 0.3$	$1.0 \pm 0.6$	1.1	$-0.4 \pm 0.9$	$1.0 \pm 2.1$	1.1
DUNK	$0.4 \pm 0.4$	$1.1 \pm 0.4$	1.2	$0.3 \pm 0.1$	$0.4 \pm 0.2$	0.5
HERS	$-0.7 \pm 0.3$	$0.5 \pm 0.5$	0.8	$-0.1 \pm 0.3$	$-0.4 \pm 0.3$	0.4
HERT	n/a	n/a		$-0.3 \pm 0.4$	$-1.0 \pm 0.9$	1.1
HURN	$0.0 \pm 0.3$	$0.0 \pm 0.3$	0.1	$-0.8 \pm 0.2$	$0.2 \pm 0.1$	0.9
IESG	$-0.6 \pm 0.1$	$1.1 \pm 0.2$	1.3	$-0.4 \pm 0.1$	$0.4 \pm 0.1$	0.6
LERW	$0.9 \pm 0.2$	$-0.4 \pm 0.3$	1.0	$0.8 \pm 0.2$	$-0.5 \pm 0.2$	0.9
MORP	$0.9 \pm 0.4$	$-1.3 \pm 0.5$	1.6	$1.5 \pm 0.8$	$1.0 \pm 0.9$	1.8
NPLD	$-0.1 \pm 0.2$	$0.0 \pm 0.4$	0.1	$-0.5 \pm 0.2$	$-0.2 \pm 0.3$	0.5
PERS	$0.3 \pm 0.1$	$0.0 \pm 0.3$	0.3	$0.2 \pm 0.2$	$-0.6 \pm 0.4$	0.7
RAL1	$0.0 \pm 0.1$	$0.9 \pm 0.4$	0.9	n/a	n/a	
SUNB	$0.3 \pm 0.2$	$1.0 \pm 0.5$	1.0	$0.3 \pm 0.3$	$-0.7 \pm 0.4$	0.8
Network RTK CGPS stations						
BLAK	n/a	n/a		$-0.2 \pm 0.2$	$0.5 \pm 0.2$	0.6
CARL	$0.0 \pm 0.1$	$0.7 \pm 0.2$	0.7	$0.0 \pm 0.1$	$0.3 \pm 0.1$	0.3
COLC	n/a	n/a		$0.4 \pm 0.1$	$0.3 \pm 0.2$	0.4
DARE	$0.5 \pm 0.1$	$0.7 \pm 0.2$	0.9	$0.5 \pm 0.1$	$0.3 \pm 0.1$	0.6
EDIN	$0.2 \pm 0.3$	$0.7 \pm 0.2$	0.7	$0.3 \pm 0.1$	$0.2 \pm 0.1$	0.4
GLAS	$0.6 \pm 0.2$	$-0.1 \pm 0.3$	0.6	$0.6 \pm 0.1$	$0.0 \pm 0.2$	0.6
INVE	$0.1 \pm 0.3$	$1.3 \pm 0.4$	1.3	$0.3 \pm 0.1$	$0.8 \pm 0.3$	0.9
IOMN	$-0.1 \pm 0.6$	$0.4 \pm 0.4$	0.4	$0.0 \pm 0.4$	$0.2 \pm 0.2$	0.2
IOMS	$0.4 \pm 0.3$	$0.4 \pm 0.2$	0.5	$0.2 \pm 0.1$	$0.3 \pm 0.2$	0.4
KING	$0.1 \pm 0.1$	$0.8 \pm 0.2$	0.8	$0.1 \pm 0.1$	$0.2 \pm 0.1$	0.3
LEED	$0.2 \pm 0.1$	$0.7 \pm 0.1$	0.8	$0.1 \pm 0.1$	$0.2 \pm 0.1$	0.2
LOND	n/a	n/a		$-0.1 \pm 0.3$	$1.1 \pm 0.5$	1.1
MALG	$-0.1 \pm 0.3$	$0.2 \pm 0.5$	0.3	$0.4 \pm 0.1$	$0.0 \pm 0.2$	0.4
NEWC	$0.0 \pm 0.1$	$0.5 \pm 0.2$	0.5	$0.0 \pm 0.1$	$0.1 \pm 0.2$	0.1
OSHQ	n/a	n/a		$-0.1 \pm 0.1$	$0.1 \pm 0.2$	0.1
THUR	$0.5 \pm 0.2$	$0.3 \pm 0.3$	0.6	$0.5 \pm 0.2$	$0.4 \pm 0.2$	0.7

multistorey brick buildings (Table 2, Figs 6a and b). As some of the time-series are still just above the minimum recommended length of 2.5 yr we show the residual horizontal station velocities against the time span used for both categories of monumentation (Figs 6c and d). Unfortunately, our results presented in Fig. 6 are inconclusive. There may be a suggestion that stations on brick buildings give similar results to those of bedrock stations, independent of solutions, as there is no clear separation. Also, the time span does not seem to have a large effect on the residual velocity magnitude. This is not necessarily what we would have expected, but it confirms some of the findings of Calais *et al.* (2006) and, in a way also, of Beavan (2005).

Overall, ignoring the five stations with very large residuals, the magnitude of the residuals is larger for those of solution DDRNF than for PPPGTF. We can confirm this by comparing Figs 6(a) and

(b), and by computing the root-mean-square (rms) statistic of the residuals, which is 1.0 and 0.7  $\text{mm yr}^{-1}$  for solutions DDRNF and PPPGTF, respectively.

From Table 8 we can also compute that for solution DDRNF the RMS of the north component residuals is less than for the east component residuals, confirming either the aforementioned possible bias in our east component due to not fixing ambiguities to integers or a symptom of the reference frame implementation for this solution. However, as the east component residuals of solution PPPGTF are just slightly larger than the north component residuals, this might be an indication that the source of the bias in solution DDRNF is largely due to the particular reference frame implementation and only to a small degree due to the float ambiguities.

Nevertheless, we have shown that overall our horizontal station velocity estimates do not appear to be affected by monumentation



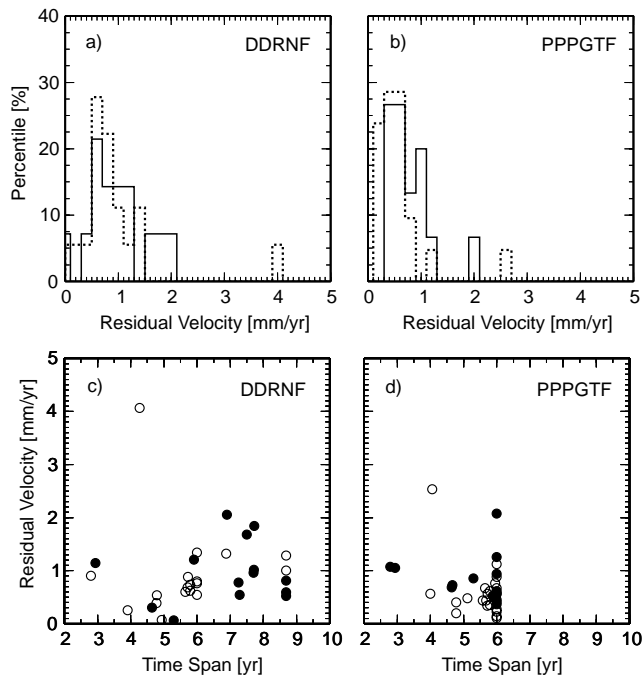


**Figure 6.** Residual horizontal station velocities distribution and residual horizontal station velocities versus time span for filtered GAS2.4 DD regional network (DDRNF) and filtered BSW5.0 globally transformed PPP (PPPGTF) coordinate time-series solutions. Solid lines in (a) and (b) and solid circles in (c) and (d) represent CGPS stations believed to be connected to bedrock either directly (carbon-fibre pole on concrete block) or via a large structure. The dotted lines and open circles represent CGPS stations mounted on roofs or walls of single to multistorey brick buildings.

or time span. Although, we cannot rule out local movements, which might explain some of the residual velocities, we have identified a list of stations that have the potential to be useful for further investigations into the horizontal crustal motion components of the GIA signal in Great Britain.

#### 4.5 Vertical crustal motions

We obtain estimates of vertical crustal motions for Great Britain from our vertical station velocity estimates if we assume that the apparent station displacement is solely due to motion of the Earth's crust and does not include any local movement associated with the location or monumentation of the CGPS station. In order to achieve this, we compare the CGPS and AG estimates of vertical station velocities with each other, compute AG-aligned CGPS estimates (Teferle *et al.* 2006) and compare the AG-aligned CGPS estimates with the independent evidence of vertical crustal motions from the Holocene sea level data for Great Britain.

Several authors have published alternative and independent evidence for vertical crustal motions in Great Britain which include estimates based on geological information, sea level observations and predictions from GIA models. As reported by Teferle *et al.* (2006), it is possible to carry out comparisons of the geodetic estimates of vertical crustal motions from AG and CGPS to those alternative data sets.

Teferle *et al.* (2006) compared their vertical station velocity estimates from CGPS and AG at Newlyn and Lerwick and found that the CGPS velocities were on average  $1.0 \pm 0.8 \text{ mm yr}^{-1}$  more positive than those from AG. When they applied this correction to

**Table 9.** Comparison of AG and CGPS estimates of vertical station velocities for the unfiltered GAS2.4 DD regional network (DDRNU), the unfiltered BSW5.0 globally transformed PPP (PPPGTU), the filtered GAS2.4 DD regional network (DDRNF), and the filtered BSW5.0 globally transformed PPP (PPPGTF) coordinate time-series solutions.

Station name	Station ID	CGPS minus AG difference			
		DDRNU (mm yr <sup>-1</sup> )	PPPGTU (mm yr <sup>-1</sup> )	DDRNF (mm yr <sup>-1</sup> )	PPPGTF (mm yr <sup>-1</sup> )
Lerwick	LERW	+1.4	+0.4	+1.3	+0.4
Newlyn TG	NEWL	+1.8	+0.9	+1.4	+0.9
Weighted mean		+1.5	+0.6	+1.3	+0.6
Standard deviation		±0.3	±0.3	±0.1	±0.3

**Table 10.** AG-aligned CGPS vertical station velocity estimates for the unfiltered GAS2.4 DD regional network (DDRNU), the unfiltered BSW5.0 globally transformed PPP (PPPGTU), the filtered GAS2.4 DD regional network (DDRNF), and the filtered BSW5.0 globally transformed PPP (PPPGTF) coordinate time-series solutions. All uncertainties are  $1\sigma$ .

Station ID	DDRNU (mm yr <sup>-1</sup> )	PPPGTU (mm yr <sup>-1</sup> )	DDRNF (mm yr <sup>-1</sup> )	PPPGTF (mm yr <sup>-1</sup> )
CGPS@TG stations				
ABER	$0.1 \pm 0.7$	$-1.5 \pm 1.0$	$0.0 \pm 0.3$	$-0.8 \pm 0.5$
BRST	$0.0 \pm 0.8$	n/a	$0.0 \pm 0.6$	n/a
LIVE	$-1.5 \pm 0.9$	$0.2 \pm 1.1$	$-0.2 \pm 0.3$	$0.5 \pm 0.4$
LOWE	$-1.5 \pm 0.6$	$-1.2 \pm 0.7$	$-1.3 \pm 0.5$	$-1.2 \pm 0.4$
NEWL	$-0.5 \pm 1.1$	$-0.5 \pm 0.9$	$-0.7 \pm 0.9$	$-0.4 \pm 0.7$
NSTG	$-1.0 \pm 1.0$	$-0.5 \pm 1.1$	$-1.2 \pm 0.8$	$-0.3 \pm 0.5$
PMTG	$-0.9 \pm 1.0$	$-1.2 \pm 1.0$	$-0.8 \pm 0.7$	$-1.1 \pm 0.5$
SHEE	$-1.1 \pm 0.6$	$-0.8 \pm 1.0$	$-0.7 \pm 0.5$	$-0.8 \pm 0.7$
Other scientific CGPS stations				
ABYW	$-0.9 \pm 0.9$	$-1.1 \pm 0.8$	$-0.4 \pm 0.6$	$-1.2 \pm 0.5$
BARK	$-1.7 \pm 0.6$	$-1.2 \pm 0.9$	$-1.4 \pm 0.5$	$-1.2 \pm 0.5$
CAMB	$-0.7 \pm 0.8$	$-2.1 \pm 0.9$	$-0.7 \pm 0.4$	$-1.3 \pm 0.6$
CARD	$0.7 \pm 2.4$	$-2.0 \pm 5.5$	$-1.2 \pm 1.9$	$-2.1 \pm 5.1$
DUNK	$-1.0 \pm 0.7$	$-0.7 \pm 1.5$	$-1.1 \pm 0.4$	$-1.4 \pm 1.1$
HERS	$-1.9 \pm 0.9$	$-0.2 \pm 1.0$	$-1.6 \pm 0.8$	$-0.4 \pm 0.7$
HERT	n/a	$0.8 \pm 1.8$	n/a	$-0.2 \pm 1.1$
HURN	$-0.9 \pm 0.9$	$-0.8 \pm 0.9$	$-1.0 \pm 0.5$	$-0.7 \pm 0.5$
IESG	$-2.4 \pm 0.6$	$-1.2 \pm 0.7$	$-2.1 \pm 0.3$	$-1.1 \pm 0.3$
LERW	$-0.6 \pm 0.8$	$-0.7 \pm 0.7$	$-0.5 \pm 0.5$	$-0.6 \pm 0.5$
NPLD	$-0.6 \pm 0.7$	$-2.4 \pm 1.0$	$-1.1 \pm 0.5$	$-0.9 \pm 0.5$
PERS	$-1.3 \pm 0.8$	$-1.9 \pm 1.0$	$-1.3 \pm 0.4$	$-1.1 \pm 0.4$
SUNB	$-2.4 \pm 0.7$	$-1.6 \pm 0.9$	$-2.1 \pm 0.6$	$-1.7 \pm 0.7$
Network RTK CGPS stations				
BLAK	n/a	$0.3 \pm 1.3$	n/a	$-0.1 \pm 0.4$
CARL	$0.3 \pm 0.8$	$-0.3 \pm 0.9$	$-0.1 \pm 0.4$	$0.1 \pm 0.4$
COLC	n/a	$-1.2 \pm 0.8$	n/a	$-0.6 \pm 0.4$
DARE	$0.0 \pm 0.7$	$-0.6 \pm 0.8$	$-0.3 \pm 0.5$	$-0.1 \pm 0.4$
EDIN	$0.8 \pm 0.8$	$0.9 \pm 0.8$	$0.9 \pm 0.5$	$1.1 \pm 0.3$
GLAS	$1.0 \pm 0.7$	$0.5 \pm 0.8$	$1.0 \pm 0.4$	$0.5 \pm 0.4$
INVE	$-0.6 \pm 0.9$	$-0.5 \pm 0.9$	$-0.2 \pm 0.5$	$-0.4 \pm 0.6$
IOMN	$0.7 \pm 1.3$	$0.2 \pm 1.2$	$0.4 \pm 1.0$	$0.6 \pm 0.9$
IOMS	$-0.1 \pm 1.0$	$-0.6 \pm 0.8$	$-0.4 \pm 0.6$	$-0.1 \pm 0.4$
KING	$-1.9 \pm 0.6$	$-0.9 \pm 0.7$	$-1.5 \pm 0.4$	$-1.1 \pm 0.3$
LEED	$-1.8 \pm 0.6$	$-0.6 \pm 0.8$	$-1.3 \pm 0.3$	$-0.8 \pm 0.3$
LOND	n/a	$-1.5 \pm 1.5$	n/a	$-0.9 \pm 1.1$
MALG	$1.7 \pm 1.8$	$0.1 \pm 0.8$	$0.9 \pm 1.0$	$0.4 \pm 0.4$
MORP	$-0.9 \pm 1.4$	$-2.6 \pm 2.5$	$-1.0 \pm 1.1$	$-2.3 \pm 2.0$
NEWC	$-1.0 \pm 0.7$	$0.8 \pm 1.0$	$-0.5 \pm 0.4$	$0.4 \pm 0.6$
THUR	$0.7 \pm 0.9$	$-0.4 \pm 0.9$	$0.4 \pm 0.4$	$-0.1 \pm 0.6$

the CGPS velocities the agreement between their CGPS estimates of vertical crustal motions and those from geology, sea level and the GIA models improved significantly.

Using our vertical station velocities from AG and CGPS, a comparison between the CGPS and AG vertical station velocities can be made for stations close to Lerwick TG on Shetland and close to or at the Newlyn TG in southwest England. We show the results of this comparison in Table 9.

As stated previously, the mean offset (and its corresponding standard deviation) between the CGPS estimates of vertical station velocity from the two software/processing strategies were  $1.1 \pm 1.1 \text{ mm yr}^{-1}$  between solutions DDRNU and PPPGTU, and  $0.7 \pm 0.6 \text{ mm yr}^{-1}$  between solutions DDRNF and PPPGTF, with the estimates of vertical station velocity based on DDRN being more positive than the estimates based on PPPGT. When considering AG, the weighted mean offset (and its corresponding standard deviation)

suggest that all four of the CGPS estimates of vertical station velocity are systematically offset from the estimates based on AG: those from solutions DDRNU and DDRNF being more positive by 1.5 or 1.3  $\text{mm yr}^{-1}$  and those from solutions PPPGTU and PPPGTF both being more positive by 0.6  $\text{mm yr}^{-1}$ .

As Teferle *et al.* (2006) reported previously, several authors have also identified systematic offsets when comparing CGPS estimates of vertical station velocity to independent evidence; Prawirodirdjo & Bock (2004) compared CGPS estimates of vertical station velocity with estimates from a GIA model and reported an offset of  $+1.1 \text{ mm yr}^{-1}$  for stations in North America and  $+1.7 \text{ mm yr}^{-1}$  for stations in northern Europe, with the CGPS estimates being more positive than the GIA model, MacMillan (2004) compared CGPS and Very Long Baseline Interferometry (VLBI) and found that CGPS estimates of vertical station velocity were  $1.5 \text{ mm yr}^{-1}$  more positive than VLBI estimates at 22 co-located global stations,

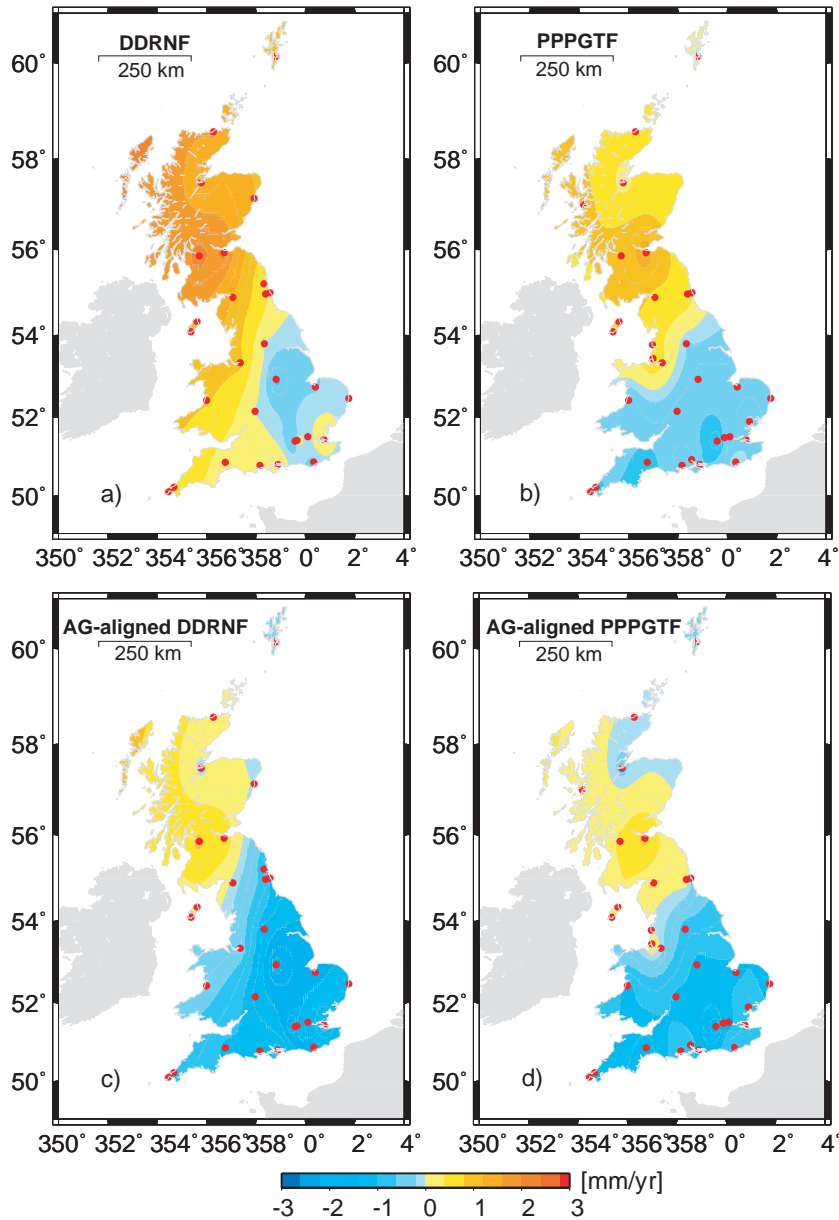


**Figure 7.** Maps of vertical crustal motions from CGPS estimates and AG-aligned CGPS estimates of vertical station velocity for filtered GAS2.4 DD regional network (DDRNF) and filtered BSW5.0 globally transformed PPP (PPPGTF) coordinate time-series solutions.

and finally, most recently, another study (Mazzotti *et al.* 2007) found their CGPS estimates of vertical station velocity to be more positive than those from AG by on average  $2.2 \pm 1.3 \text{ mm yr}^{-1}$  for the northern Cascadia in the United States and Canada.

Presently, the general consensus in the international community is that current CGPS estimates of vertical station velocity may be systematically biased, which is due to a combination of: the use of models for relative antenna phase centre variations, that is, inadequate modelling of satellite and receiver antenna phase centres in a changing satellite constellation (e.g. Ge *et al.* 2005; Cardellach *et al.* 2007); the use of current terrestrial reference frames, such as ITRF2000 and ITRF2005 (e.g. Blewitt *et al.* 2006); and, in the case of solutions DDRNU and DDRNF, limitations in using a regional rather than a global network and reference frame implementation, for which we have already shown a systematic offset of  $+1.1$  or  $+0.7 \text{ mm yr}^{-1}$  when compared to solutions PPPGTU and PPPGTF, respectively.

With this in mind, we now assume that the presented vertical station velocity estimates for solutions PPPGTU and PPPGTF are truly with respect to ITRF2000. We have shown that in both cases these are systematically offset, that is, more positive, when compared to those from AG. The update to ITRF2005, the most recent terrestrial frame realization, however, brought about an increase of this systematic bias in our CGPS velocity estimates for both solutions. Altamimi *et al.* (2007) pointed out that due to a rate in the Z-translation of the ITRF2005 with respect to ITRF2000, the vertical component of ITRF2005 will differ by  $+1.8 \times \sin(\phi) \text{ mm yr}^{-1}$  to that of ITRF2000, with  $\phi$  being the station latitude. At the same time, the ITRF2000 scale rate was shown to be  $0.08 \text{ ppb yr}^{-1}$  with respect to ITRF2005, which would reduce the contribution of the Z-translation rate to the vertical station velocity differences by  $0.5 \text{ mm yr}^{-1}$ . This means that for Great Britain, which lies between the latitudes of  $50^\circ\text{N}$  and  $60^\circ\text{N}$ , the ITRF2005 vertical station velocities will be about  $0.9\text{--}1.1 \text{ mm yr}^{-1}$ , respectively, larger than those of ITRF2000. However, with the current concerns about the correctness of the Z-translation rate (Altamimi *et al.* 2007; Argus 2007) and the other aforementioned issues related to antenna phase centre and atmospheric modelling, we decided to present our results based on ITRF2000. Interestingly, if we assume that the ITRF2000 scale rate, as determined with respect to ITRF2005, is correct, then the associated change in the vertical station velocities of  $0.5 \text{ mm yr}^{-1}$  would agree favourably with our systematic bias of  $0.6 \text{ mm yr}^{-1}$  between the CGPS and AG estimates of vertical station velocity for solutions PPPGTU and PPPGTF.

Teferle *et al.* (2006) presented a very simple procedure for combining CGPS and AG estimates of vertical station velocity, based on aligning the CGPS estimates to the AG estimates using the systematic offset between them. Following this procedure, we compute AG-aligned CGPS estimates of vertical station velocity, the systematic offset relating to a particular CGPS solution being basically subtracted from the CGPS estimate of vertical station velocity for a station. Through this procedure, the CGPS estimates of vertical station velocity presented in Table 7 are changed to the AG-aligned CGPS estimates given in Table 10, which only shows the reliable estimates (based on the discussions above).

It is clear from Table 10 that the AG-aligned CGPS estimates of vertical station velocity from solutions DDRNU, DDRNF, PPPGTU and PPPGTF are in much better agreement than the corresponding CGPS estimates of vertical station velocity. We show that the mean offset (and its corresponding standard deviation) between the estimates of vertical station velocity from the two CGPS software/processing strategies are reduced from  $+1.1 \pm 1.1$  to

$+0.1 \pm 1.1 \text{ mm yr}^{-1}$  between solutions DDRNU and PPPGTU, and from  $+0.7 \pm 0.6$  to  $+0.0 \pm 0.6 \text{ mm yr}^{-1}$  between solutions DDRNF and PPPGTF, when aligning the CGPS to the AG results. Appendix C includes further evidence for the validation of the AG-alignment procedure carried out, through comparison of the CGPS and AG-aligned CGPS estimates of vertical station velocity for ABER, BRST and NEWL with results from Wöppelmann *et al.* (2007), a recent analysis as part of the IGS TIGA Pilot-Project.

The effect of the AG-alignment procedure on the vertical crustal motions for Great Britain can be clearly seen in Fig. 7. This figure shows maps of vertical crustal motions from CGPS estimates and AG-aligned CGPS estimates of vertical station velocity for solutions DDRNF and PPPGTF.

For comparison we also show a map of vertical crustal motions for Great Britain derived from the geological information. Although Fig. 8 is based on the complete geological data set (Shennan & Horton 2002; Shennan *et al.* 2006) it only shows the sites mentioned in this study.

Clearly visible in these vertical crustal motion maps are the similarities in the primary areas of uplift in Scotland and subsidence in England and Wales. However, the outline of areas undergoing uplift or subsidence in Figs 7(c) and (d) are quite dissimilar in that the map based on solution DDRNF suggests that the whole west coast of Great Britain is rising with respect to the easterly regions of

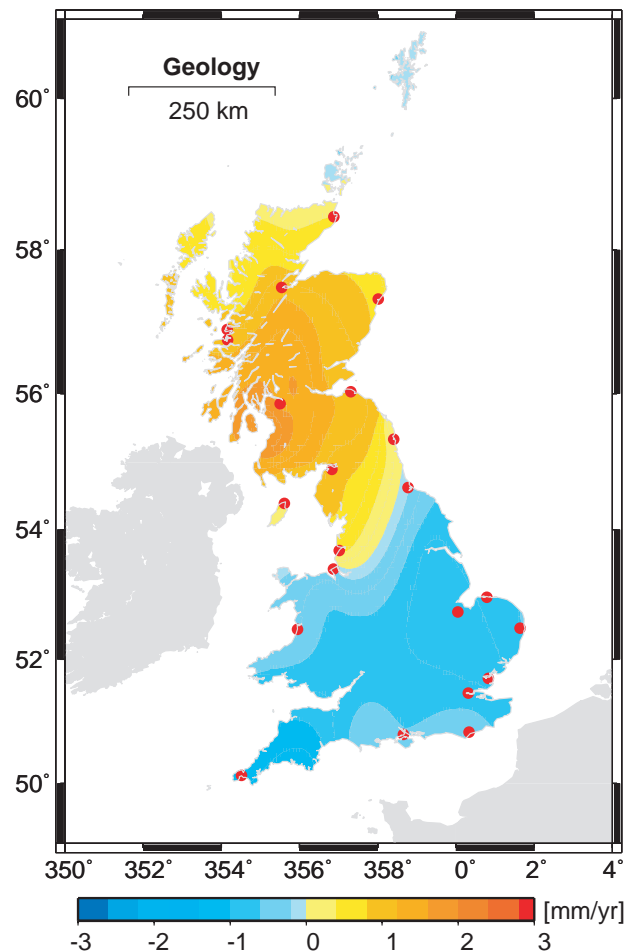


**Figure 8.** Map of vertical crustal motions derived from Holocene sea level data. Red dots indicate geological sites of Table 4.

England, whereas solution PPPGTF suggests a pattern of uplift and subsidence which is more consistent with that previously published based on Holocene sea level data (Shennan & Horton 2002, Fig. 8).

For solution DDRNF, Figs 7(a) and (c) suggest a possible tilt along a south-westerly to north-easterly axis, i.e. roughly from Newlyn to Lerwick. As this tilt is not apparent in Figs 7(b) and (d), we assume it is due to the regional reference frame implementation which uses IGS stations on the European mainland, all lying in the area to the south and east of Great Britain, and note that this is clearly not being removed through the current AG-alignment procedure.

For solution PPPGTF, Figs 7(b) and (d), the situation is quite different. First, there does not seem to be a network tilt and secondly, it is more difficult to argue in favour of the alignment.

This can be further investigated by directly comparing the AG-aligned CGPS estimates of vertical crustal motions to those from the geological information presented in Table 4. The table gives vertical crustal motions for a number of geological sites, which can be assigned a close-by CGPS station for comparison. We show a comparison of these motions for locations along the western and eastern coasts of Great Britain for solutions DDRNF and PPPGTF in Fig. 9. Figs 9(a) and (b) show the locations from southwest England

to western and northern Scotland along the coastlines with the Irish Sea and the Atlantic Ocean and Figs 9(c) and (d) show those from southern England to northeast Scotland along the coastlines with the English Channel and North Sea.

It is worth noting that we should not necessarily expect perfect agreement between the last decade, as represented by the AG-aligned CGPS estimates of vertical crustal motion, and the last 4000 yr (Holocene), as represented by the estimates based on geological studies. Nevertheless, it can be seen that for both CGPS solutions, the AG-aligned CGPS estimates are generally more negative than the geology; with the principal exception of the CGPS@TG station NEWL, which has AG-aligned CGPS estimates of vertical crustal motion which are consistently less negative than those from the geological information and more consistent with those suggested by Gehrels (2006) and Massey *et al.* (2008) (see also Appendix C). Figs 9(b)–(d) do however also suggest a slight overcorrection of the CGPS estimates of vertical station velocity through the current AG-alignment procedure.

Furthermore, we compute the mean offset (and its corresponding standard deviation) and the rms statistic between the CGPS estimates of vertical crustal motion and those from geological

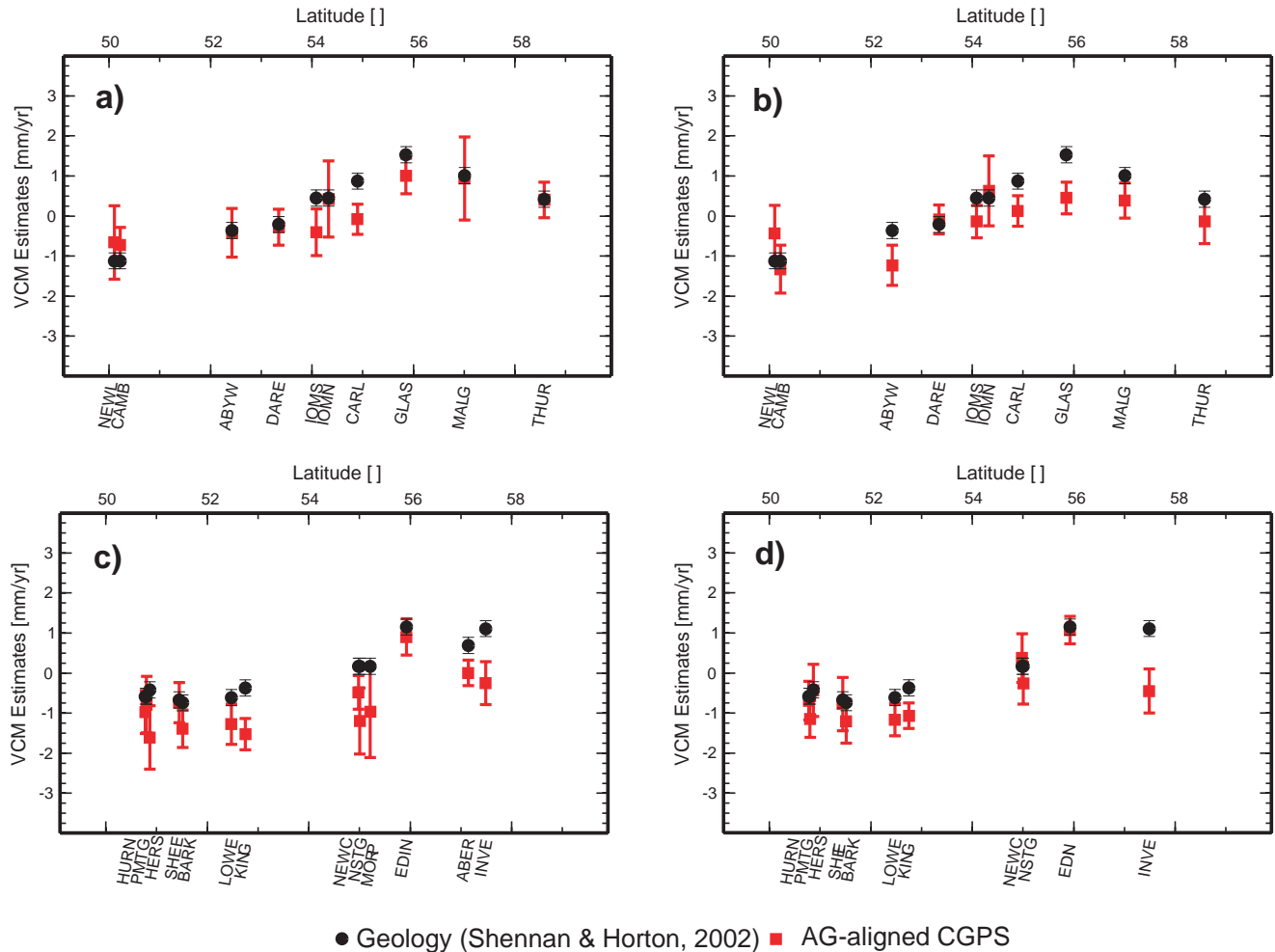


**Figure 9.** Comparison of AG-aligned CGPS estimates of vertical crustal motions (VCM) from filtered GAS2.4 DD regional network (DDRNF) (a and c) and filtered BSW5.0 globally transformed PPP (PPPGTF) (b and d) coordinate time-series solutions to those from geological information (Shennan & Horton 2002). The top row shows the locations from southwest England along the western coastline to the north of Scotland, whereas the bottom row shows those along the coastlines of the English Channel and the North Sea. Uncertainties are  $1\sigma$ .

information, and between the AG-aligned CGPS estimates of vertical crustal motion and those from geological information, for solutions DDRNF and PPPGTF. For solution DDRNF we compute mean offsets of  $+0.8 \pm 0.5$  and  $-0.5 \pm 0.5$  mm yr<sup>-1</sup> and rms of 1.0 and 0.7 mm yr<sup>-1</sup> for the CGPS and AG-aligned CGPS estimates, respectively. For solution PPPGTF we compute mean offsets of  $+0.2 \pm 0.7$  and  $-0.4 \pm 0.7$  mm yr<sup>-1</sup> and rms of 0.7 and 0.8 mm yr<sup>-1</sup> for the two estimates, respectively. This suggests that the AG-alignment procedure does improve the agreement with geological information for solution DDRNF even when the network of stations is expanded from those in Teferle *et al.* (2006) to the current network. This outcome seems at first not to be repeated for the case of solution PPPGTF, where we see an increase in the mean offset and RMS statistic between the geological and the AG-aligned CGPS estimates of vertical crustal motion, when compared to using the CGPS estimates. However, if we take into account the effect of ocean siphoning, as mentioned previously, this would lower all of the geological vertical crustal motion estimates by between 0.2 and 0.4 mm yr<sup>-1</sup> and hence lead to a further reduction of the mean offsets and rms between the AG-aligned CGPS and geological vertical crustal motion estimates.

We note that this comparison does not account for any differential vertical motions between the sites of the CGPS stations and geological information. If we consider the station separation from Table 4 it is clear that this assumption may not hold true in all cases, and this potentially explains some of the differences seen at GLAS, INVE and IOMS on the western coast and at KING and NEWC on the eastern coast, which suggests that the vertical station velocity estimates at these stations may not represent vertical crustal motions. Interestingly, we can, however, confirm that the vertical station velocity estimates for the CGPS@TG stations do appear to represent vertical crustal motions and that there is no local scale subsidence evident (see Fig. 10).

Fig. 10 also shows that there is no visible correlation between the difference in vertical crustal motion from the AG-aligned CGPS estimates of solution PPPGTF and the geological evidence, with distance between the CGPS station and the geological site, at least up to 50 km.

## 5 CONCLUSIONS

Over the last decade the geodetic evidence from CGPS and AG data collected in Great Britain has reached a level of maturity that allows the interpretation of this evidence as present-day crustal motions. Together with estimates of motion using Holocene sea level data from sites close to those of CGPS and AG measurements, we have introduced a comprehensive data set useful for studies of crustal motion information for Great Britain.

We derived horizontal crustal motions for Great Britain from our CGPS estimates of horizontal station velocity under the assumption that the CGPS stations only experience displacements due to horizontal crustal motions. The apparent crustal motion signal follows the predicted motions of the ITRF2000 plate motion model with residual velocities being generally smaller than 1 mm yr<sup>-1</sup>. The residual velocities are apparently random, there is no discernible internal deformation, and they show no dependence on station monumentation or time-series length. Our results do not confirm the previously reported residual motion signal in southeast England.

We derived vertical crustal motions for Great Britain from our CGPS and AG-aligned CGPS estimates of vertical station velocity under the assumption that the CGPS and AG stations only

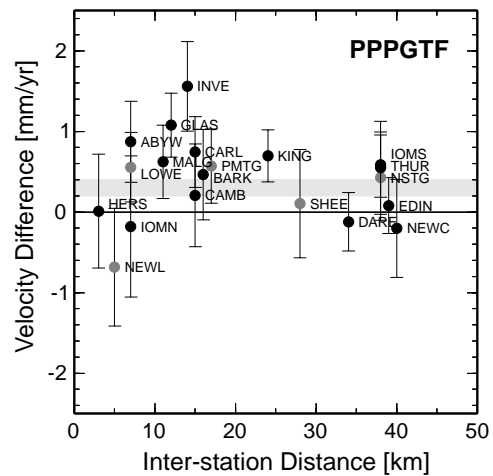


**Figure 10.** Differences between geodetic and geological vertical crustal motion estimates versus their interstation distances. Differences were computed between the AG-aligned CGPS estimates of vertical crustal motion, from the filtered BSW5.0 globally transformed PPP (PPPGTF) coordinate time-series solution, and those from geological information (Shennan & Horton 2002). Grey circles indicate CGPS@TG stations, and black circles other scientific and network RTK CGPS stations. The grey-shaded area indicates the region of 0.2–0.4 mm yr<sup>-1</sup> agreement between the motion estimates if the geological evidence were corrected for ocean siphoning. Uncertainties are  $1\sigma$ .

experience displacements due to vertical crustal motions. Overall our results confirmed the expected pattern of subsidence on Shetland, uplift in most areas of Scotland, and subsidence in large areas of England and Wales, and suggest that, in general, the pattern of present-day vertical crustal motions based on geodetic data is consistent with the pattern of vertical crustal motions based on Holocene sea level data, that is, no substantial difference is apparent between the present-day and Holocene vertical motions.

Using the vertical crustal motions from the geological information based on Holocene sea level data we investigated the effectiveness of the AG-alignment procedure to eliminate biases inherent in current CGPS results and the associated estimates of vertical station velocity. With the overall uncertainty associated with current terrestrial reference frames, the AG-alignment clearly provided improved estimates of vertical station velocity for both the regional and global reference frame implementations.

Although we expect further improvements in our CGPS results through a reprocessing of the CGPS data for Great Britain using an updated processing strategy, this will only be possible once the required products have been made available by the IGS. At this stage an inclusion of the new AG station at Herstmonceux will also benefit the computation of the alignment and together with an expansion of the AG station network, a more sophisticated AG-CGPS combination process could be derived.

For now we have provided a comprehensive data set of present-day crustal motions in Great Britain which has already supported the work described in Woodworth *et al.* (2009) and Bradley *et al.* (2009), and highlighted the importance of the complementary nature of the geodetic techniques of CGPS and AG, and of the requirement for independent data sets, that is, the geological information.

## ACKNOWLEDGMENTS

The work presented was partly funded through the UK Department for Environment Food and Rural Affairs, the Environment Agency

and the Natural Environment Research Council (NERC). The CGPS data from the UK was made available through the NERC funded BIGF (<http://www.bigf.ac.uk>), all other CGPS data and related GPS products were taken from the IGS (Beutler *et al.* 1999). We also like to acknowledge useful critics and suggestions provided by John Beavan and two anonymous reviewers, which greatly improved the content of this paper.

## REFERENCES

- Altamimi, Z., Sillard, P. & Boucher, C., 2002. ITRF2000: a new release of the International Terrestrial Reference Frame for Earth science applications, *J. geophys. Res.*, **107**(B10), 2214, doi:10.1029/2001JB000561.
- Altamimi, Z., Sillard, P. & Boucher, C., 2004. CATREF software: combination and analysis of terrestrial reference frames, Tech. Rep. LAREG Technical Note SP08, Institut Géographique National, Paris, France.
- Altamimi, Z., Collilieux, X., Legrand, J., Garayt, B. & Boucher, C., 2007. ITRF2005: a new release of the International Terrestrial Reference Frame based on time series of station positions and Earth orientation parameters, *J. geophys. Res.*, **112**, B09401, doi:10.1029/2007JB004949.
- Aoki, Y. & Scholz, C.H., 2003. Vertical deformation of the Japanese islands *J. geophys. Res.*, **108**(B5), 2257, doi:10.1029/2002JB002129.
- Argus, D.F., 2007. Defining the translational velocity of the reference frame of Earth, *Geophys. J. Int.*, **169**(3), 830–838, doi:10.1111/j.1365-246X.2007.03344.x.
- Beavan, J., 2005. Noise properties of continuous GPS data from concrete pillar geodetic monuments in New Zealand and comparison with data from U.S. deep drilled braced monuments, *J. geophys. Res.*, **110**, B08410, doi:10.1029/2005JB003642.
- Bell, F.G., Donnelly, L.J., Genske, D.D. & Ojeda, J., 2005. Unusual cases of mining subsidence from Great Britain, Germany and Colombia, *Environ. Geol.*, **47**(5), 620–631.
- Bennett, R.A. & Hreinsdóttir, S., 2007. Constraints on vertical crustal motion for long baselines in the central Mediterranean region using continuous GPS, *Earth planet. Sci. Lett.*, **257**(3–4), 419–434, doi:10.1016/j.epsl.2007.03.008.
- Beutler, G., Rothacher, M., Schaer, S., Springer, T., Kouba, J. & Neilan, R.E., 1999. The International GPS Service (IGS): an interdisciplinary service in support of Earth sciences, *Adv. Space Res.*, **23**(4), 631–635.
- Blewitt, G., 2003. Self-consistency in reference frames, geocenter definition, and surface loading of the solid Earth *J. geophys. Res.*, **108**(B2), 2103, doi:10.1029/2002JB002082.
- Blewitt, G. & Lavallée, D., 2002. Effect of annual signals on geodetic velocity, *J. geophys. Res.*, **107**(B7), 2145, doi:10.1029/2001JB000570.
- Blewitt, G., Davies, P., Gregorius, T.L.H., Kwar, R. & Sanli, U., 1997. Sustainable geodetic monitoring of the natural environment using the IGS, in *Methods for Monitoring Sea Level: GPS and Tide Gauge Benchmark Monitoring and Altimeter Calibration*, pp. 69–83, Jet Propulsion Laboratory, California Institute of Technology, Pasadena.
- Blewitt, G. *et al.*, 2006. Geodetic observations and global reference frame contributions to understanding sea level rise and variability, in *Understanding Sea-Level Rise and Variability—A World Climate Research Programme Workshop and a WCRP contribution to the Global Earth Observation System of Systems*, pp. 127–144, World Climate Research Programme, Paris, 6–9 June 2006.
- Böhm, J., Niell, A.E., Tregoning, P. & Schuh, H., 2006. Global Mapping Function (GMF): a new empirical mapping function based on numerical weather model data, *Geophys. Res. Lett.*, **33**, L07304, doi:10.1029/2005GL025546.
- Bradley, S., Milne, G.A., Teferle, F.N., Bingley, R.M. & Orliac, E.J., 2009. Glacial isostatic adjustment of the British Isles: new constraints from GPS measurements of crustal motion, *Geophys. J. Int.*, in press, doi:10.1111/j.1365-246X.2008.04033.x.
- Bruyninx, C., Becker, M. & Stangl, G., 2001. Regional densification of the IGS in Europe using the EUREF Permanent GPS Network (EPN), *Phys. Chem. Earth*, **26**(6–8), 531–538.
- Caccamise, D.J., Merrifield, M.A., Bevis, M., Foster, J., Firing, Y.L., Schenewerk, M.S., Taylor, F.W. & Thomas, D.A., 2005. Sea level rise at Honolulu and Hilo, Hawaii: GPS estimates of differential land motion, *Geophys. Res. Lett.*, **32**, L03607, doi:10.1029/2004GL021380.
- Calais, E., Han, J.Y., DeMets, C. & Nocquet, J.-M., 2006. Deformation of the North American plate interior from a decade of continuous GPS measurements, *J. geophys. Res.*, **111**, B06402, doi:10.1029/2005JB004253.
- Canning, J.C., Henney, P.J., Morrison, M.A., Van Calsteren, P.W.C., Gaskarth, J.W. & Swarbrick, A., 1998. The Great Glen Fault: a major vertical lithospheric boundary, *J. Geol. Soc., Lond.*, **155**, 425–428, doi:10.1144/gsjgs.155.3.0425.
- Cardellach, E., Elósegui, P. & Davis, J.L., 2007. Global distortion of GPS networks associated with satellite antenna model errors, *J. geophys. Res.*, **112**, B07405, doi:10.1029/2006JB004675.
- Curry, G.B., 1986. Fossils and tectonic along the Highland Boundary Fault in Scotland, *J. Geol. Soc., Lond.*, **143**, 193–198, doi:10.101144/gsjgs.143.1.0193.
- Dach, R., Hugentobler, U., Fridez, P. & Meindl, M., eds, 2007. *Bernese GPS Software Version 5.0*, Atronomical Institute, University of Bern, Bern.
- de Linage, C., Hinderer, J. & Rogister, Y., 2007. A search for the ratio between gravity variation and vertical displacement due to a surface load, *Geophys. J. Int.*, **171**(3), 986–994.
- Dong, D., Yunck, T.P. & Heflin, M.B., 2003. Origin of the International Terrestrial Reference Frame *J. geophys. Res.*, **108**(B4), 2200, doi:10.1029/2002JB002035.
- Dong, D., Fang, P., Bock, Y., Webb, F.H., Prawirodirdjo, L., Kedar, S. & Jamason, P., 2006. Spatiotemporal filtering using principal component analysis and Karhunen-Loeve expansion approaches for regional GPS network analysis, *J. geophys. Res.*, **111**, B03405, doi:10.1029/2005JB003806.
- Donnelly, L.J., 2006. A review of coal mining induced fault reactivation in Great Britain, *Quart. J. Eng. Geol. Hydrogeol.*, **39**, 5–50.
- Edwards, R.J., 2006. Mid- to late-Holocene relative sea-level change in southwest Britain and the influence of sediment compaction, *Holocene*, **16**(4), 575–587.
- Ellison, R.A., Woods, M.A., Allen, D.J., Forster, A., Pharoah, T.C. & King, C., 2004. Geology of London. Memoir of the British Geological Survey, Sheets 256 (North London), 257 (Romford), 270 (South London) and 271 (Dartford), England and Wales, British Geological Survey.
- Francis, O. *et al.*, 2005. Results of the International comparison of absolute gravimeters in Walferdange (Luxembourg) of November 2003, in *Gravity, Geoid and Space Missions GGSM 2004, IAG International Symposia*, Vol. 129, pp. 272–275, Springer, Heidelberg, Berlin New York, Porto, Portugal. August 30–September 3, 2004.
- Fritsche, M., Dietrich, R., Knöfel, A., Rülke, A., Vey, S., Rothacher, M. & Steigenberger, P., 2005. Impact of higher-order ionospheric terms on GPS estimates, *Geophys. Res. Lett.*, **32**, L23311, doi:10.1029/2005GL024342.
- Ge, M., Gendt, G., Dick, G., Zhang, F.P. & Reigber, C., 2005. Impact of GPS satellite antenna offsets on scale changes in global network solutions, *Geophys. Res. Lett.*, **32**, L06310, doi:10.1029/2004GL022224.
- Gehrels, W.R., 2006. Sea-level rise and coastal subsidence in southwest England, *Reports and Transactions of the Devonshire Association for the Advancement of Science*, **138**, 25–42.
- Geirsson, H. *et al.*, 2006. Current plate movements across the Mid-Atlantic Ridge determined from 5 years of continuous GPS measurements in Iceland, *J. geophys. Res.*, **111**, B09407, doi:10.1029/2005JB003717.
- Hernández-Pajares, M., Juan, J.M., Sanz, J. & Orús, R., 2007. Second-order ionospheric term in GPS: implementation and impact on geodetic estimates, *J. geophys. Res.*, **112**, B08417, doi:10.1029/2006JB004707.
- Hill, T.C.B., Woodland, W.A., Spencer, C.D. & Marriott, S.B., 2007. Holocene sea-level change in the Severn Estuary, southwest England: a diatom-based sea-level transfer function for macrotidal settings, *Holocene*, **17**(5), 639–648.
- Hopewell, H., 2003. Environmental and Instrumental Effects of High Precision Gravimetry—a case study in Britain, *PhD thesis*, University of Edinburgh.
- Humphries, L., 2001. A review of relative sea level rise caused by



- mining-induced subsidence in the coastal zone: some implications for increased coastal recession, *Clim. Res.*, **18**(1–2), 147–156.
- Johansson, J.M. et al., 2002. Continuous GPS measurements of postglacial adjustment in Fennoscandia I. geodetic results, *J. geophys. Res.*, **107**(B8), ETG 3/1–3/27.
- Kedar, S., Hajj, G.A., Wilson, B.D. & Heflin, M.B., 2003. The effect of the second order GPS ionospheric correction on receiver positions *Geophys. Res. Lett.*, **30**(16), 1829, doi:10.1029/2003/GL017639.
- Kierulf, H.P. et al., 2008. Comparison of GPS analysis strategies for high-accuracy vertical land motion, *Phys. Chem. Earth*, **33**(3–4), 194–204, doi:10.1016/j.pce.2006.11.003.
- King, R.W. & Bock, Y., 2005. *Documentation for the GAMIT GPS Analysis Software Version 10.2*, Dept. of Earth, Atmospheric, and Planetary Sciences, Mass. Inst. of Technol., Cambridge, USA.
- Kreemer, C., Lavallée, D.A., Blewitt, G. & Holt, W.E., 2006. On the stability of a geodetic no-net-rotation frame and its implication for the International Terrestrial Reference Frame, *Geophys. Res. Lett.*, **33**, L17306, doi:10.1029/2006GL027058.
- Lambeck, K., 1993a. Glacial rebound of the British Isles I: preliminary model results, *Geophys. J. Int.*, **115**, 941–959.
- Lambeck, K., 1993b. Glacial rebound of the British Isles II: a high-resolution, high-precision model, *Geophys. J. Int.*, **115**, 960–990.
- Lambeck, K., Johnston, P.J., Smither, C. & Nakada, M., 1996. Glacial rebound of the British Isles III: constraints on mantle viscosity, *Geophys. J. Int.*, **125**, 340–354.
- Lambert, A., Courtier, N., Sasagawa, G.S., Klopping, F., Winester, D., James, T.S. & Liard, J.O., 2001. New constraints on Laurentide postglacial rebound from absolute gravity measurements, *Geophys. Res. Lett.*, **28**(10), 2109–2112.
- Lambert, A., Courtier, N. & James, T.S., 2006. Long-term monitoring by absolute gravimetry: tides to postglacial rebound, *J. Geodyn.*, **41**(1–3), 307–317.
- Langbein, J. & Johnson, H.O., 1997. Correlated errors in geodetic time series: implications for time-dependent deformation, *J. geophys. Res.*, **102**(B1), 591–603, doi:10.1029/96JB02945.
- Larson, K.M. & van Dam, T.M., 2000. Measuring postglacial rebound with GPS and absolute gravity, *Geophys. Res. Lett.*, **27**(23), 3925–3928.
- Lidberg, M., Johansson, J.M., Scherneck, H.G. & Davis, J.L., 2007. An improved and extended GPS-derived 3D velocity field of the glacial isostatic adjustment (GIA) in Fennoscandia, *J. Geod.*, **81**, 213–230, doi:10.1007/s00190-006-0102-4.
- MacMillan, D., 2004. Rate difference between VLBI and GPS reference frame scales, *EOS, Trans. Am. geophys. Un.*, **85**(47), Fall Meet. Suppl., G21B-5.
- Mao, A., Harrison, C.G.A. & Dixon, T.H., 1999. Noise in GPS coordinate time series, *J. geophys. Res.*, **104**(B2), 2797–2818.
- Massey, A.C., Gehrels, W.R., Charman, D.J., Milne, G.A., Peltier, W.R., Lambeck, K. & Selby, K.A., 2000. Relative sea-level change and post-glacial isostatic adjustment along the coast of south Devon, United Kingdom, *J. Quater. Sci.*, **23**(5), 415–433, doi:10.1002/jqs.1149.
- Mazzotti, S., Lambert, A., Courtier, N., Nikolaishen, L. & Dragert, H., 2007. Crustal uplift and sea level rise in northern Cascadia from GPS, absolute gravity, and tide gauge data, *Geophys. Res. Lett.*, **34**, L15306, doi:10.1029/2007GL03020283.
- Mazzotti, S., Jones, C. & Thomson, R.E., 2008. Relative and absolute sea level rise in western Canada and northwestern United States from a combined tide gauge-GPS analysis, *J. geophys. Res.*, **113**, C11019, doi:10.1029/2008JC004835.
- Milne, G.A., Davies, J.L., Mitrovica, J.X., Scherneck, H.G., Johansson, J.M., Vermeer, M. & Koivula, H., 2001. Space-geodetic constraints on glacial isostatic adjustment in Fennoscandia, *Science*, **291**, 2381–2385.
- Milne, G.A. et al., 2006. Modelling the glacial isostatic adjustment of the UK region, *Phil. Trans. Roy. Soc., Part A*, **364**, 931–948, doi:10.1098/rsta.2006.1747.
- Mitrovica, J.X. & Milne, G.A., 2002. On the origin of late holocene sea-level highstands within equatorial ocean basins, *Quat. Sci. Rev.*, **21**, 2179–2190.
- Mitrovica, J.X. & Peltier, W.R., 1991. On post-glacial Geoid subsidence over the equatorial oceans, *J. geophys. Res.*, **96**, 20 053–20 071.
- Mitrovica, J.X., Davis, J.L. & Shapiro, I.I., 1994. A spectral formalism for computing three-dimensional deformations due to surface loads 2. present-day glacial isostatic adjustment, *J. geophys. Res.*, **99**, 7075–7101.
- Niebauer, T.M., Sasegawa, G.S., Faller, J.E., Hilt, R. & Klopping, F., 1995. A new generation of absolute gravimeters, *Metrol.*, **32**, 159–180.
- Nikolaïdis, R.M., 2002. Observation of Geodetic and Seismic Deformation with the Global Positioning System, *PhD thesis*, University of California.
- Nocquet, J.M. & Calais, E., 2003. Crustal velocity field of western Europe from permanent GPS array solutions, 1996–2001, *Geophys. J. Int.*, **154**, 72–88.
- Nocquet, J.M., Calais, E., Altamimi, Z., Sillard, P. & Boucher, C., 2001. Intraplate deformation in western Europe deduced from an analysis of the International Terrestrial Reference Frame 1997 (ITRF97) velocity field, *J. geophys. Res.*, **106**(B6), 11 239–11 257.
- Peltier, W.R., 2001. Global glacial isostatic adjustment and modern instrumental records of relative sea level history, in *Sea Level Rise History and Consequences*, Vol. 75 of International Geophysics Series, p. 232, eds Douglas, B.C., Kearney, M.S. & Leatherman, S.P., Academic Press, San Diego.
- Peltier, W.R., Shennan, I., Drummond, R. & Horton, B., 2002. On the post-glacial isostatic adjustment of the British Isles and the shallow viscoelastic structure of the Earth, *Geophys. J. Int.*, **148**(3), 443–475.
- Prawirodirdjo, L. & Bock, Y., 2004. Instantaneous global plate motion model from 12 years of continuous GPS observations, *J. geophys. Res.*, **109**, B08405, doi:10.1029/2003JB002944.
- Prawirodirdjo, L., Ben-Zion, Y. & Bock, Y., 2006. Observation and modeling of thermoelastic strain in Southern California Integrated GPS Network daily position time series, *J. geophys. Res.*, **111**, B02408, doi:10.1029/2005JB003716.
- Shennan, I., 1989. Holocene crustal movements and sea-level changes in Great Britain, *J. Quater. Sci.*, **4**, 77–89.
- Shennan, I. & Horton, B., 2002. Holocene land- and sea-level changes in Great Britain, *J. Quater. Sci.*, **17**(5–6), 511–526, doi:10.1002/jqs.710.
- Shennan, I., Peltier, W.R., Drummond, R. & Horton, B., 2002. Global to local scale parameters determining relative sea-level changes and the post-glacial isostatic adjustment of Great Britain, *Quatern. Sci. Rev.*, **21**(1–3), 397–408.
- Shennan, I., Bradley, S.L., Milne, G.A., Brooks, A., Bassett, S.E. & Hamilton, S., 2006. Relative sea-level changes, glacial isostatic modelling and ice-sheet reconstructions from the British Isles since the Last Glacial Maximum, *J. Quater. Sci.*, **21**(6), 585–599, doi:10.1002/jqs.1049.
- Steigenberger, P., Rothacher, M., Dietrich, R., Fritsche, M., Rülke, A. & Vey, S., 2006. Reprocessing of a global GPS network, *J. geophys. Res.*, **111**, B05402, doi:10.1029/2005JB003747.
- Stewart, M., Strachan, R.A., Martin, M.W. & Holdsworth, R.E., 2001. Constraints on early sinistral displacements along the Great Glen Fault Zone, Scotland: structural setting, U-Pb geochronology and emplacement of the syn-tectonic Clunes tonalite, *J. Geol. Soc., Lond.*, **158**, 821–830.
- Stewart, M.P., Ffoulkes-Jones, G.H., Ochieng, W.Y., Shardlow, P.J., Penna, N.T. & Bingley, R.M., 2002. *GAS: GPS Analysis Software User Manual*. Version 2.4, IESSG, University of Nottingham, Nottingham.
- Teferle, F.N., 2003. Strategies for long-term monitoring of tide gauges with GPS, *PhD thesis*, University of Nottingham, Available at: <http://theses.nottingham.ac.uk>.
- Teferle, F.N., Bingley, R.M., Dodson, A.H. & Baker, T.F., 2002. Application of the dual-CGPS concept to monitoring vertical land movements at tide gauges, *Phys. Chem. Earth*, **27**(32–34), 1401–1406.
- Teferle, F.N., Bingley, R.M., Dodson, A.H., Apostoloidis, P. & Staton, G., 2003. RF interference and multipath effects at continuous GPS installations for long-term monitoring of tide gauges in UK harbours, in *Proceedings of the 16th Technical Meeting of the Satellite Division of the Institute of Navigation, ION GPS/GNSS 2003, Portland, Oregon, 9–12 September 2003*, p. 12, Institute of Navigation, Washington, DC.
- Teferle, F.N., Bingley, R.M., Williams, S.D.P., Baker, T.F. & Dodson, A.H., 2006. Using continuous GPS and absolute gravity to separate vertical land movements and changes in sea level at tide gauges in the UK, *Phil. Trans. Roy. Soc., Part A*, **364**, 917–930, doi:10.1098/rsta.2006.1746.

- Teferle, F.N., Orliac, E.J. & Bingley, R.M., 2007. An assessment of bernese GPS software Precise Point Positioning using IGS final products for global site velocities, *GPS Sols.*, **11**(3), 205–213, doi:10.1007/s10291-006-0051-7.
- Teferle, F.N., Williams, S.D.P., Kierulf, H.P., Bingley, R.M. & Plag, H.P., 2008. A continuous GPS coordinate time series analysis strategy for high-accuracy vertical land movements, *Phys. Chem. Earth*, **33**(3–4), 205–216, doi:10.1016/j.pce.2006.11.002.
- Tregoning, P. & Van Dam, T., 2005. Atmospheric pressure loading corrections applied to GPS data at the observation level, *Geophys. Res. Lett.*, **32**, L22310, doi:10.1029/2005GL024104.
- Van Camp, M., Williams, S.D.P. & Francis, O., 2005. Uncertainty of absolute gravity measurements, *J. geophys. Res.*, **110**, B05406.
- van Dam, T.M., Wahr, J., Milly, P.C.D., Shmakin, A.B., Blewitt, G., Lavallée, D. & Larson, K.M., 2001. Crustal displacements due to continental water loading, *Geophys. Res. Lett.*, **28**(4), 651–654.
- Vey, S., Dietrich, R., Fritsche, M., Rülke, A., Rothacher, M. & Steigenberger, P., 2006. Influence of mapping function parameters on global GPS network analysis: comparisons between NMF and IMF, *Geophys. Res. Lett.*, **33**, L01814, doi:10.1029/2005GL024361.
- Vitushkin, L. *et al.*, 2002. Results of the sixth international comparison of absolute gravimeters, ICAG-2001, *Metrol.*, **39**(5), 407–424.
- Wahr, J., Dazhong, H. & Turpin, A., 1995. Predictions of vertical uplift caused by changing Polar ice volumes on a viscoelastic earth, *Geophys. Res. Lett.*, **22**(8), 977–980.
- Wdowinski, S., Bock, Y., Zhang, J., Fang, P. & Genrich, J., 1997. Southern California Permanent GPS Geodetic Array: Spatial filtering of daily positions for estimating coseismic and postseismic displacements induced by the 1992 Landers earthquake, *J. geophys. Res.*, **102**(B8), 18 057–18 070, doi:10.1029/97JB01378.
- Wdowinski, S. *et al.*, 2004. GPS measurements of current crustal movements along the Dead Sea Fault, *J. geophys. Res.*, **109**, B05403, doi:10.1029/2003JB002640.
- Williams, S.D.P., 2003. The effect of coloured noise on the uncertainties of rates estimated from geodetic time series, *J. Geod.* **76**(9–10), 483–494, doi:10.1007/s00190-002-0283-4.
- Williams, S.D.P., 2008. CATS: GPS coordinate time series analysis software, *GPS Sols.*, **12**(2), 147–153, doi:10.1007/s010291-10007-10086-10294.
- Williams, S.D.P., Baker, T.F. & Jeffries, G., 2001. Absolute gravity measurements at UK tide gauges, *Geophys. Res. Lett.*, **28**(12), 2317–2320, doi:10.1029/2000GL012438.
- Williams, S.D.P., Bock, Y., Fang, P., Jamason, P., Nikolaidis, R.M., Prawirodirdjo, L., Miller, M. & Johnson, D., 2004. Error analysis of GPS position time series, *J. geophys. Res.*, **109**, B03412, doi:10.1029/2003JB002741.
- Woodworth, P., Teferle, F.N., Bingley, R.M. & Shennan, I., 2009. Trends in UK mean sea level revisited, *Geophys. J. Int.*, **176**, 19–30, doi:10.1111/j.1365-246X.2008.03942.x.
- Woodworth, P.L., Tsimplis, M.N., Flather, R.A. & Shennan, I., 1999. A review of the trends observed in British Isles mean sea level data measured by tide gauges, *Geophys. J. Int.*, **136**(3), 651–670.
- Wöppelmann, G., Martin Miguez, B., Bouin, M.N. & Altamimi, Z., 2007. Geocentric sea-level trend estimates from GPS analyses at relevant tide gauges world-wide, *Global Planet. Change*, **57**(3–4), 396–407, doi:10.1016/j.gloplacha.2007.02.002.
- Wu, X., Argus, D.F., Heflin, M.B., Ivins, E.R. & Webb, F.H., 2002. Site distribution and aliasing effects in the inversion for load coefficients and geocenter motion from GPS data *Geophys. Res. Lett.*, **29**(24), 2210, doi:10.1029/2002GL016324.
- Zhang, J., Bock, Y., Johnson, H.O., Fang, P., Williams, S.D.P., Genrich, J., Wdowinski, S. & Behr, J., 1997. Southern California Permanent GPS Geodetic Array: error analysis of daily position estimates and site velocities, *J. geophys. Res.*, **102**(B8), 18 035–18 055.
- Zong, Y.Q. & Tooley, M.J., 1996. Holocene sea-level changes and crustal movements in Morecambe Bay, northwest England, *J. Quatern. Sci.*, **11**(1), 43–58.

## APPENDIX A: SPATIAL FILTERING

Teferle (2003) found that overall best filtering results were obtained by using as many stations as possible during the bias computation and by carefully selecting and/or excluding individual coordinate components. After close inspection of solutions DDRNU and PPPGTU we selected 20 and 24 stations, respectively, and their coordinate components for the computation of the daily common mode bias (Table 11). Our stations-of-choice were those with long time spans, few coordinate offsets and those not exhibiting any station-specific characteristics, such as unusual or larger periodic signals or features (e.g. the north component of SHEE, Fig. S1). As can be seen, as a result of this selection process, none of the IGS stations located in Great Britain (HERS, HERT, MORP and NPLD) were included to compute the bias. Also, we note that judging from the coordinate time-series for BLAK, COLC and OSHQ, and THUR (Fig. S3), it is unlikely that their additional use in the bias computation for solution PPPGTU had a noticeable effect on the bias compared to solution DDRNU and the filtered coordinate time-series thereafter, as the bias estimate was based on 20 or more stations from early 2000 onwards (Fig. 11). Also, on days with less

**Table 11.** Station and coordinate components used for the computation of the daily common mode bias.

Station	Component	Station	Component
ABYW	ne-	LEED	neu
BARK	ne-	LERW	neu
BLAK*	neu	LOWE	neu
CAMB	neu	MALG	neu
CARL	neu	NEWC	neu
COLC*	neu	NEWL	neu
DARE	neu	OSHQ*	neu
EDIN	neu	PERS	neu
GLAS	neu	PMTG	neu
IESG	neu	SHEE	--u
INVE	neu	SUNB	neu
KING	neu	THUR*	neu

Note: Asterisk indicates stations only available to coordinate time-series solution PPPGTU.

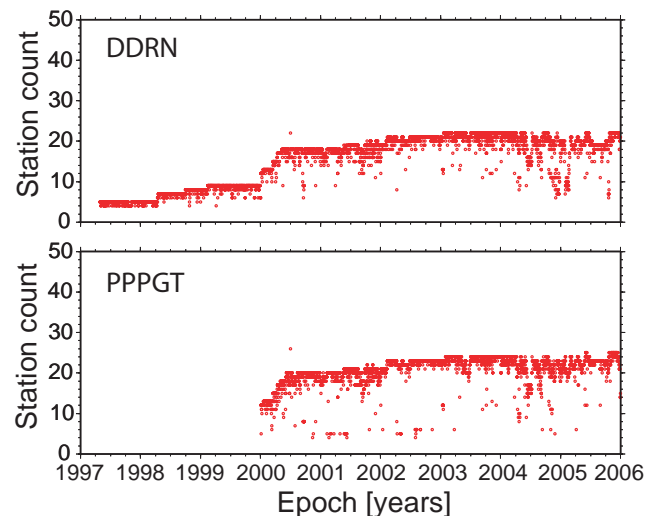


**Figure 11.** Number of stations used in the computation of the daily common mode bias for the GAS2.4 DD regional network (DDRNU) and the BSW5.0 globally transformed PPP (PPPGT) solutions.

than three available stations, we did not compute a common mode bias estimate and for such days, we did not obtain filtered coordinate estimates (Nikolaïdis 2002).

## APPENDIX B: STABILITY OF CGPS@TG STATION NEWL USED IN THE AG-ALIGNMENT PROCESS

The CGPS@TG station NEWL is founded on the pier at Newlyn tide gauge near to Land's End in southwest England. The stability, in a local and regional context, of NEWL could have an impact on the nature of the apparent systematic offset between the CGPS estimate of vertical station velocity and the AG estimate, which is for the AG station located in the church at Paul about 1.5 km away.

The mean sea level records from the Newlyn tide gauge for the period 1915–21 were used to define Ordnance Datum Newlyn (ODN) and the Tidal Observatory has remained in the same location since that time. The primary tide gauge benchmark (PTGBM) at Newlyn is a bolt, adjacent to the stilling well, inside the Tidal Observatory. The PTGBM was first connected to the primary levelling network in 1915 and was last verified by precise levelling (line G001) in 1990. The TGBM network is effectively formed from seven benchmarks, comprising the PTGBM, two benchmarks on the pier, two benchmarks in the village and two fundamental benchmarks (FBMs), located at Tolcarne, about 900 m northwest of the PTGBM and at Paul, about 1.4 km southwest of the PTGBM. The FBMs are founded on solid rock, whereas all of the other inland benchmarks are Ordnance Survey flush brackets set into walls. The TGBM network was first connected to the PTGBM in 1952 and last verified by precise levelling (line G001) in 1990. The results of the repeated precise levelling surveys showed no significant changes (i.e. less than 0.1 mm) in height within the TGBM network over the period from 1952 to 1990, which suggests that the pier on which the tide gauge and the CGPS@TG station are located did not experience any uplift or subsidence relative to any of the benchmarks, including the two FBMs founded on solid rock, and is stable in a local context.

A further confirmation of this can be obtained for a regional context by considering the vertical station velocities estimated for NEWL along with the vertical station velocities estimated for the scientific CGPS station CAMB, which is at Camborne about 20 km away and founded on solid rock (Table 2). In this respect, it can be reported that the CGPS estimates of vertical station velocity for CAMB were  $+0.8 \pm 0.8$  and  $+0.5 \pm 0.4$  mm yr<sup>-1</sup> for solutions DDRNU and DDRNF, respectively, which agree with the estimates for NEWL (Table 7) of  $+1.1 \pm 1.1$  and  $+0.6 \pm 0.9$  mm yr<sup>-1</sup> to within 0.3 and 0.1 mm yr<sup>-1</sup>.

Considering these two different sets of results, therefore, we conclude that the apparent systematic offsets of +1.8, +0.9, +1.4 and

+0.9 mm yr<sup>-1</sup> (Table 9) between the CGPS and AG estimates of vertical station velocity for Newlyn are not due to relative movements between the CGPS@TG station NEWL founded on the pier adjacent to Newlyn tide gauge and the AG station founded on solid rock in the church at Paul, some 1.5 km away.

Unfortunately, a similar assessment cannot be carried out for the AG and CGPS stations at Lerwick on Shetland as similar data to that presented for Newlyn is not available, but at least considering Newlyn, this serves to validate the AG-alignment process carried out.

## APPENDIX C: COMPARISONS AT CGPS@TG STATIONS ABER, BRST AND NEWL

For ABER, BRST and NEWL it is possible to compare our vertical station velocity estimates to results from Wöppelmann *et al.* (2007), a recent analysis as part of the IGS TIGA Pilot-Project which used over 200 globally distributed CGPS stations. Their vertical station velocity estimates were computed using the GAMIT (King & Bock 2005) and CATREF (Altamimi *et al.* 2004) software, applying the new absolute satellite and receiver antenna phase centre corrections (Ge *et al.* 2005), new tropospheric delay modelling (Böhm *et al.* 2006) and atmospheric pressure loading corrections (Tregoning & Van Dam 2005). Their reference frame implementation was based on IGB00, so includes an equivalent set of stations as for our implementation in the solutions based on PPPGT. Using a time span of 6.7 years, Wöppelmann *et al.* (2007) computed vertical station velocity estimates for ABER, BRST and NEWL to be  $0.2 \pm 0.1$ ,  $-1.2 \pm 0.1$  and  $-1.0 \pm 0.2$  mm yr<sup>-1</sup>, respectively. When comparing these to our CGPS and AG-aligned CGPS estimates (Tables 7 and 10), we show a reduction in the velocity differences for ABER, BRST and NEWL from +1.1, +2.5, and +1.7 mm yr<sup>-1</sup> to -0.2, +1.2 and +0.4 mm yr<sup>-1</sup>, respectively for solution DDRNF, and for NEWL from 1.2 to 0.6 mm yr<sup>-1</sup> for solution PPPGT. Again, this serves to validate the AG-alignment process carried out.

## SUPPORTING INFORMATION

Additional Supporting Information may be found in the online version of this article:

**Appendix S1.** Three supplementary tables and four supplementary figures, which are referred to in the text.

Please note: Wiley-Blackwell are not responsible for the content or functionality of any supporting materials supplied by the authors. Any queries (other than missing material) should be directed to the corresponding author for the article.